5-2014

The effects of shielding on Non-Destructive Analysis (NDA) and the use of Small-angle Compton scattering to overcome those effects

Cory Jake Hudson
University of Tennessee - Knoxville, chudso10@utk.edu

To the Graduate Council:

I am submitting herewith a thesis written by Cory Jake Hudson entitled "The effects of shielding on Non-Destructive Analysis (NDA) and the use of Small-angle Compton scattering to overcome those effects." I have examined the final electronic copy of this thesis for form and content and recommend that it be accepted in partial fulfillment of the requirements for the degree of Master of Science, with a major in Nuclear Engineering.

Laurence F. Miller, Major Professor

We have read this thesis and recommend its acceptance:

Lawrence H. Heilbronn, Ronald E. Pevey

Accepted for the Council:
Carolyn R. Hodges

Vice Provost and Dean of the Graduate School

(Original signatures are on file with official student records.)

The effects of shielding on Non-Destructive Analysis (NDA) and the use of Small-angle Compton scattering to overcome those effects

A Thesis Presented for the

Master of Science

Degree

The University of Tennessee, Knoxville

Cory Jake Hudson

May 2014

ACKNOWLEDGEMENTS

I would like to thank Dr. Laurence Miller for his continued guidance and support throughout this thesis project. His experience, in-depth knowledge, and overall willingness to help were invaluable during this process. I would also like to thank my committee members Dr. Lawrence Heilbronn and Dr. Ronald Pevey for their support in completing this thesis project. Finally, I would like to thank Dr. Richard Oberer, Dr. Lisa Chiang, and Ms. Cynthia Gunn for their innovation and impressive research toward the concepts of Small-angle Compton scattering. I would also like to thank them for giving me access to their research, letting me be involved in selected measurements, and for taking time to teach me about the theory and application of their methods. The concepts and knowledge I have gained from this experience have been instrumental in my personal growth as a Nuclear Engineer and in forming the critical aspects of this thesis project.

ABSTRACT

The use of passive Non-Destructive Analysis (NDA) equipment and techniques are very beneficial tools in the nuclear industry that have a plethora of applications and advantages over destructive or more invasive measurement methods. Of course, NDA techniques also have many limitations including dealing with many unknown parameters, overcoming the effects of gamma ray shielding, and the reliance on making many gross assumptions in the analysis of non-destructively acquired data. These limitations can lead to biased results or extremely difficult analysis which often introduces inaccurate conclusions and/or high levels of uncertainty.

This thesis paper will focus on specific NDA equipment and analysis techniques and discuss how they work, what their advantages are, what their disadvantages are, and some critically important real-world applications and uses of these NDA measurement techniques. The main focus of this discussion will explore great details about the theory, validation, and application of a newly developed NDA measurement technique called “Small-angle Compton scattering” which is a naturally occurring phenomenon in gamma energy spectrum that occurs when gamma rays are shielded by materials directly between a radioactive source and a detector. This paper will explain how this phenomenon can be observed and interpreted to give critical information about the effects of attenuation on a radioactive source, help improve non-destructive analysis techniques, and improve the overall results of difficult yet common measurement conditions of radioactive materials, principally Uranium-235 (U-235).

TABLE OF CONTENTS

LIST OF TABLES

LIST OF FIGURES

LIST OF ABBREVIATIONS

NDA – Non-Destructive Analysis or sometimes Non-Destructive Assay

HPGe – High Purity Germanium

NaI(Tl) – Sodium Iodide (Thallium Doped)

ALARA – As Low As Reasonably Achievable

MCA – Multi-Channel Analyzer

GGH – Generalized Geometry Holdup

U-235 – A fissile isotope of Uranium

UNH - Uranyl Nitrate Hexahydrate

TMU – Total Measurement Uncertainty

Chapter 1: Introduction

Non-Destructive Analysis (NDA) is a highly utilized nuclear measurement technique that is applied to many different situations in the nuclear world and industry. It can be used to locate, characterize, and even quantify various radioactive isotopes for applications in Environmental and Waste Management, Nuclear Materials Accounting, Nuclear Criticality Safety, and even Non-Proliferation. NDA can also be used as a technical extension of a nuclear security program as a quick, accurate, and cost effective deterrent to theft and diversion of nuclear materials. Non-Destructive measurement systems and techniques are so beneficial for many reasons. The first and most obvious is that they are typically passive measurements that don't alter the state of the radioactive source. In many cases they usually don't require close proximity, handling, or even seeing the radioactive material you are measuring. This supports the ALARA (As Low As Reasonably Achievable) principle for radiation exposure and makes NDA extremely safe compared to other radioactive measurement methods that require more hazardous destructive testing that can create additional radioactive waste compared to an non-destructive measurement. Second, NDA equipment is highly portable meaning that measurements and analysis can be done in a true field situation compared to destructive NDA techniques which are typically restricted to a laboratory setting. Also, NDA measurements can often be taken and analyzed fairly quickly in any location making critical results available in almost real time. All of these together make NDA measurement techniques very useful and cost effective compared to more difficult destructive analysis methods.

As with any technical solution that offers a long list of benefits, there are also critical limitations associated with non-destructive measurement techniques. Because seeing or handling radioactive materials inside a container is often impossible or not ideal, many educated guesses or assumptions must be made in order to properly analyze a suspect material. The accuracy or in-accuracy of these assumptions can give results with wide degrees of uncertainty. In some situation, this might be acceptable, but in other more critical safety and non-proliferation situations, this might be a problem. Also, since the NDA techniques I will be discussing in this thesis are passive methods that rely on detecting gamma radiation emitting from a radioactive

source, strategic or even unintentional shielding can play a huge role in altering gamma rays and negatively affecting the accuracy and capabilities of non-destructive measurements. This is especially true for radioactive materials that emit lower energy gamma rays that are more easily attenuated like the fissile U-235 material.

One of the core topics of this thesis is to discuss a newly developed NDA measurement technique called "Small-angle Compton scattering" that helps account for shielding between a radioactive source and a gamma detector by providing valuable information about the thickness of the shielding material which allows NDA engineers to accurately account and correct for it in their analysis. This technique, which was conceptualized by Dr. Richard Oberer and developed with support from Dr. Lisa Chiang and Ms. Cynthia Gunn, uses the Small-angle Compton scatters within the gamma spectrum to assess the amount of material that the gamma rays are traversing before they are detected in the detector. This research mainly focuses on the U-235 isotope because of its worldwide use and desirable nature toward the creation of atomic energy and weapons, but it can be used to non-destructively evaluate other radioactive isotopes as well. Because Small-angle Compton scattering produces a well known discontinuity in the energy peaks of any radioactive isotope (See Figure 1 below), Dr. Oberer and his colleagues were able to devise predictive mathematical formulas to pull useful data out of this observed discontinuity and apply it to their overall measurement analysis. The end result was more accurate NDA data, especially for situations involving shielding and potential intervening material between a source and your detector.

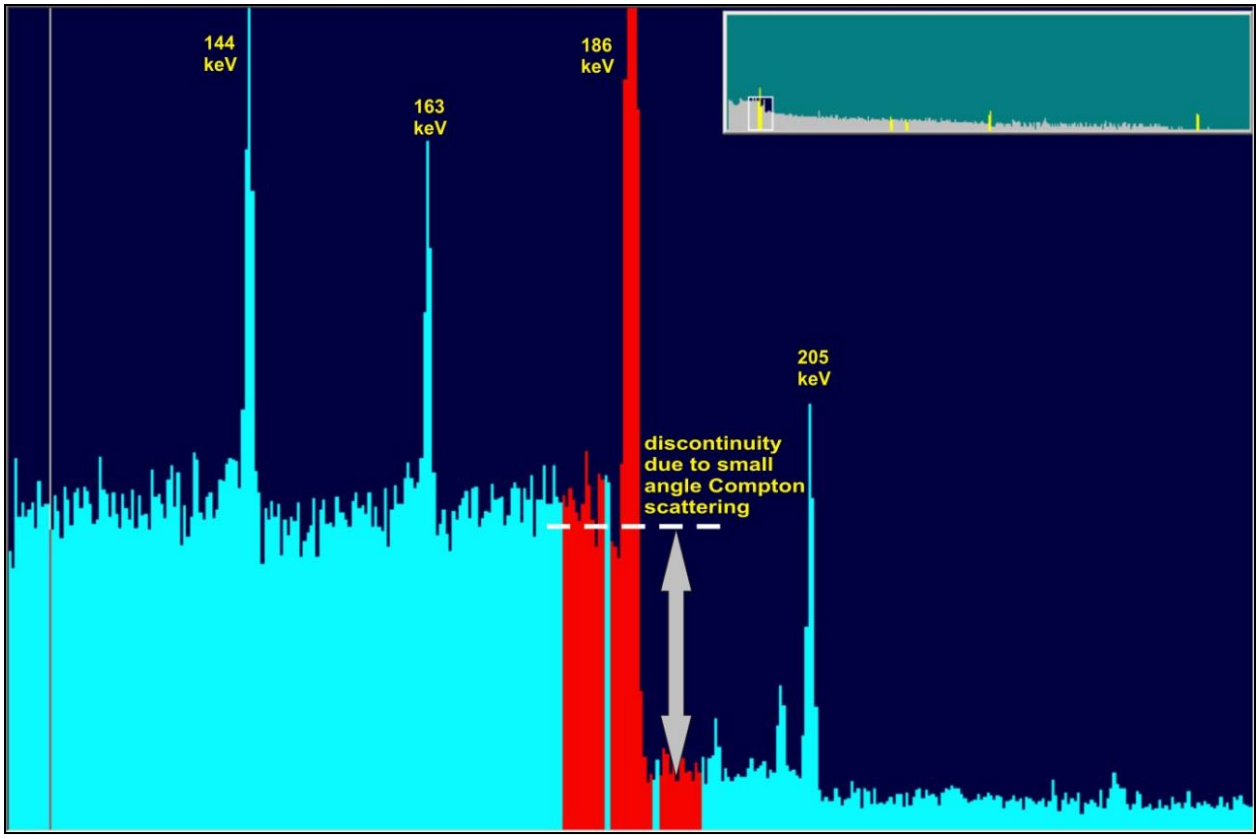

Figure 1: The phenomenon of Small-angle Compton scattering is shown by the discontinuity in the primary 185.72 keV gamma peak from a high resolution spectrum of U-235 material.

a. Objective

Within this thesis project I plan to not only explain some of the benefits and limitations of various NDA equipment and techniques, but also share extensive details about the newly developed NDA method involving Small-angle Compton scattering which has many real-world applications and can help overcome some well-known challenges that exist in non-destructive measurements. This project will provide details into the theory, validation, and application of Small-angle Compton scattering as well as a variety of potential uses and future work that could be accomplished if this method and research were continued to be developed.

b. Background

It is a well known fact that NDA measurements utilizing gamma rays are dependent on a variety of factors that can affect the quality of your results. To get ideal NDA results, accurate models must be built to represent the conditions of your measurements. These models and the accuracy of NDA measurements in general are based on key things such as geometry and the affects of attenuation as described in Table 1 below. Building accurate models helps to account and correct for the various influences that affect NDA measurements, but being able to accurately define all the items from Table 1 is almost impossible. In ideal circumstances, typical NDA measurements can be replicated using 'standard based' methods so that accurate models can be built using known radioactive sources with defined quantities to help improve the accuracy and ability to measure unknown radioactive elements in similar configurations. Unfortunately, the vast majority of 'real world' applications of NDA measurements are not conducive with 'standard based' modeling. Gamma emitting radiation is present in a variety of forms and locations making reliance on representative standards impractical and in many cases impossible. Therefore, Small-Angle Compton Scattering was born out of the necessity to develop theoretical corrections that would improve modeling assumptions in real world applications of NDA measurements.

The discontinuity in the gamma-ray peak caused by Small-angle Compton scattering was previously considered an annoyance in determining peak area, but it turns out to be a valuable tool for determining the composition and amount of material between the source and detector. The ability to accurately gauge the amount of attenuating material between radioactive source and the detector significantly reduces many of the variables that drive uncertainty in NDA measurements.

Table 1: Critical influences on modeling and analysis for NDA gamma measurements.

Influence:	**Details:**

Geometry	• Distance
	  ○ Distance between source and detector
	• Physical Dimensions
	  ○ Dimensions of container holding radioactive material
	  ○ Dimensions of radioactive source itself

Attenuation	• Process Knowledge
	  ○ Matrix Composition
	  ○ Bulk Density
	  ○ Net Weight
	• Matrices
	  ○ Container or other materials interfering or shielding gamma rays of interest
	  ○ Comingling of radioactive materials within non-radioactive materials
	• Material Forms
	  ○ Homogeneous and low density material is ideal for NDA measurements
	  ○ Heterogeneous or material clumping causes self-attenuation issues or biased results depending on detector placement.
	• Self-Shielding
	  ○ Small concentrations of Uranium can self-shield gamma rays
	  ○ Thick concentrations of Uranium can completely shield gamma rays

c. Motivations

One of the original motivations that led to this research being conducted on Small-angle Compton scattering was its potential application to quantifying U-235 material in solution form that was spilled onto concrete floors in a Uranium Chemical Operations facility. If U-235 solution is spilled onto a porous concrete floor at various locations and in various quantities over decades of production, quantifying how much material has become trapped or embedded in the floor as holdup is an important task for both criticality safety and material accounting purposes. The estimated quantity of U-235 in a concrete floor can vary considerably based on assumptions made about the depth of penetration the U-235 solution made into the concrete. For example, using common NDA measurement techniques that utilize decay count rates from the principle gamma ray of U-235 (185.72keV) to analyze U-235 content in the floor can produce great variations in estimated quantities if you assume the absorbed U-235 solution is all concentrated near the surface of the concrete compared to if the solution absorbed deeper into the concrete. Furthermore, the quantities could be grossly miscalculated if the U-235 solution found a crack in the foundation and made its way several inches into the concrete or if the actual condition of the floor does not match your assumptions. Based on actual NDA measurements performed in this scenario, it was noticed that estimates of U-235 holdup in a concrete floor can vary by as much 50% and be on the magnitude of 10-20 kilograms of difference in U-235 quantity by simply varying the assumed depth of penetration of U-235 solution into the concrete floor from just 0 to 1 inch.

See Figure 2 below for a visual explanation of these different U-235 solution penetration conditions into a concrete floor.

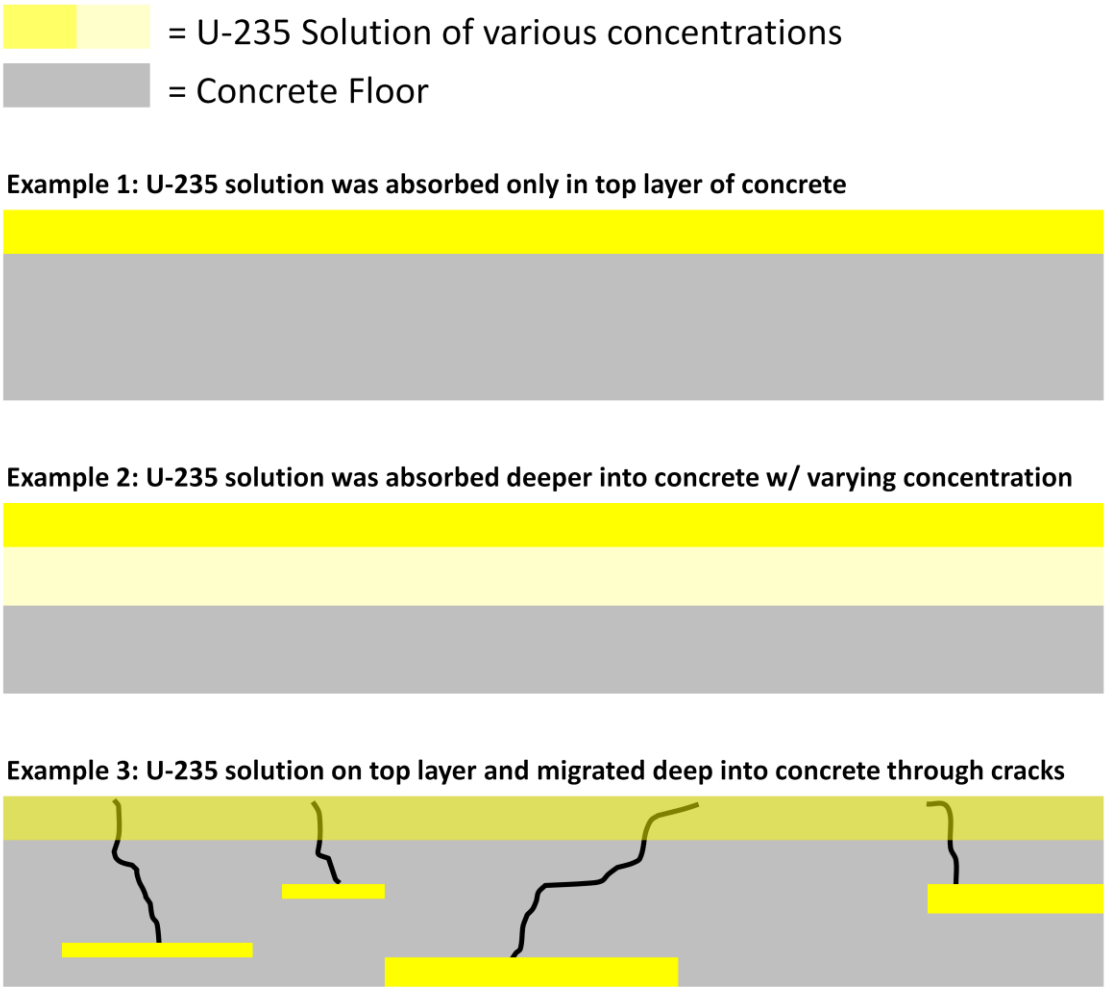

Figure 2: Various possible holdup conditions and penetration depths of U-235 solution spilled onto a concrete floor.

Other motivations that also perpetuated this research into Small-angle Compton scattering are its applications to nuclear security, nuclear inspections, and non-proliferation efforts. Figure 3 below shows a simple situation in which not knowing the amount of shielding present between a gamma detector and a radioactive source can give the appearance of similar amounts of U-235 when in fact the true situation is very different. As shown, both rate meters calibrated to the gamma energies of U-235 show the same 1000cps displayed from the source, but the unknown thickness of shielding can make 1kg appear the same as 10kg. This situation could be very practical if the source was embedded in some unknown container or material, or if

someone was going through great lengths to make a nuclear inspector think less U-235 material is present by trying to shield it from the detection equipment. The use of Small-angle Compton scattering can be used to overcome these obstacles and provide valuable information about shielding and gamma-ray attenuation.

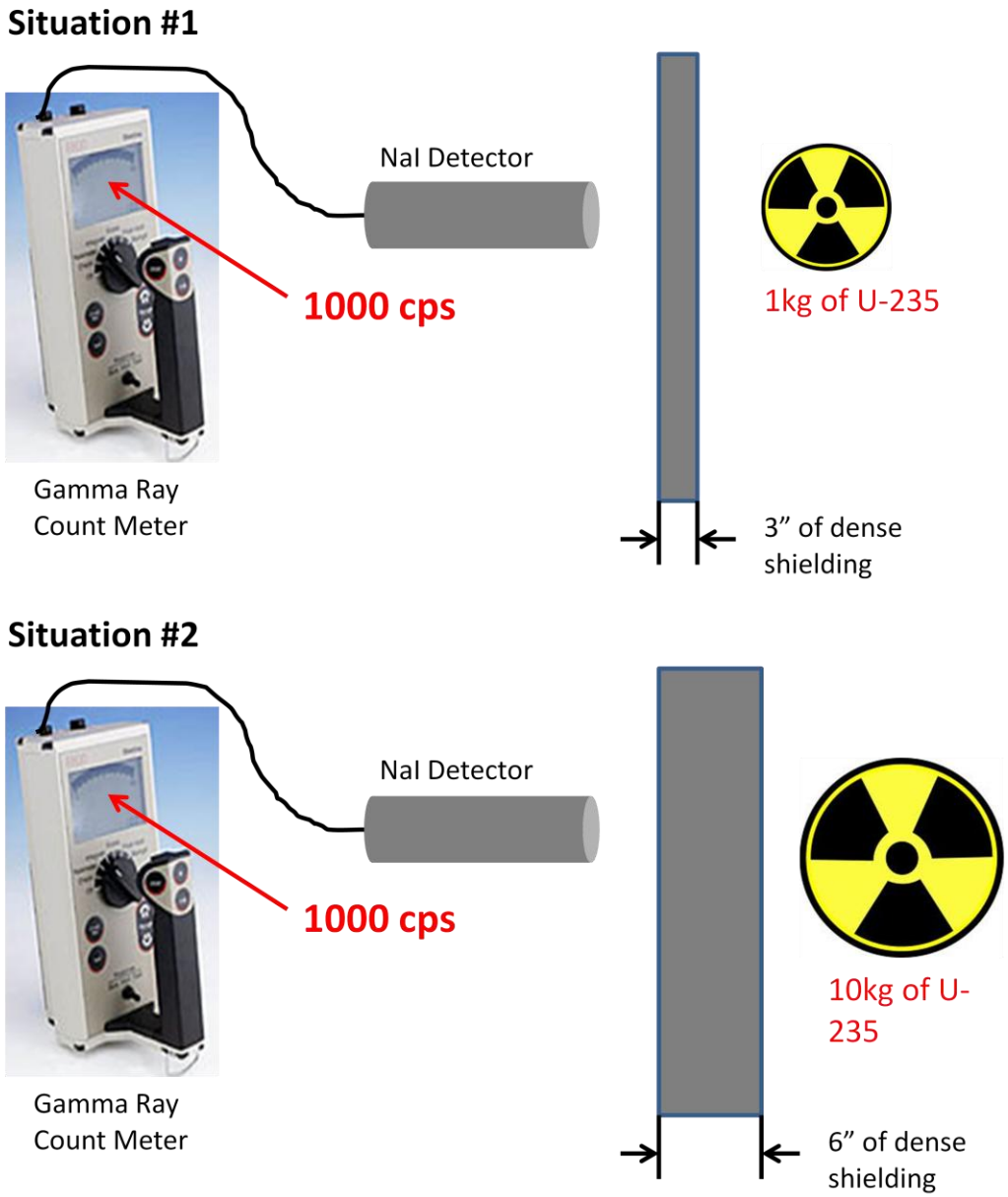

Figure 3: Unknown thicknesses of shielding make proper NDA corrections for attenuation impossible and can make very different nuclear situations look similar.

Chapter 2: Description of Equipment

Various types of equipment are available for measuring and quantifying radioactive materials using non-destructive methods. The main equipment that supports the measurements and validations associated with Small-angle Compton scattering and its real-world applications are a thallium activated sodium iodide (NaI[Tl]) gamma ray energy spectrometer and a High Purity Germanium (HPGe) detector. The main differences between these two devices are that NaI detectors typically display gamma ray spectrum with low resolution and are calibrated in a way that allows them to measure and analyze a specific radioactive isotope of interest. For this particular research, this isotope is U-235. HPGe detectors display gamma ray spectrum with a much higher resolution and allow the user to observe and quantify multiple radioactive isotopes at one time using energies throughout the spectrum (typically from 60keV – 2734keV). The high resolution of the HPGe detector also allows the distinction between multiple, closely positioned gamma rays from the same radioactive isotope which improves the ability to achieve better modeling accuracy and make better analysis correction. Figures 4 and 5 below show the key distinction between a low resolution spectrum from a NaI detector and a high resolution spectrum from an HPGe detector.

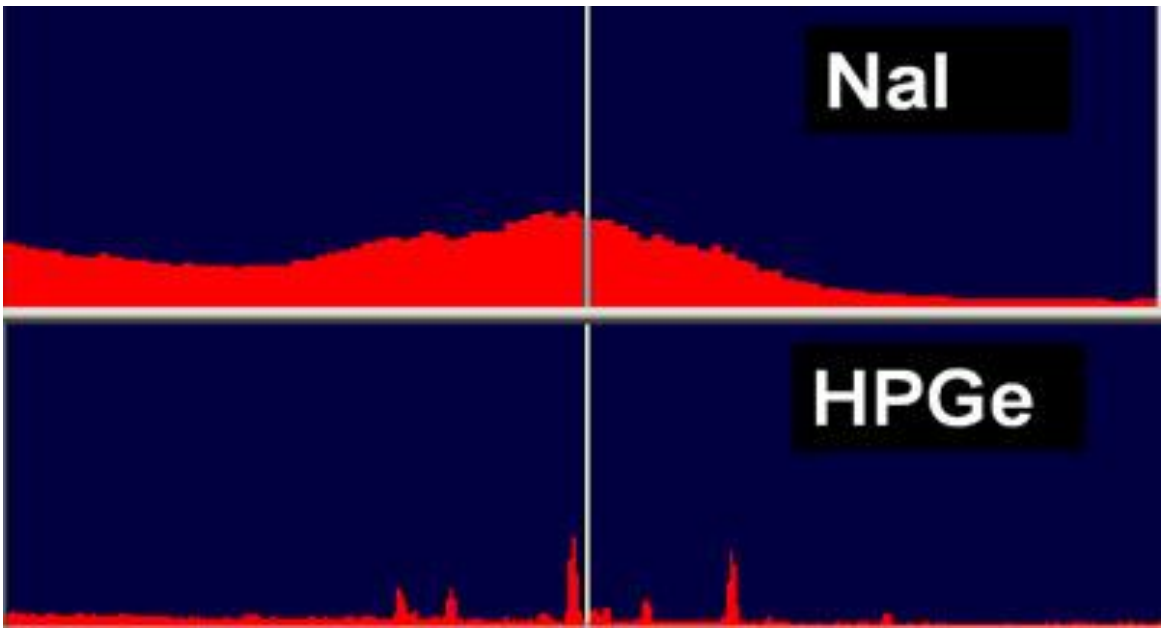

Figure 4: Visual distinction between low resolution (NaI) and high resolution spectrum (HPGe).

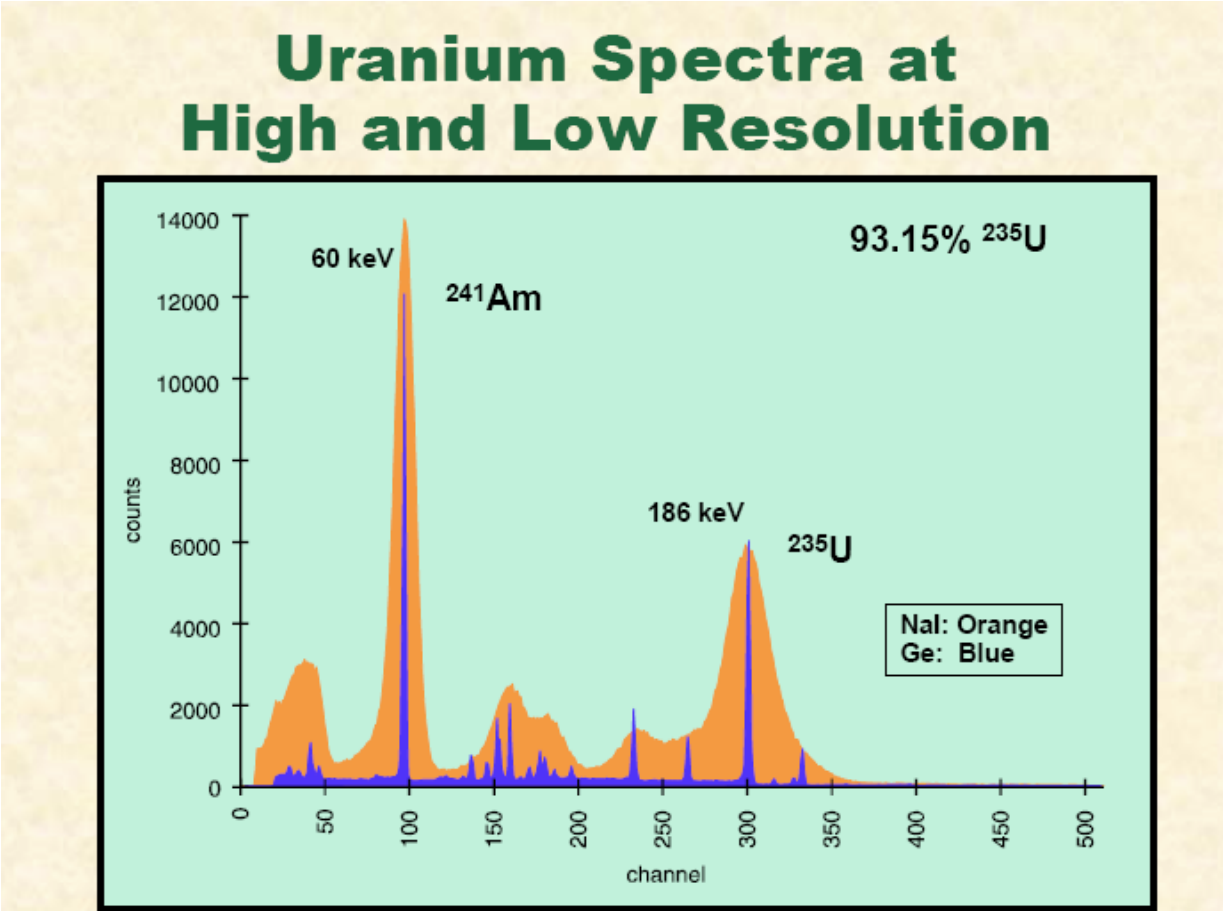

Figure 5: U-235 and Am-241 spectra at high and low resolution.

d. Sodium Iodide (NaI) Gamma Ray Spectrometer

A thallium activated sodium iodide (NaI[Tl]) gamma ray energy spectrometer, when properly calibrated, is able to make quantifiable assessment of U-235 holdup in the presence of other uranium isotopes and prevailing background radiation. The benefits of this type of measurement equipment are that it is portable, lightweight, and has quick data acquisition times. An example of this type of NDA detection equipment is shown below in Figure 6.

Figure 6: Example of typical NaI detection equipment including detector, multi-channel analyzer (MCA), and hand-held computer.

The use and calibration of this type of non-destructive measurement equipment is based upon the methodologies defined by Phyllis Russo in LA-14206, where detection efficiency determination protocols are defined (called Generalized Geometry Holdup [GGH]). The GGH methodology together with attenuation correction algorithms and other modeling parameters are combined to provide a comprehensive tool for conducting in situ gamma-ray measurements. Figure 7 below shows a picture of a NaI(Tl) detection element and its housing as well as a schematic diagram of the spectrometers primary system components. The detector element is a 1.0 inch diameter by 0.5 inch thick scintillation crystal of NaI(Tl). Incident radiation photons from the source material of interest, and for that matter, non-source generated interfering background radiation interacting in the crystal, result in the generation of photons in the crystal in the near visible region. A photomultiplier tube is utilized to convert the deposited photon energy into an output current pulse with an output proportional to the energy input. The output current pulse is processed into a form and shape suitable for pulse height analysis.

This pulse output is then received by a pulse height analyzer where its height is measured and stored. Input pulses are collected for a set period of time so that an energy spectrum can be formed and displayed.

An Am-241 source is positioned on the scintillator to provide a constant reference source of gamma-rays at 60keV. This provides a constant full energy peak that does not interfere with the observation of U-235 events. This peak provides a data quality check and an electronic gain stabilization signal for the electronics system of the detector.

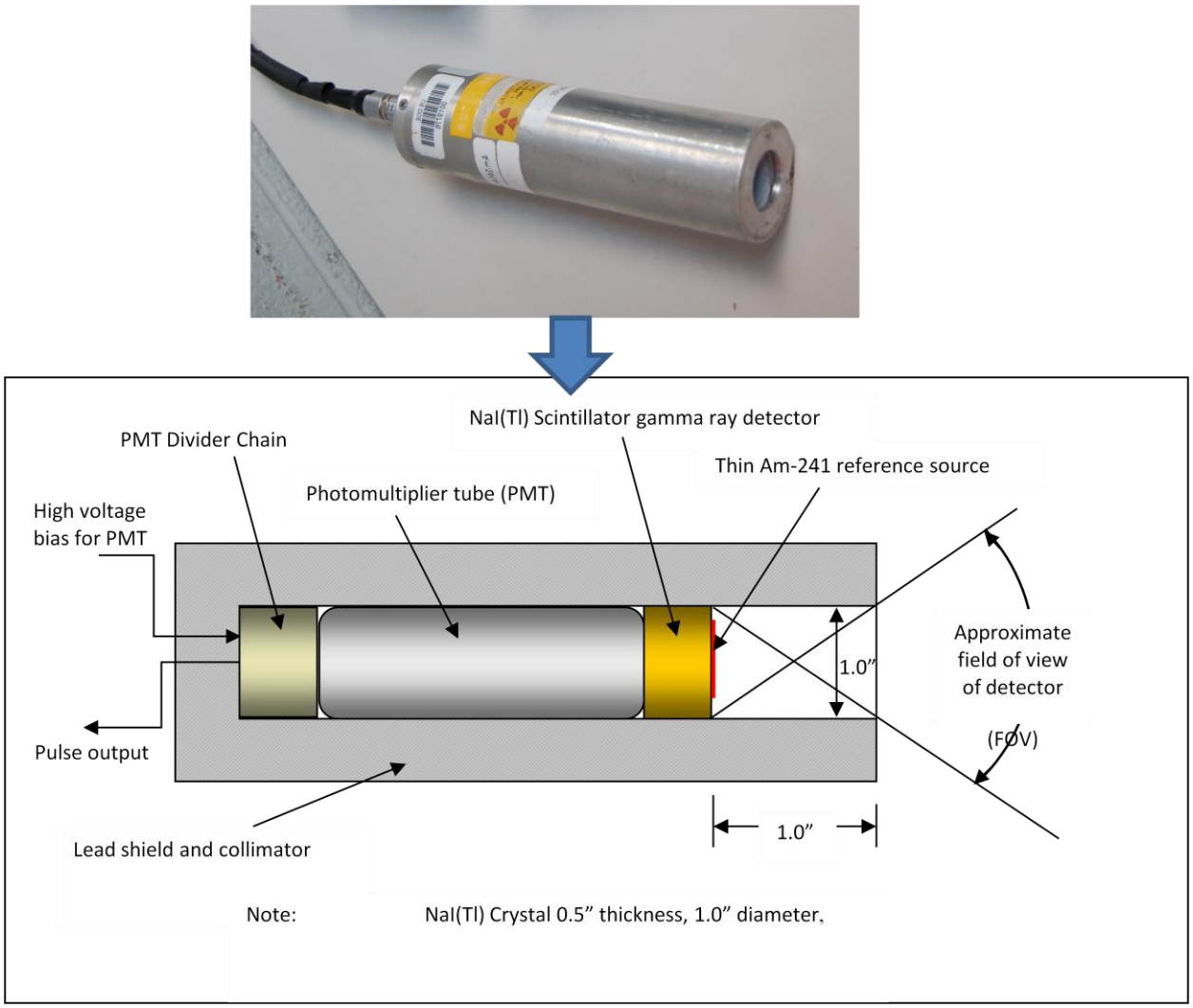

Figure 7: NaI(Tl) detection element and its housing and a schematic diagram of the spectrometer primary system components.

Gamma rays emitted from various radionuclides have characteristic energies of emission that are fixed, regardless of any external effects or criteria. Each radionuclide emits a unique energy (or range of energies) whose precise measurement can allow the identification of the presence of that radionuclide. In the case of the uranium isotope series of interest, each disintegration results in the emission of an alpha particle immediately followed by one or more mono-energetic photons. If the response of the detector is proportional to the energy deposited in its volume, then the detector has an energy measurement capability and can be useful as an energy spectrometer. Because the NaI(Tl) crystal is optically transparent, a gamma ray interacting in the crystal transfers some, or all of its energy to an electron via a Compton interaction or the photoelectric effect. This energetic electron then travels through the crystal lattice, losing energy to the crystal lattice through lattice excitation, the generation of more electrons, and the generation of Bremstrahlung X-rays. These are typically reabsorbed into the crystal lattice. The crystal then de-excites through the emission of a number of visible region photons. The light is generated as a light "pulse" whose intensity is proportional to the energy deposited in the crystal. This light is detected and amplified by use of a device called a photo multiplier tube (PMT).

Figure 8 below shows how a typical scintillation crystal and a photomultiplier are coupled together to make a complete detection element. The photomultiplier requires a voltage distribution so that the avalanche of electrons can be accelerated down the tube to provide an output current pulse. This device is very sensitive to changes in voltage and as a consequence requires care in use to ensure its gain stability.

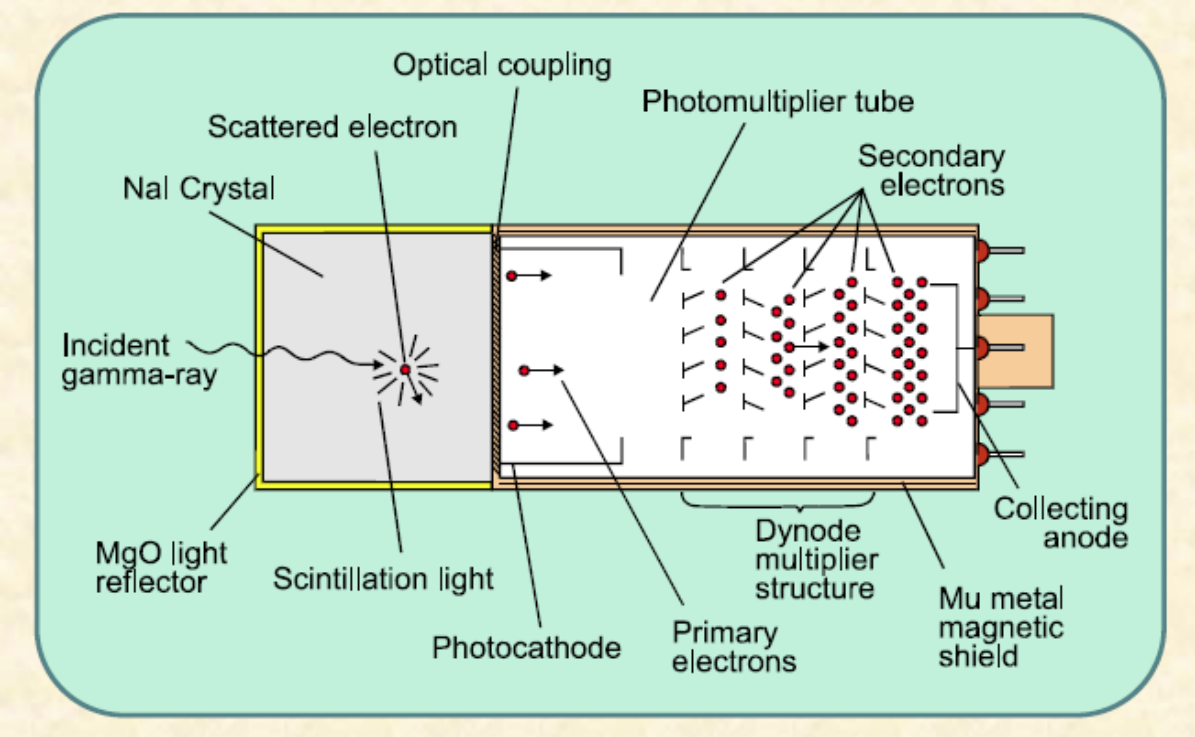

Figure 8: A typical scintillation crystal and a photomultiplier coupled together to make a complete detection element.

e. High Purity Germanium (HPGe) Detector

High Purity Germanium (HPGe) is one of the best radiation detection technologies that provide sufficient information to accurately and reliably identify all critical radionuclides from their passive gamma ray emissions. HPGe detectors have a 20-30x improvement in resolution as compared to that of Sodium Iodide (NaI) detectors. In addition, NaI detectors, unlike HPGe detectors, have been shown to perform poorly in mixed isotope, shielded, stand-off, and high background scenarios.

Every radionuclide of concern in homeland security naturally emits a unique set of one or more gamma ray energies from which it can be uniquely identified, analogous to how a fingerprint uniquely identifies an individual person. These energies are measured in units of electron volts (eV) or Kiloelectron volts (KeV) and most are found within the range of 30 KeV to 3000 KeV.

They are not however uniformly spread across this range. Many are tightly spaced with only a few KeV or less between them. To make identification of these radionuclides possible, one needs to be able to measure these energies to approximately 1/10th of 1 percent (0.1%). HPGe detectors can provide this level of accuracy while NaI detectors provide only about 6 parts in 100. This problem is obvious when you look at the comparable spectra produced by NaI and HPGe detectors. Also, unlike NaI detectors, HPGe detectors are more resistant to signal degradation caused by changes in background radiation, shielding, multiple radionuclide interference, and temperature variations. Figure 9 below shows a typical setup of an HPGe detector.

Figure 9: Typical setup of an ORTEC HPGe detector with collimator.

HPGe detectors have been used for over quarter of the century. However, because germanium has relatively low band gap, these detectors must be cooled in order to reduce the thermal generation of charge carriers, and therefore reverse leakage current, to an acceptable level. Otherwise, leakage current induced noise destroys the energy resolution of the germanium detector. Liquid nitrogen, which has a temperature of 77 °K is the common cooling medium for

such detectors and is stored in the 3 liter dewar seen on the left side of the detector in Figure 9 above. The germanium detector is mounted in a vacuum chamber which is attached to or inserted into a LN_2 Dewar. The sensitive detector surfaces are thus protected from moisture and condensable contaminants. Since this type of equipment must operate at cryogenic temperatures and they require highly accurate supporting electronics, HPGe detectors have typically been large and expensive laboratory instruments that are not as suitable for field use as the NaI detectors, although improvements have been made to make HPGe detectors more portable and acceptable for field use. Figure 10 below shows how the liquid nitrogen from a mother dewar is used to cool the germanium crystal in and HPGe crystal which allows it to properly detect gamma ray emissions in a passive manner.

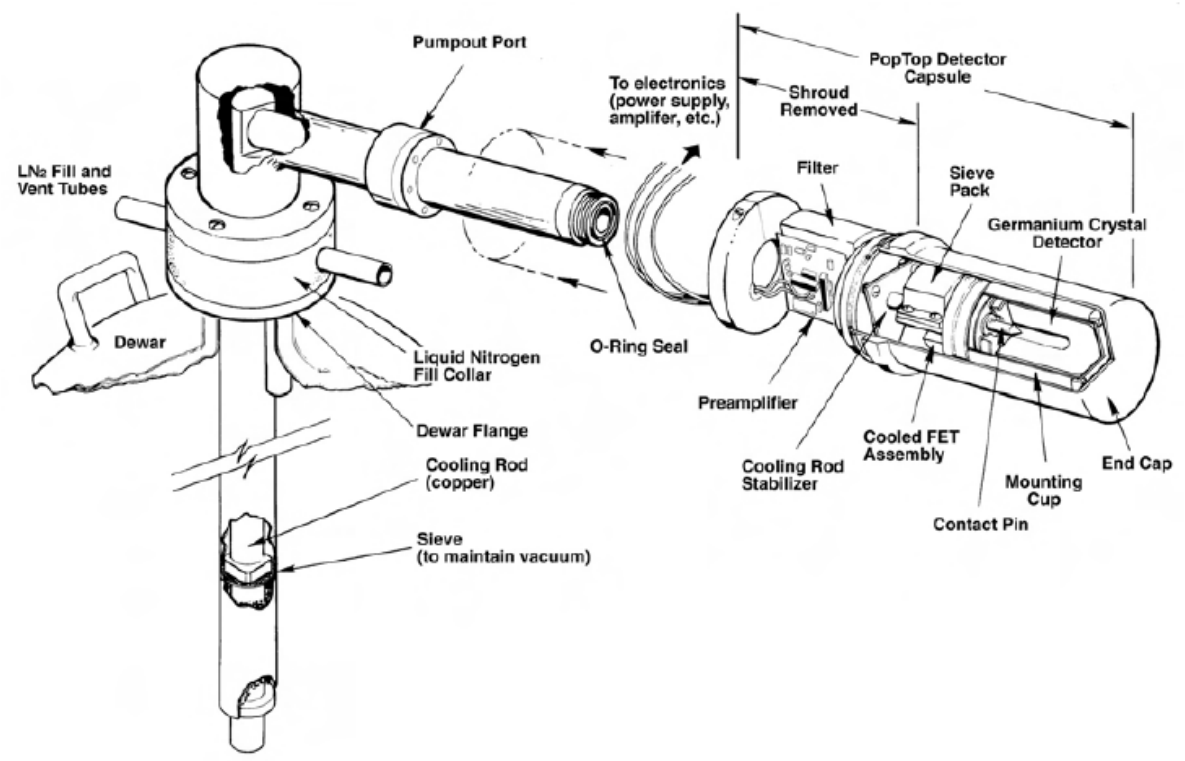

Figure 10: Exploded view of a PopTop HPGe detector capsule with horizontal dipstick cryostat attached to a liquid nitrogen dewar.

Chapter 3: Theory of approach for Small-angle Compton scattering

Now that an understanding of the measurement equipment has been established, the theory behind Small-angle Compton scattering will be discussed. But, before getting into the theory and approach of using Small-angle Compton scattering, the meaning and origin of this 'Small-Angle' term should be shared. It is well known that the principal mechanisms of energy deposition by photons in matter are photoelectric absorption, Compton scattering, pair production, and photonuclear reactions. The theory and application discussed in this thesis project revolves solely around Compton scattering which occurs when an incident gamma ray is deflected from its original path by an interaction with an electron. The gamma ray loses part of its energy from Compton scattering. The ratio of this new energy E to the original gamma-ray energy E_γ is given by the equation:

$$\left(\frac{E}{E_\gamma}\right) = \frac{1}{1 + \frac{E_\gamma}{m_e c^2}(1 - \cos(\theta))}$$

When the scattering angle θ approaches zero, the scattered gamma ray has the same or nearly the same energy as the original gamma ray. It is the effect of this Small-angle Compton scattering that produces the discontinuity at the gamma-ray peak that is shown below in Figure 11. The theory of this research is based around the thought that because the scattered gamma ray continues on in nearly the same direction as the original, it can only be caused by material directly between the source and detector. From that, it was postulated by Dr. Oberer that the magnitude of this discontinuity with respect to the gamma-ray peak is an indicator of the amount of material or shielding directly between the gamma-ray source and the detector. The ability to accurately gauge the amount of attenuating material between radioactive source and the detector helps develop much more accurate analysis models which will in turn significantly reduce one of the critical variables that drives uncertainty in NDA measurement.

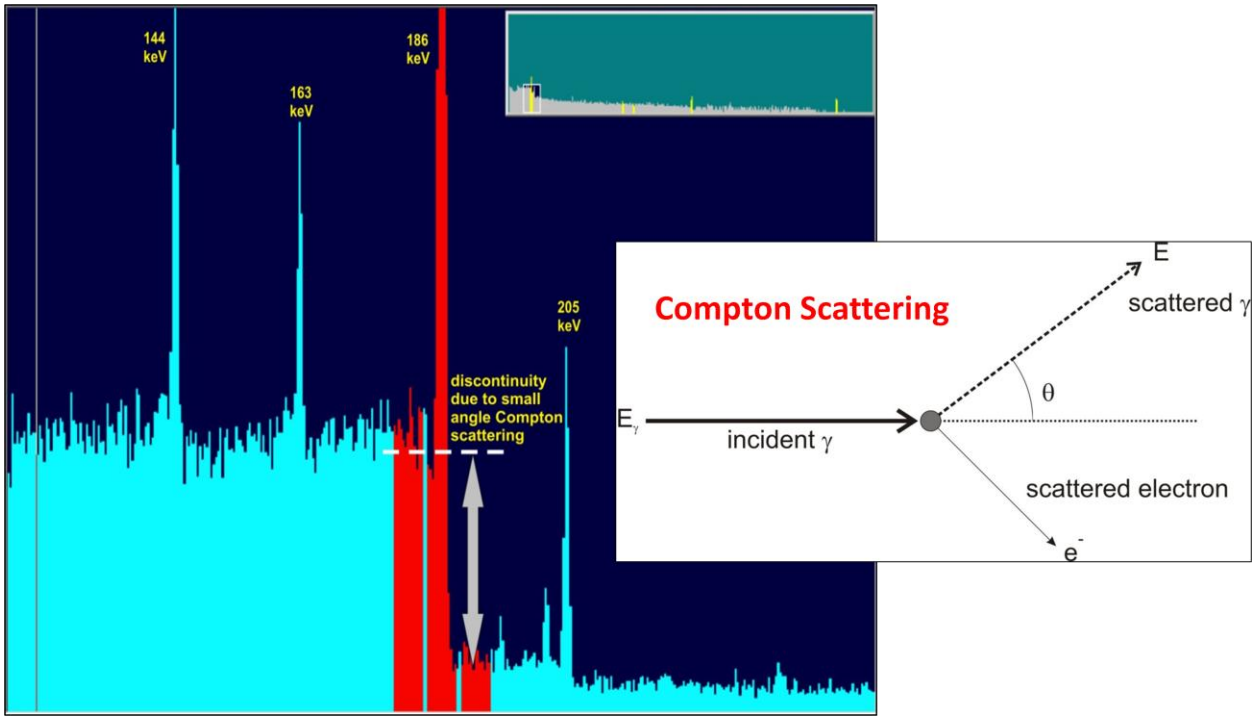

Figure 11: Example of Compton scattering at very small angles which creates a discontinuity in the gamma peak.

f. Attenuation of Gamma Rays

There are three main factors that affect the attenuation of gamma rays. The first is the thickness of the material that the gamma ray must travel through to get to the detector, *x*. The second factor is the density of this intervening material, ρ. The third is the mass-attenuation coefficient, μ. The mass-attenuation coefficient is statistically based on the probability per unit distance traveled that a gamma ray interacts with the intervening material. This coefficient is directly dependent on the composition of the material being traversed and the energy of the gamma ray. The probability of a gamma ray traversing a distance of x in a material is given by the equation:

$$T = e^{-\mu\rho x}$$

Because the mass-attenuation coefficient is dependent on the energy of the gamma ray, the product ρx of the intervening material can be determined by comparing gamma rays of different energies emitted by the same isotope. When dealing with highly enriched uranium, the energies emitted from the isotope of U-235 are the most useful. These energies and branching ratios are shown below in Table 2. The 185.72keV gamma ray is the primary peak of U-235 due to its much higher branching ratio compared to the other energies. It should be noted that U-235 gamma rays are typically considered low-energy gamma rays compared to other radioactive isotopes which makes them more susceptible to the affects of shielding and attenuation and therefore more difficult to analyze in certain situations. It should also be noted that uranium is a highly dense material itself and in certain masses and configurations can be considered infinitely thick. This means that the outer layers of uranium completely shield out inner layers of the same piece or configuration of uranium and make detection and accurate analysis with detectors virtually impossible.

Table 2: Gamma ray energies and branching ratios for U-235.

Energies emitted by U-235	Branching Ratio
143.76keV	10.5%
163.35keV	4.7%
185.72keV	54.0%
202.12keV	1.0%
205.31keV	4.7%

The measured count rate of a gamma ray is determined as a net peak area per count time from an acquired spectrum. The count rate of a signature gamma ray is directly proportional to the amount of U-235 present if all background and attenuation effects are properly accounted for and corrected. Attenuation of a gamma ray signal can be caused by interaction of the gamma rays with any intervening materials between the source and the detector. Interactions occur with container walls, matrix materials mixed with the source material, and by interaction within

the source material itself. Background interference is caused by sources coming into the detector from items other than that which is being measured and can severely affect intended results if it is not low and/or controlled. Background radiation is also caused by Compton scattering of the signature gamma rays of the source material or from Compton interactions from higher energy peaks that form the Compton continuum of a spectrum. This Compton radiation has lost the identity of its original energy and cannot be used to quantify the amount of radioactive source material present.

g. Process of Differential Attenuation

When measuring a container or fixed location containing radioactive material, the net weight, container/location dimensions, and general characteristics of material making up matrix material must be identified and included in calculating the attenuation of the measured gamma rays. These calculations operate on the assumption that the radioactive isotopes are uniformly distributed throughout the contents of the intervening material. In other words, the radioactive material should have a homogeneous presence throughout the matrix material it is contained within. In reality, this condition is rarely achieved and leads to spectrum being under or over corrected based on incorrect assumptions. Since the gamma rays of differing energies from the same isotope will experience different degrees of attenuation, assumptions used in creating a mathematical model of the measured matrix can be adjusted until the corrected activities for each of the gamma rays of a given isotope are equal. This technique of relying on a multi gamma-ray analysis approach for a given radioisotope is referred to as differential attenuation.

A gamma ray spectrum can be analyzed using a differential attenuation technique that converts the measured, uncorrected activities to corrected activities from which the mass of an isotope can be computed. In order to apply differential attenuation appropriately, the measured activity of a specific isotope must be noticeably above the background level in the measurement environment and appropriately corrected for the effects of attenuation and geometry. Theoretically, all of the gamma-rays measured from a single isotope should have the

same activity as the primary energy of the isotope. For example, the activity from the primary peak of U-235 shown in Table 2 above (185.72keV) should be the same as the secondary peaks at the 143.73keV, 163.35keV, 202,12keV, and 205.31keV gamma ray energies. If the incorrect attenuation correction factors are used, then the computed activities for the different gamma rays for that isotope will differ.

The concept of differential attenuation is shown below in Figures 12 using a user interface from a software product developed by the company ORTEC called ISOTOPIC. The blue dots represent the various gamma rays from the U-235 isotope shown above in Table 2. The larger blue dot on the line signals the reference peak for U-235 (185.72keV) because it is the most prominent peak based on its much higher branching ratio compared to the other peaks. All the other gamma ray activities from the U-235 isotope are referenced to this main 185.72keV peak with the intention of adjusting three key parameters to make the activities of all gamma ray energies from U-235 as equal as possible.

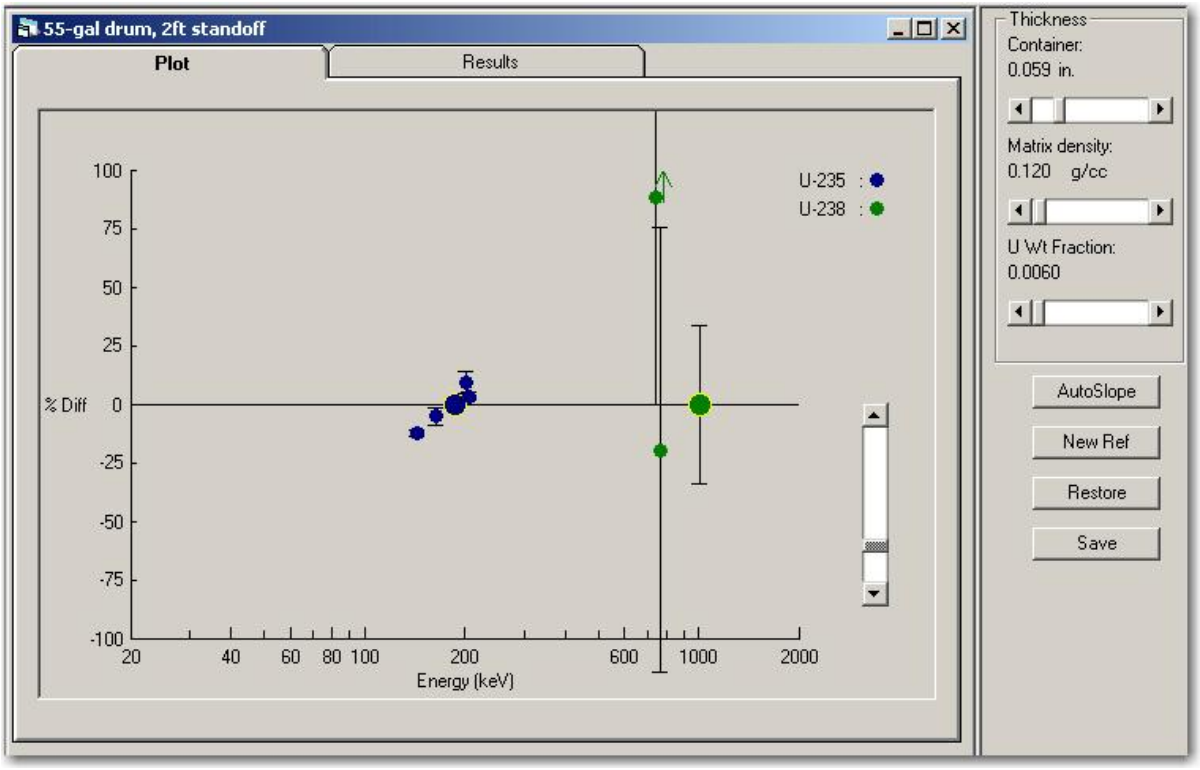

Figure 12: Differential attenuation plot from ISOTOPIC software before any corrections are made.

The three parameters that can be adjusted to appropriately correct the spectrum for attenuation are shown with slide-bars on the top-right of Figure 12 and are:

1. Thickness Container (in) – Thickness of the container or material the gamma rays must traverse to get to the detector (Note: container material and density would already be set up in the analysis model built within the ISOTOPIC software).
2. Matrix Density (g/c^3) – The density of the material containing the U-235 or other radioactive isotope you are trying to measure (Note: Matrix can be almost any material including concrete, combustibles, water, other metals, or Uranium itself).
3. U Wt. Fraction – Percentage of Uranium by weight compared to the other materials in the matrix.

Attenuation effects may be corrected for by using theoretical relationships relating the attenuation of a gamma ray of a given energy to the density, thickness, and mass attenuation coefficient of the material with which the gamma ray is interacting. The difficulty in calculating the total self-attenuation comes from the fact that the fraction of uranium present in the matrix must be included with the composition of the matrix material, which is an unknown. The relationship used to correct for self-attenuation of a radioactive source mixed with a matrix material is provided in the equation below.

$$CF_{Self-Atten} = \frac{\mu_m \rho_m x_m}{(1 - e^{-\mu_m \rho_m x_m})}$$

Where μ_m = Mass-attenuation coefficient for the matrix material

ρ_m = Bulk density for the matrix material

X_m = Thickness of the matrix material

In the first plot in Figure 12 above, the gamma rays are under corrected and therefore show a large difference between the various dots representing gamma ray energies. As an example, Figure 13 below shows a corrected plot where the U Wt Fraction was adjusted from 0.006 to 0.863 which moves most of the energy dots in almost perfect line with the main 185.72keV reference dot. In other words, the activities reported by these multiple gamma rays are nominally the same as the main reference peak. The 202.12keV peak is the only dot not in line with the rest due to its comparatively low branching ratio (1.0%). If all energy peaks cannot be perfectly in line with the main reference peak, then the focus should be on the gamma ray energies with the highest branching ratios compared to the reference peak which is 185.72keV for U-235.

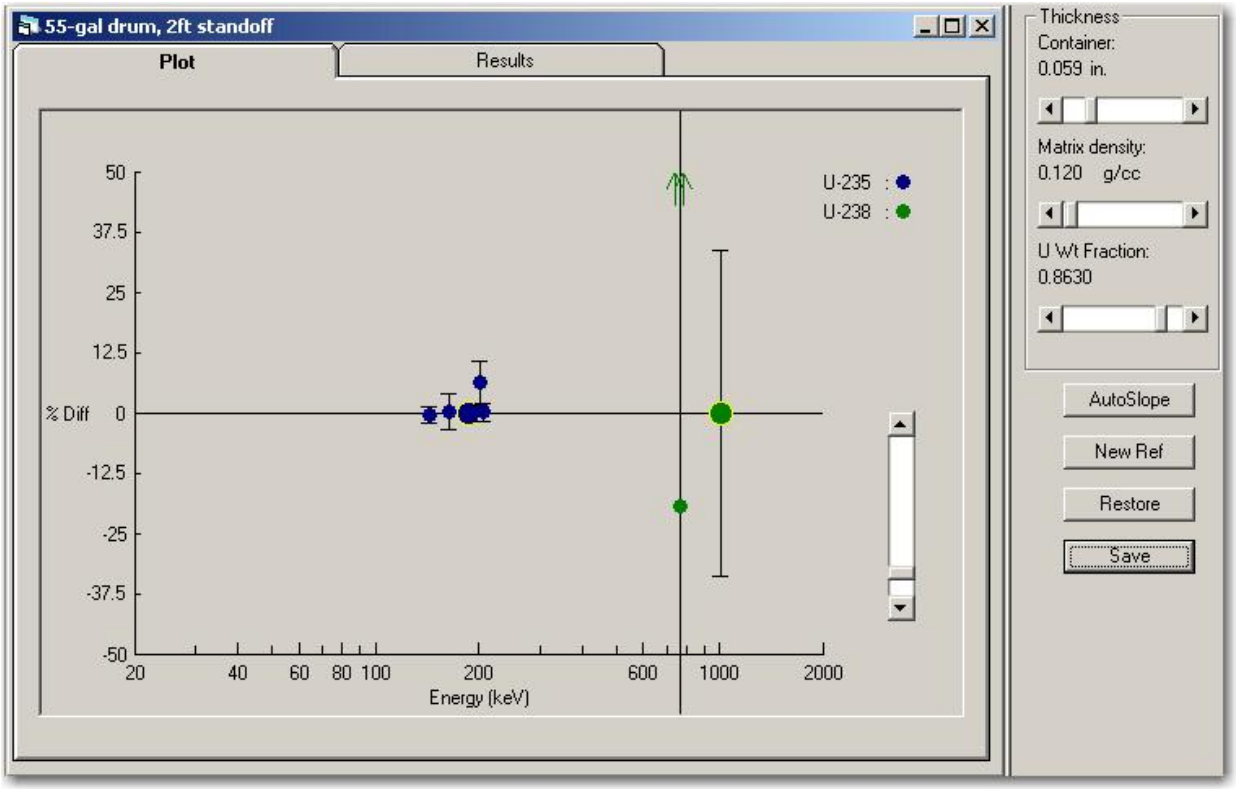

Figure 13: Differential attenuation plot from ISOTOPIC software with U Wt Fraction correction (0.006 → 0.863) to align all gamma-ray energies from U-235.

The standard differential attenuation analysis can be performed either directly in the ISOTOPIC software, or it can be computed from the raw spectra data by using the following physical equations that convert the measured activities to an attenuation and geometry corrected set of activities that can be converted to a mass.

Equation 1 shows the fundamental gamma NDA equation which relates the total detection efficiency$\epsilon_{i,E}$, the correction factors for attenuation by the container and matrix: CF_c, CF_m, and geometry G.

$$Q_{i,E} = \frac{R_{i,E}}{Y_{i,E}\epsilon_{i,E}} \qquad \text{Equation 1}$$

where, $Q_{i,E}$ Activity of nuclide *i* from gamma-ray of energy *E*.
$R_{i,E}$ Peak count rate from gamma-ray energy *E* from nuclide *i*.
$Y_{i,E}$ Branching ratio for gamma-ray energy *E* from nuclide *i*.
$\epsilon_{i,E}$ Total detection efficiency

The total detection efficiency is a function of the intrinsic efficiency, attenuation, and distance between the source material and the detector as shown in

$$\epsilon_{i,E} = \frac{\epsilon(E) C_{attn}}{G} \qquad \text{Equation 2}$$

where, $\epsilon(E)$ Intrinsic detection efficiency at energy *E* (absolute efficiency for a non-attenuating point source at distance r_0).

C_{attn} Effects from attenuation: container, CF_c; matrix, CF_m
G Effects from geometry (spatial distribution)

C_{attn} can be rewritten as a function of the gamma-ray transmission through the container and matrix.

$$C_{attn} = \frac{1}{CF_c}\frac{1}{CF_m}$$

$$= T_c \frac{T_m - 1}{\ln(T_m)}$$

$$C_{attn} = \frac{1}{e^{\mu_c \rho_c x_c}} \frac{1 - e^{-\mu_m \rho_m x_m}}{\mu_m \rho_m x_m} \qquad \text{Equation 3}$$

Finally, the geometry factor *G* is a function of the spatial distribution of the source material with respect to the detector.

$$G = \left(\frac{\bar{r}}{r_0}\right)^2 \qquad \text{Equation 4}$$

where, G Effects from geometry (spatial distribution)
$\bar{r}$ Average distance between source and detector
r_0 Calibration distance

Combining Equation 2 through Equation 4 into Equation 1, yields the final NDA equation:

$$Q_{i,E} = \left(\frac{R_{i,E}}{Y_{i,E}\epsilon(E)}\right)\left(\frac{\bar{r}}{r_0}\right)^2 (e^{\mu_c\rho_c x_c})\left(\frac{\mu_m\rho_m x_m}{(1-e^{-\mu_m\rho_m x_m})}\right) \qquad \text{Equation 5}$$

where, $Q_{i,E}$ Activity of nuclide *i* from gamma-ray of energy *E*.
$R_{i,E}$ Peak count rate from gamma-ray energy *E* from nuclide *i*.
$Y_{i,E}$ Branching ratio for gamma-ray energy *E* from nuclide *i*.
$\epsilon(E)$ Intrinsic detection efficiency at energy *E* (absolute efficiency for non-attenuation point source at distance r_0).
$\bar{r}$ Average distance to source from the detector.
r_0 Calibration distance
μ_c Mass-attenuation coefficient for the container material.
ρ_c Density of the container material.
x_c Thickness of the container.
μ_m Mass-attenuation coefficient for the matrix.
ρ_m Bulk density of the matrix.
x_m Thickness of the matrix.

The previously mentioned ISOTOPIC software uses these same equations, but the software determines the values of these parameters by having the user build an analytical model within the program that describes the container, matrix, and source-to-detector geometry. Then when the analysis is performed on the spectrum, the user is allowed to interactively change the

container thickness, matrix density, and uranium weight fraction as show by the slide bars in the top right corner of Figures 12 and 13 above. These corrections in theory seem very easy when the parameters that are adjustable are well known, but in real-world situations, this is rarely the case. Often times, NDA personnel making critical analysis of collected spectrum must make educated guesses and account for their probable errors by increasing the reported uncertainty in their answers. Also, adjusting Matrix Density compared to U Wt. Fraction can have hugely different effects on the final results in done incorrectly. The concept of Small-angle Compton scattering was developed to help overcome this difficulty because it is a tool that is able to accurately estimate the density-thickness of a radioactive isotope behind or within a highly attenuating material which will ultimately reduce the number of unknowns when trying to analyze gamma ray spectrum.

h. Theory of Small-Angle Compton Scattering

In a gamma-ray spectrum, one can frequently observe a discontinuity in the Compton background at a gamma-ray peak. For the U-235 isotope shown again below in Figure 14, this discontinuity is shown at the 185.72keV gamma peak. Although the other secondary gamma ray energies produced by U-235 are shown in Figure 14 and undergo the same effects of Small-angle Compton scattering, the discontinuity is not as pronounced and therefore is not useable in the same way that the discontinuity at the principal peak of 185.72keV is. So, although Small-angle Compton scattering can be applied to other radionuclides besides U-235, it should be noted that this analysis tool should be concentrated on the principal peak of an isotope and in situations where a reasonable peak of the desired isotope is detected.

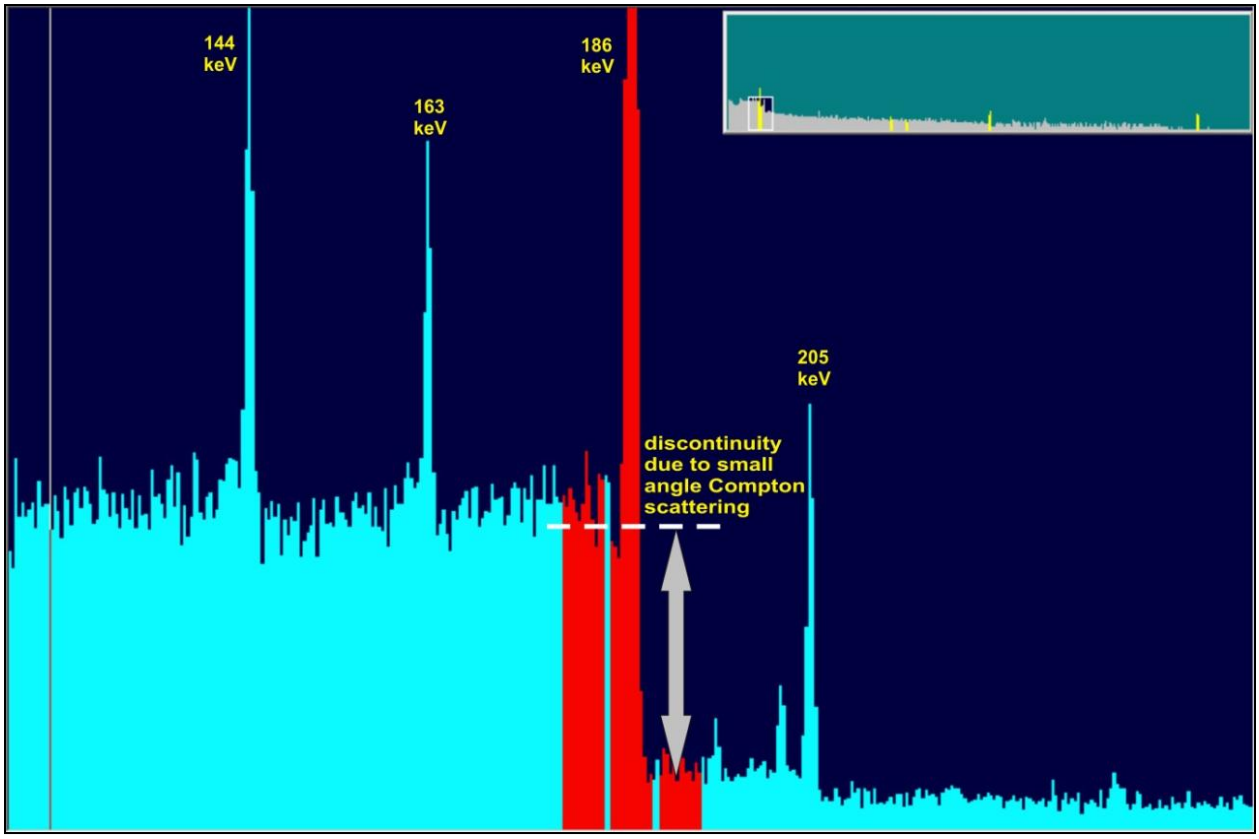

Figure 14: High-resolution spectrum of HEU showing a discontinuity in the Compton background due to small-angle scattering of 185.72keV gamma rays as a result of interactions with surrounding materials.

The Compton continuum is caused by Compton scattering in the detector from higher energy gamma rays, but the discontinuity at a specific gamma-ray peak, on the other hand, is caused by Small-angle Compton scattering in material directly between the gamma-ray source and the detector. These small-angle scatters reduce the gamma-ray energy by an incredibly small amount from the initial peak energy.

This familiar discontinuity in the peak was originally thought to be a degradation of the spectrum that needed to be removed to accurately determine the net peak count rate, but research and testing originated by Dr. Richard Oberer and his colleagues proved that this discontinuity actually contains valuable information about the amount of attenuation the gamma rays undergo as well as information about the type and thickness of material between

the detector and the gamma ray source. The small-angle scattering discontinuity divided by the gamma-ray peak can be used with the familiar variables of the attenuation calculation for a container or for a matrix to estimate the depth of a gamma-ray source in a material. The fraction of gamma-ray interactions that are small-angle Compton scatters is a function of the gamma-ray energy and the atomic number, Z, of the matrix or container material similar to the mass-attenuation coefficient. In fact, it is actually the fraction of the mass-attenuation coefficient attributed to small-angle scattering per energy of the scattered gamma ray. Furthermore, the magnitude of this discontinuity can be described and predicted by the mathematical formulas presented below where the only variables are atomic-number Z, gamma-ray energy E_γ, mass-attenuation coefficient μ, density ρ, and depth x of a gamma-ray source. When the small-angle discontinuity is measured, density-thickness ρx can be calculated from these equations either directly from Equation 8 below or by interpolation using Equation 9. It can then be used together with the analysis techniques of differential attenuation which were explained above.

The small-angle scattering differential cross-section is determined by Equation 6 from the atomic-number Z and gamma-ray energy, E_γ.

$$\left.\frac{d\sigma}{d\mathrm{E}}\right|_{\theta=0} = 254.9(\mathrm{keV}\cdot\mathrm{barn})\left(\frac{\mathrm{Z}}{\mathrm{E_\gamma}^2}\right) \qquad \text{Equation 6}$$

Dividing this differential cross-section by the total cross-section σ gives the fraction k of interactions which are small-angle Compton scatters from Equation 7 and 8.

$$k = \frac{\left.\frac{d\sigma}{d\mathrm{E}}\right|_{\theta=0}}{\sigma} \qquad \text{Equation 7}$$

$$k = 254.9(\text{keV} \cdot \text{barn})\left(\frac{\text{Z}}{\sigma \times \text{E}_\gamma{}^2}\right) \qquad \text{Equation 8}$$

The derivation of Equations 6 and 8 is shown in detail in Appendix A.

Multiplying this fraction *k* by the mass-attenuation coefficient μ_c, density ρ_c, and depth x_c of a discrete gamma-ray source gives the magnitude of small-angle scattering discontinuity divided by the peak height which is shown in Equation 9.

$$\frac{N_{sa}(x)}{N_\gamma(x)} = k\mu_c\rho_c x_c \qquad \text{Equation 9}$$

A continuous, uniform distribution in a matrix to a depth x_m is given from the same variables (μ_m, ρ_m, x_m) in Equation 10 below.

$$\frac{N_{sa}(x)}{N_\gamma(x)} = \frac{k[1 - e^{-\mu_m\rho_m x_m}(1 + \mu_m\rho_m x_m)]}{(1 - e^{-\mu_m\rho_m x_m})} \qquad \text{Equation 10}$$

The ratio comparing the number of gamma rays that undergo Small-angle Compton scattering while traversing a distance of *x* through a material $N_{sa}(x)$ compared to the number of gamma rays that traverse a distance of *x* through a material without interacting $N_\gamma(x)$ can be used to determine the amount of intervening matter between a gamma-ray source and detector. It can also be used in addition to differential attenuation, or independently when differential attenuation cannot be used in the instance of a single gamma ray source such as Cs-137. This depth is useful in estimating the attenuation of the gamma rays or can help determine the structure of a nuclear device in a forensic situation.

i. Formulas for Attenuation and Small-Angle Compton Scattering

This section will focus on some of the more familiar equations for gamma ray attenuation and the relationship to the equations for the peak discontinuity formed by Small-angle Compton scattering. As previously mentioned, as a gamma ray travels through matter, it interacts and loses energy via the photoelectric effect, Compton scattering, and pair production. The number of gamma rays interacting while traversing a distance *x* through the material with a density ρ and mass-attenuation coefficient μ is proportional to the number of gamma rays N_γ:

$$\frac{dN_\gamma}{dx} = -\mu\rho N_\gamma \qquad \text{Equation 11}$$

The solution to this differential equation is:

$$N_\gamma(x) = N_0 e^{-\mu\rho x} \qquad \text{Equation 12}$$

N_γ represents the gamma-rays that travel through the intervening material without interaction while N_o represents the number of gamma rays when no intervening material is present.

Of these gamma rays interacting with the material, a fraction *k* of these interactions are small-angle Compton scatters. As the scattering angle approaches zero, the energy loss of the gamma ray also approaches zero. The number of small-angle gamma rays $N_{sa(x)}$ is therefore increased by *k* times the number of gamma-rays interacting, $\mu\rho N_\gamma$. However, because these small-angle gamma rays have virtually the same energy as the original gamma rays, they interact at the same rate $\mu\rho$ proportional to the number N_{sa} there are. The differential equation for number of small-angle gamma rays is:

$$\frac{dN_{sa}}{dx} = k\mu\rho N_\gamma - \mu\rho N_{sa} \qquad \text{Equation 13}$$

The solution to this differential equation is:

$$N_{sa(x)} = kN_0\mu\rho x e^{-\mu\rho x} \qquad \text{Equation 14}$$

Finally, the ratio of the number of gamma-rays undergoing small-angle Compton scatters compared to the uninteracted gamma rays is:

$$\frac{N_{sa}(x)}{N_\gamma(x)} = k\mu\rho x \qquad \text{Equation 15}$$

It is important to remember that the relation of the gamma ray peak to the discontinuity depends on the density, thickness, and composition of the material directly intervening between the gamma ray source and the detector. Equation 15 can now be used to predict the magnitude of the discontinuity that will be observed at a peak in a spectrum acquired from a radioactive source shielded by a layer of material of known density, thickness, and composition.

Of course, there is another possible scenario for attenuation of a radioactive source that is homogeneously mixed with a matrix material. In this scenario, rather than a having a source N_o at a discrete depth in the matrix material, it would be a distributed source mixed within the matrix at a concentration *c*. Therefore the number of gamma rays increases with the depth in the matrix, but also decreases from attenuation giving the following differential equation:

$$\frac{dN_\gamma}{dx} = \mathrm{c} - \mu\rho N_\gamma \qquad \text{Equation 16}$$

The solution of this differential equation is:

$$N_\gamma(x) = \frac{\mathrm{c}}{\mu\rho}(1 - e^{-\mu\rho x}) \qquad \text{Equation 17}$$

The small-angle scattered gamma rays are therefore fed by the distributed source, but also decreased by attenuation giving the following equations:

$$\frac{dN_{sa}}{dx} = k\mu\rho N_{\gamma} - \mu\rho N_{sa} \qquad \text{Equation 18}$$

where N_{γ} comes from Equation 17. The solution of this differential equation becomes

$$N_{sa(x)} = \frac{ck}{\mu\rho}[1 - e^{-\mu\rho x}(1 + \mu\rho \mathrm{x})] \qquad \text{Equation 19}$$

And again, the ratio of the number of gamma-rays undergoing small-angle Compton scatters compared to the un-interacted gamma-rays is determined by:

$$\frac{N_{sa}(x)}{N_{\gamma}(x)} = \frac{k[1-e^{-\mu\rho x}(1+\mu\rho \mathrm{x})]}{(1-e^{-\mu\rho x})} \qquad \text{Equation 20}$$

Equation 20 can be used to predict the magnitude of the discontinuity from a radioactive source distributed in a matrix material of known density, thickness and composition. Other distributions of the radioactive source can be solved in this manner. Again, for an exponentially distributed source, c is multiplied by an exponential.

Chapter 4: Validation Study for Small-Angle Compton Scattering

Now that the theory behind Small-angle Compton scattering has been fully discussed, the next portion of this thesis will explain the validation of the theory through a practical experiment. The following sections share the details of a validation study that was conducted to prove the concepts of the Small-angle Compton scattering method before it was applied to any real-world applications.

j. Introduction

Gamma ray spectroscopy is a valuable tool that provides a lot of useful information about various radionuclides in an object or a container. Gamma ray spectroscopy is such a valuable tool because it is passive and doesn't alter the material being evaluated. It is also typically cheaper, safer, and more versatile than traditional destructive methods.

In this particular validation study that was completed, the focus was on the fissile nuclide of U-235. U-235 the most critical component in nuclear weapons and therefore, the use of Small-angle Compton scattering has a lot of applications within the DOE Weapons Program as well as non-proliferation efforts around the world. Any country that is illegally trying to possess or enrich dangerous quantities of U-235 will most likely try to hide it our shield it from detection by inspectors or regulatory watchdogs. Therefore, it was the isotope of interest when trying to validate the theory of Small-angle Compton scattering as a method to accurately quantify U-235 under shielded conditions.

When using NDA measurement techniques, the net count rate determined from characteristic peaks of a gamma ray spectrum can be related to the quantity of the radionuclide. Of course, this relationship can be influenced at varying degrees by the intrinsic efficiency of the detector you are using, the branching ratios (or emissions per disintegration) of the gamma ray, the geometry between the detector and the source, and the effects of attenuation. In this case, attenuation refers to gamma rays that interact with the matter between the source and the detector and therefore are absent from the spectrum peak.

Again, since Small-angle Compton Scattering is caused by the composition and amount of intervening material between the source and the detector, the discontinuity that is created in the gamma peak of interest is used to provide information about the intervening material. The magnitude of this discontinuity is related to the prevalence of this Small-angle Compton scattering which is in turn related to the composition and amount of matter between the source and detector. Being able to determine this information and better account for the effects of attenuation in your NDA analysis will eliminate unknowns, reduce uncertainty, and provide overall better estimates of U-235 or other radio nuclides of interest in non-ideal and heavily shielded measurement situations.

Figure 15 and Figure 16 below show some additional examples of the spectral discontinuity created by small-angle Compton scattering of the principle 185.72keV peak from U-235 material. Figure 15 shows the simple step-height fall-off of the spectrum when concrete material is used between a source and a detector. The magnitude of the discontinuity can be predicted from the mathematical expressions discussed in the sections above and it is heavily dependent on the amount and composition of the material that is between the source and the detector.

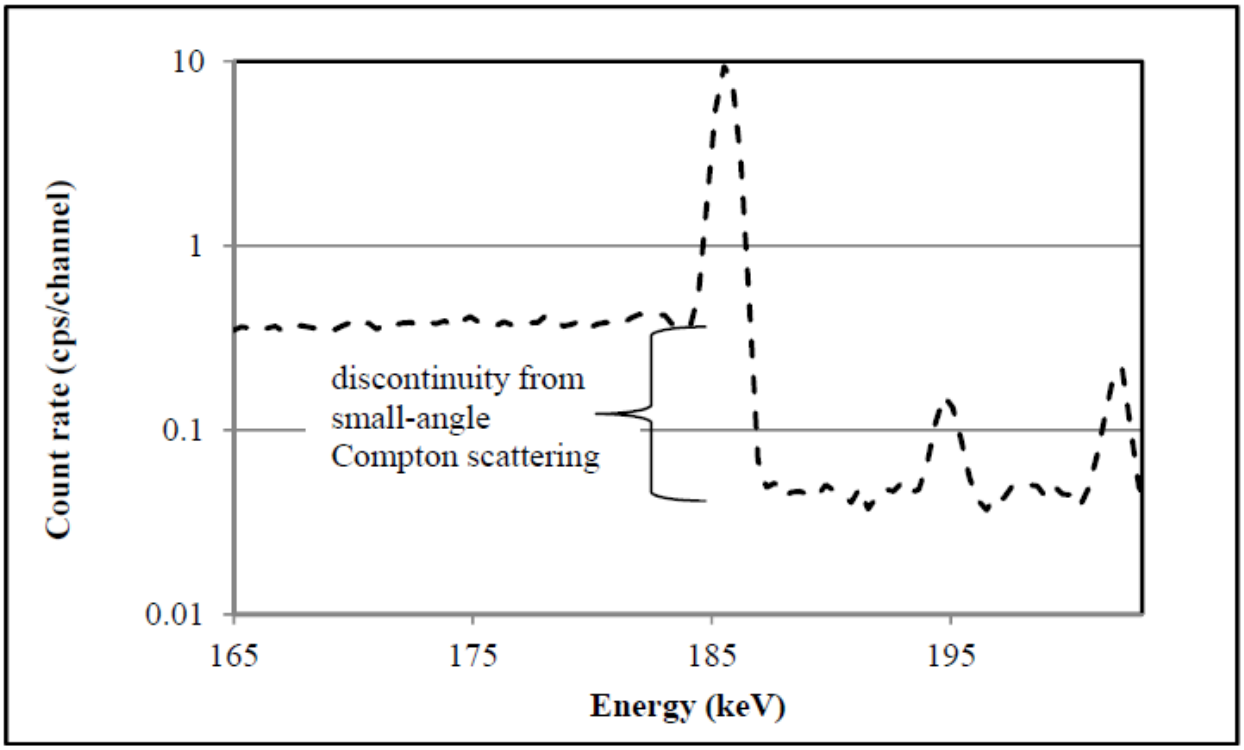

Figure 15: The small-angle Compton scattering discontinuity at the 185.72keV gamma-ray from U-235 attenuated by concrete.

Figure 16 below is another example which clearly shows how the magnitude of the discontinuity changes when the thickness of the intervening concrete is changed between the U-235 source and the detector. Because the count rates are on a linear scale in Figure 16 and are normalized, it is easy to see how the spectrum discontinuity grows at the 185.72keV energy as the thickness of intervening concrete between the source and detector is increased from 0 inches to 1.5 inches and on to 3.75 inches.

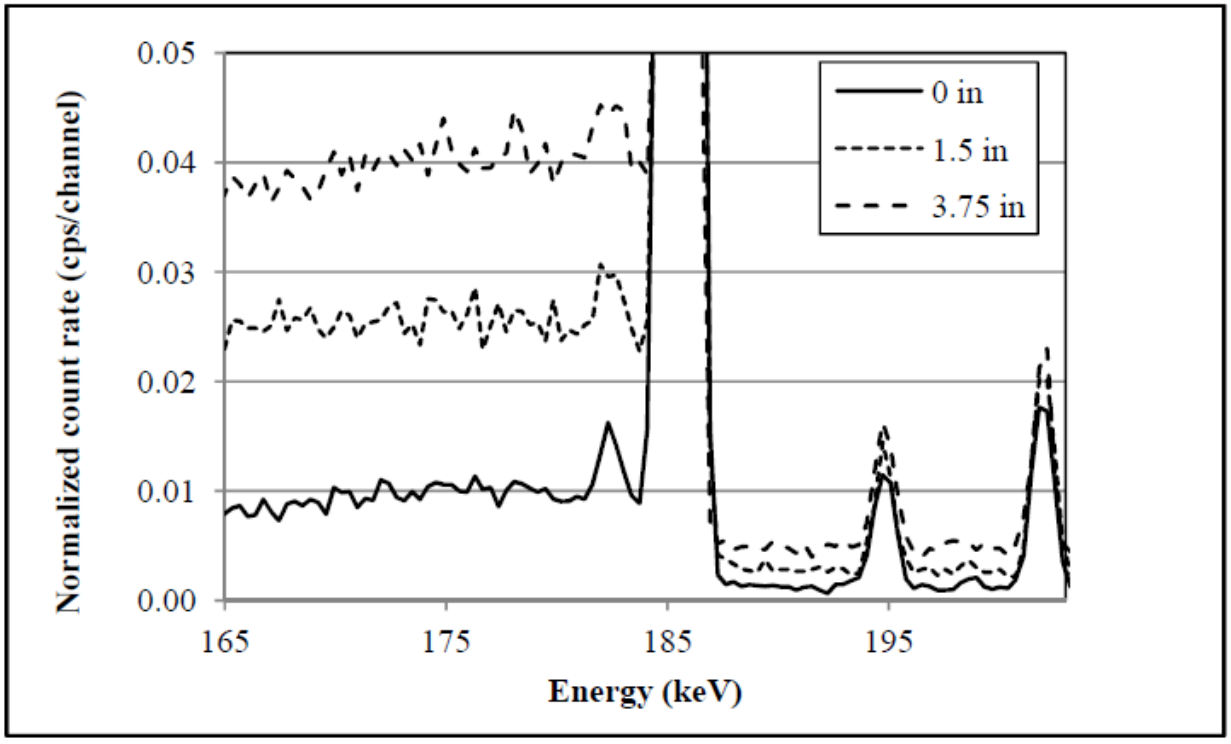

Figure 16: The small-angle Compton scattering discontinuity at the 185.72keV gamma ray from U-235 for three different thicknesses of concrete placed between an HEU source and the detector.

It should be reiterated that only a fraction of the interactions between gamma rays and intervening matter are Small-angle Compton scatters. For this experiment and validation study, the generation and attenuation of gamma rays by Small-angle Compton scattering is examined for various known U-235 sources that are either placed at discrete depths behind a concrete material or are uniformly distributed from the face of the detector to some depth. The validation of the Small-angle Compton scattering method is accomplished by comparing the predicted discontinuities from the mathematical equations to the experimental results from the known U-235 sources attenuated by concrete.

k. Experimental Setup

The setup for this experiment was done by using known planar sources containing varying, but known quantities of U-235 and measuring them behind different thicknesses of concrete. To be able to easily vary the position of the U-235 sources and the thickness of the intervening concrete between the detector and the sources, several thin concrete tiles were used. The setup is shown below in Figure 17 where you have the HPGe detector on the left and 15 individual pieces of ¼"concrete tile on the right. Also shown in Figure 17 are several heavy-duty lead collimators which are used to shield out any background gamma rays that might interfere with the experiment. Although the experiment was done in a relatively low background area, this might not always be the case when trying to apply this method in real world situations. For that reason, the experimental setup was done in the most conservative manner to make sure this method could be recreated in other situations where background interference is present.

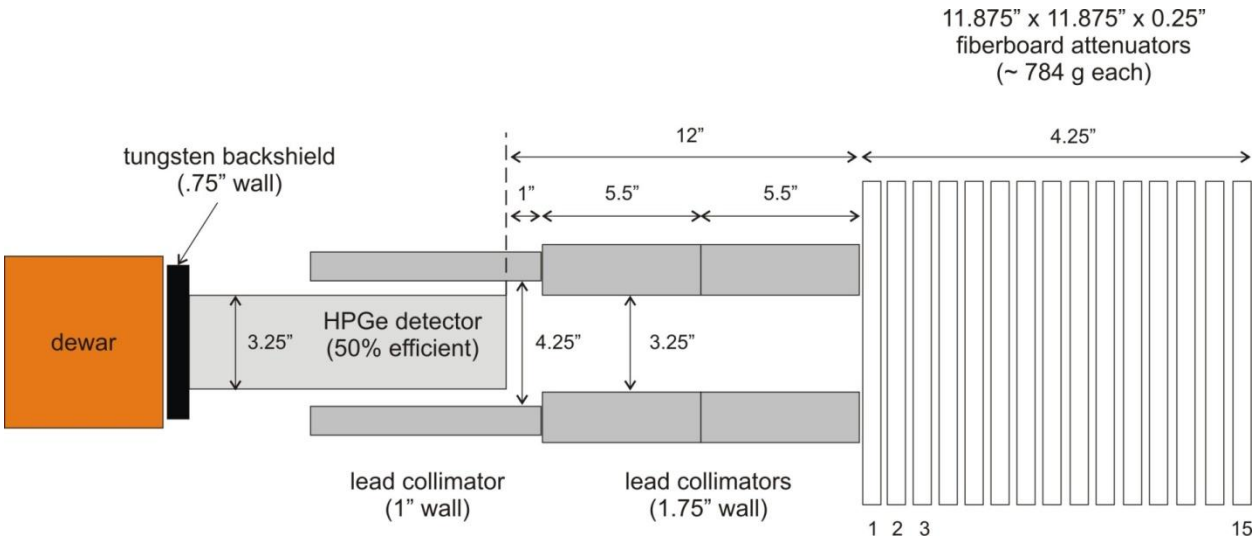

Figure 17: Theoretical setup showing the fifteen concrete Hardy board tiles, collimator, and detector. An HEU planar source was placed between the Hardy-board tiles at various depths.

The concrete tiles were cut into 11-7/8" squares and each tile weighed 784g +/- 7g. Therefore, the calculated density was 1.36g/cm^3. Six planar U-235 standards were used in conjunction with this setup because the planar standards could easily fit in any position between the concrete tiles. The standards were created from 96.312% enriched uranyl nitrate Hexahydrate (UNH) and the mass fraction of uranium is 0.4971gU/gUNH. The specifications of the uranium standards used in this validation study are summarized below in Table 3. The values for the declared amounts of U-235 are computed by multiplying the mass of UNH by the product of 0.4971gU/gUNH and 0.96312gU-235/gU. The planar sources were constructed with UNH deposited on 3 plies of absorbent pads sandwiched between two 1/16" sheets of polyethylene terephthalate (PET) glycol. The 3 plies of hazmat absorbent are 0.047" thick.

Table 3: Specifications of planar U-235 standard used for calibration exercise.

ID	UNH mass (g)	U-235 mass (g)	U-235 areal density (g/cm^2)
P1	44.80	24.45 ± 0.52	0.0333
F1	4.60	2.2 ± 0.19	0.0022
F2	14.30	6.85 ± 0.24	0.0065
F3	14.30	6.85 ± 0.24	0.0065
F4	34.72	16.62 ± 0.42	0.0160
F5	46.30	22.17 ± 0.53	0.0212

I. Instrument Calibration and Setup

As shown above, a heavily collimated high-resolution HPGe detector was used for this study. The collimators were used to not only shield out background, but also to limit the various source to detector pathways that are possible. A tungsten back shield was also added to minimize interference entering the detector crystal through the back of the detector.

Furthermore, the detector and collimators were aligned so that the detector was exactly centered within each of the collimators used. The instrument setup used for the calibration is shown below in Figure 18.

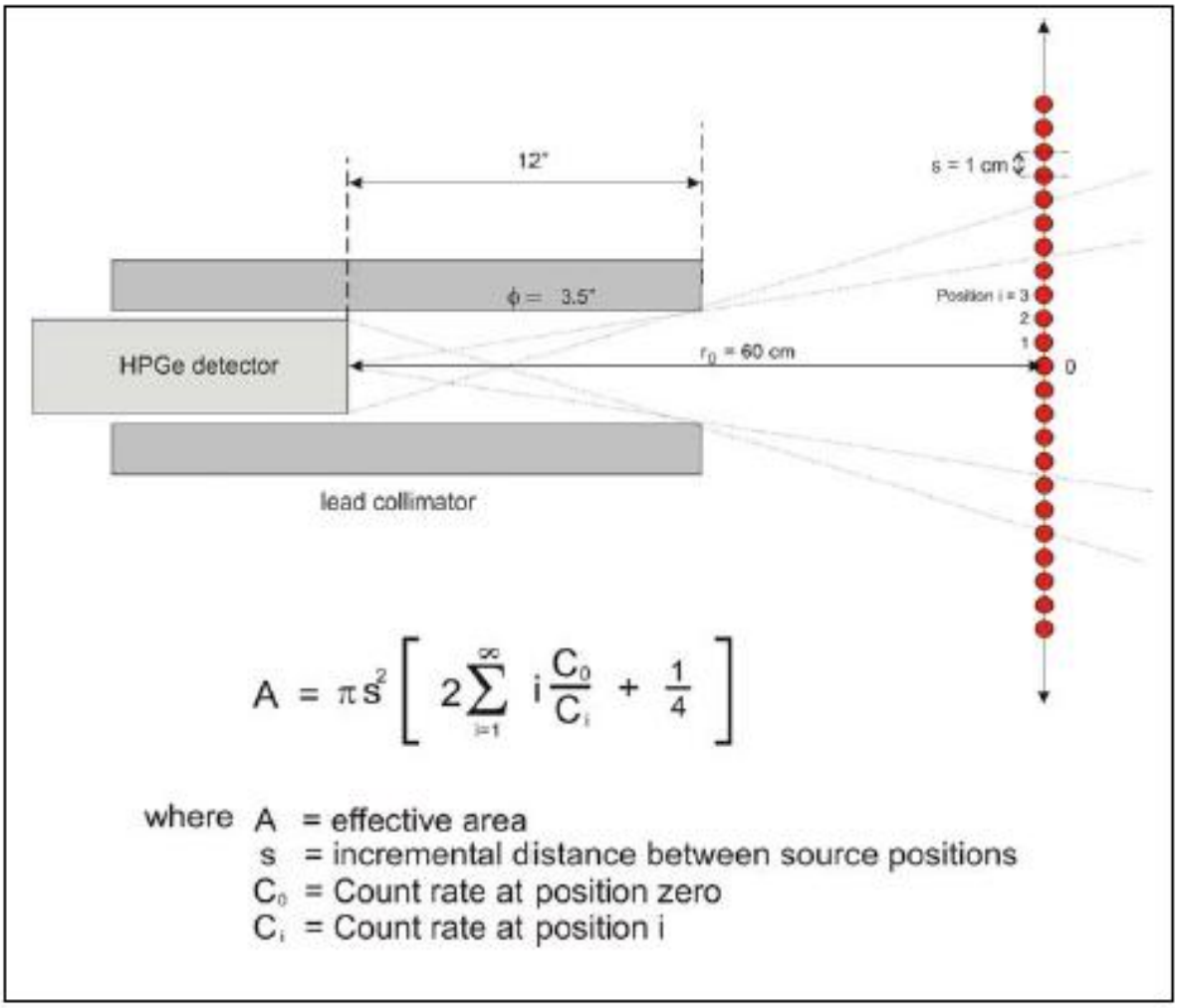

Figure 18: Detector setup for HPGe calibration showing effective area calibration.

The calibration of the detector for this validation study was done in three stages. First, an energy and intrinsic counting efficiency calibration was completed for the detector using a mixed-gamma multi-energy calibration source. Next, the radial response of the detector was calculated using a U-235 source in a traditional generalized-geometry holdup (GGH) calibration. By GGH methodology, the effective area of the detector is determined experimentally by

stepping a point source along a line orthogonal the detector axis and integrating the response for an area source calibration. The radial response was done using an 11g U-235 calibration source measured along a line 60 cm from the detector axis, and stepped 1 cm at a time covering both directions as shown in Figure 18. Figure 19 below shows the radial response curve generated by this calibration. As can be seen, the efficiency of the detector remains pretty high and consistent as the source is moved between 0 and 7 cm off center, but then it begins to fall off exponentially. This is a good example of why geometry is such an important part of modeling and analysis when dealing with NDA equipment and measuring methods.

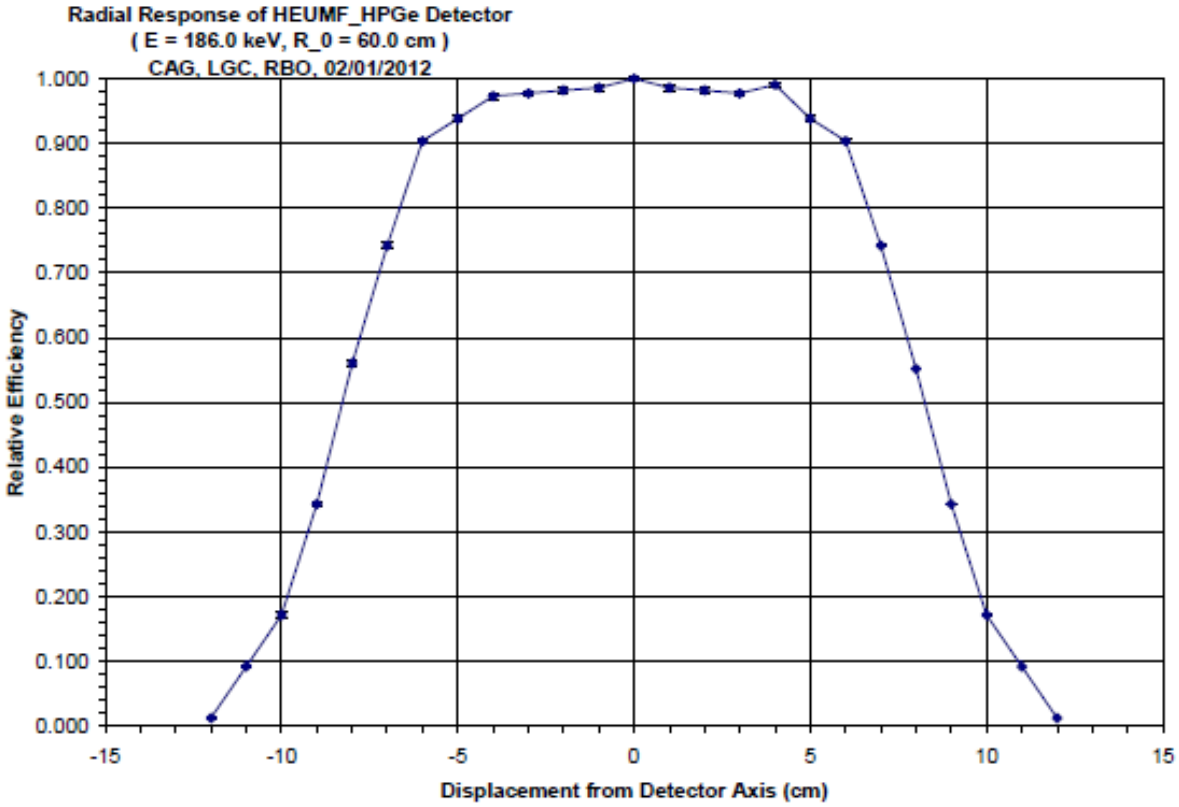

Figure 19: Radial response curve from GGH calibration which stepped an 11g U-235 source along an axis in both directions 60cm away from the HPGe detector.

The final stage in the calibration required a measurement of a planar source placed directly at the face of the 12” collimator. The spectrum obtained was used to determine the small-angle step height caused by the collimator itself. The calibration results are given directly below.

Calibration results of HPGe detector:

```
Calibration
49-TP50599A, NIST 83310-681, Annual calibration

Energy Calibration

Zero offset: 0.252 keV
Gain: 0.354 keV/channel
Quadratic: 3.019E-08 keV/channel^2


Efficiency Calibration

Type: Polynomial
Uncertainty: 0.388 %
Coefficients:     -0.277340 -7.625097 0.527058
                  -0.072410 0.004320 -0.000102
Stand off: 30 cm

Generalized Geometry Calibration

Effective Area: 224.27 cm2
radius0: 1.69 in
geometric CF: 0.018
collimator S/P: 0.041 (at face of 12” collimator)
```

Final experimental preparations were done to calibrate the effect of Small-angle Compton scattering using Standard P1 from Table 3 above. This standard was placed at various positions within the concrete tiles and spectrums are collected at each position using the HPGe detector. For example, at position 0, the standard is placed before the concrete tiles and therefore the detector should not be affected by any gamma-ray attenuation from the concrete tiles. At position 1, the standard is placed after the first ¼” thick concrete tile. Measurements would continue in step-wise fashion as a spectrum is collected on the source for each position amongst the concrete tiles going all the way back to position 15.

The net count rate in the 185.72keV gamma-ray peak at the various depths from position 0 to 15 is shown below in Figure20. Figure 20 also shows an exponential function that was fit to the experimental data based on Equation 12 above $N_\gamma(x) = N_0 e^{-\mu\rho x}$. The dotted line comes from this equation while the diamonds show actual experimental data from measuring the U-235 source at each of the 16 possible positions. At position 0, the following parameters were used: N_o = 144.57cps, μ = 0.136cm2/g.

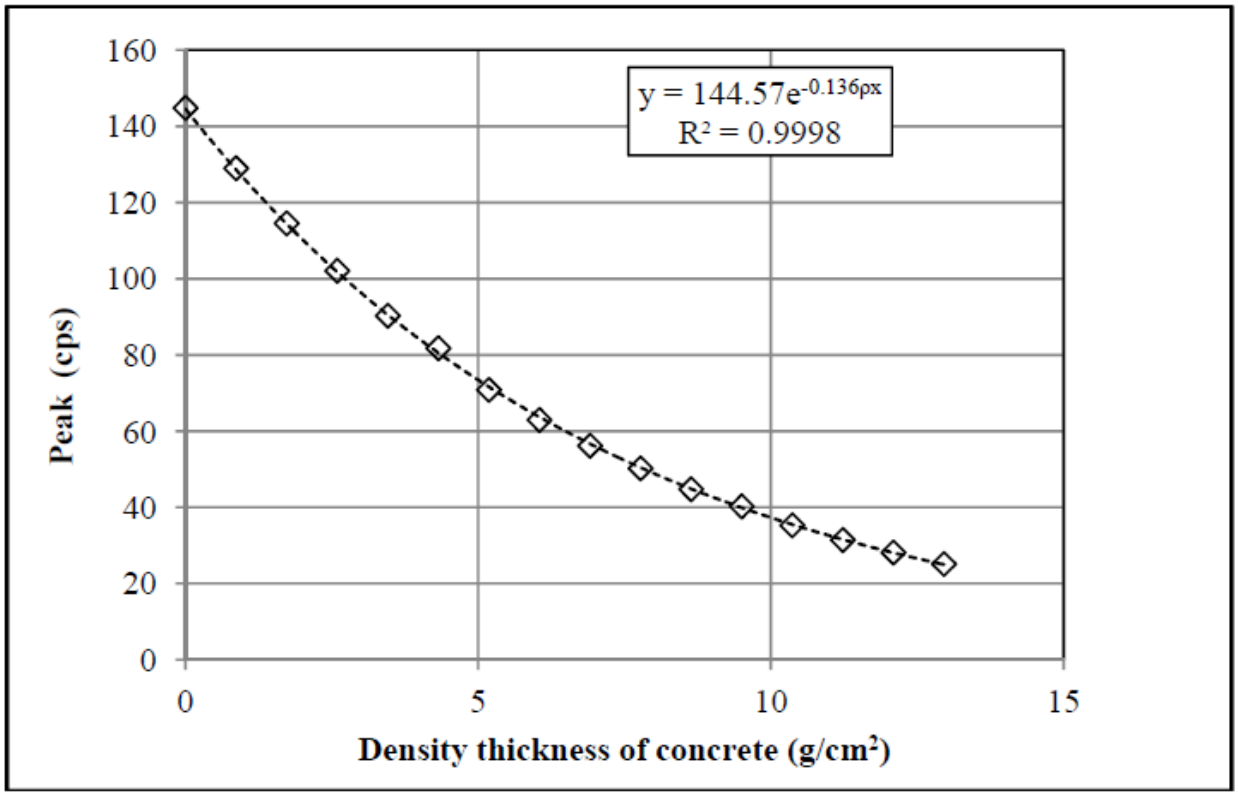

Figure 20: Attenuated count rate from U-235 standard placed in varying position (0 to 15) within concrete tiles.

It has also been proven that from the step height of the discontinuity created by Small-angle Compton scattering, we can calculate a linear relationship with the density thickness of the

material intervening between the source and the detector. So by computing the step/height, you can actually theoretically compute the density thickness of the interacting material. Figure 21 below shows this relationship where the dotted line was based on Equation 12 above ($N_\gamma(x) = N_0 e^{-\mu\rho x}$) and from Equation 15 above ($\frac{N_{sa}(x)}{N_\gamma(x)} = k\mu\rho x$) while the diamonds again show actual experimental data from measuring the U-235 source at each of the 16 possible positions.

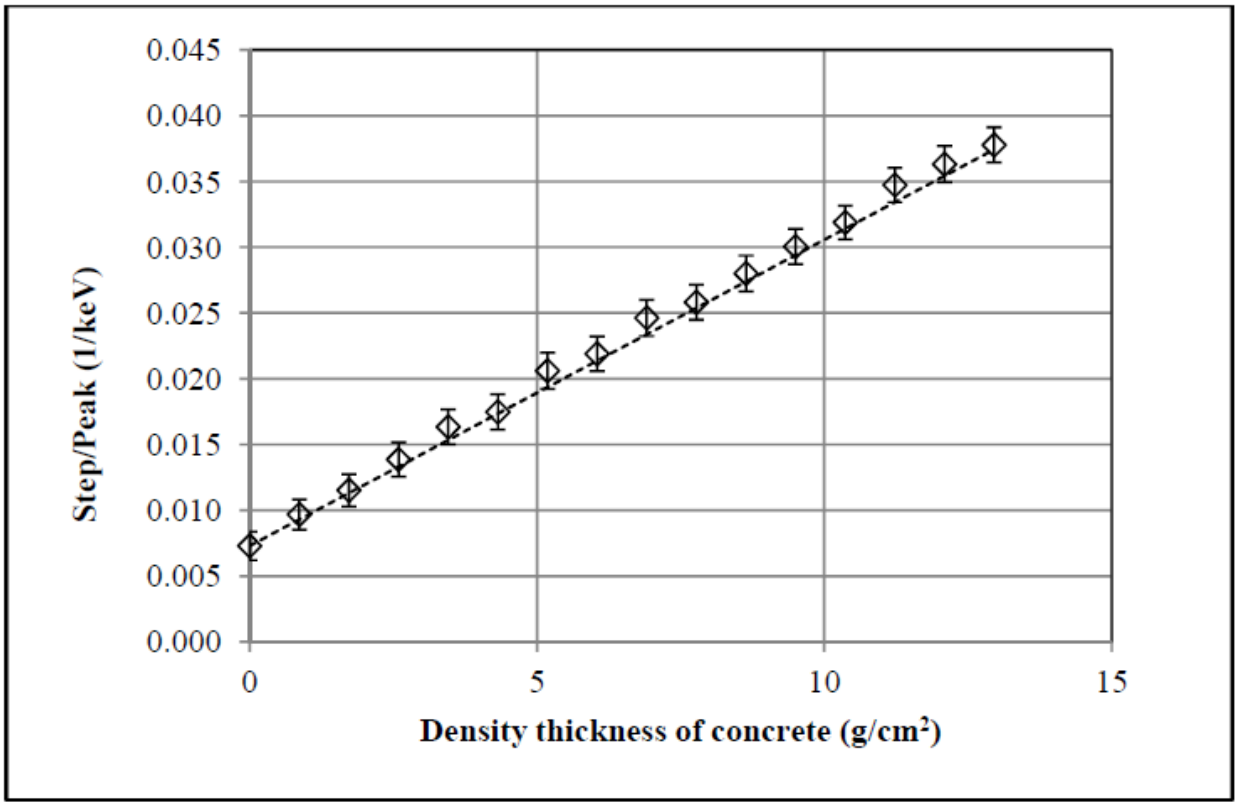

Figure 21: Small angle discontinuity produced from a U-235 standard placed in varying position (0 to 15) within concrete tiles.

These calibrations and confirmations show good agreement between the theoretical and experimental data which gives validation to the equations and the theories behind this Small-

Angle Compton scattering analysis method. One note on Figure 21 above is that the expectation at position 0 where there is no intervening material is that no small-angle scattering should occur. As can be seen, a small step/peak ratio of about 0.007 is detected at position 0. This occurs because small-angle scattering comes from several other sources in this setup. First, the U-235 source itself causes some self-attenuation. Also, the detector housing, the possibility of a dead layer on the Germanium crystal, and the plastic encasing the source produce some attenuation and small-angle scattering. These sources of attenuation are still considered to be intervening material between the source and the detector, so they should be expected to cause this minimal amount of small-angle scattering. With these calibrations and initial setup applications showing promising results, more elaborate experiments and validations can be discussed.

m. Experimental Analysis

The concept of Small-angle Compton scattering was first developed and envisioned as a way to measure the amount of enriched uranium that has been spilled as a solution and deposited at various depths and concentrations into a concrete floor. Therefore, the gamma spectrometry analysis requires input regarding the amount of concrete present with which the uranium solution deposit will interact. The information is extremely difficult to determine because there is no exact way to tell how a uranium solution will deposit itself into a porous concrete floor. Will it remain at the surface? Will it absorb in to pores or cracks to some unknown depth? The only way to overcome this unknown and determine an accurate density-thickness of the uranium deposit in concrete was to utilize the concept of Small-angle Compton scattering. As previously mentioned, interactions of gamma rays with intervening material between the source and the detector cause a discontinuity in the Compton continuum that provide useful information in determining the density-thickness of a uranium deposit in concrete.

The discontinuity in the Compton continuum caused by Small-angle scattering for enriched uranium is at the 185.72keV gamma-ray peak. Determining the magnitude of the discontinuity

is a critical step in this analysis process and the step height is determined by finding the count rate in the region of interest (ROI) before the 185.72keV peak and subtracting the count rate from the ROI after the peak then dividing by the energy width of the ROI containing the 185.72keV peak. This is detailed out in Figure 22 below.

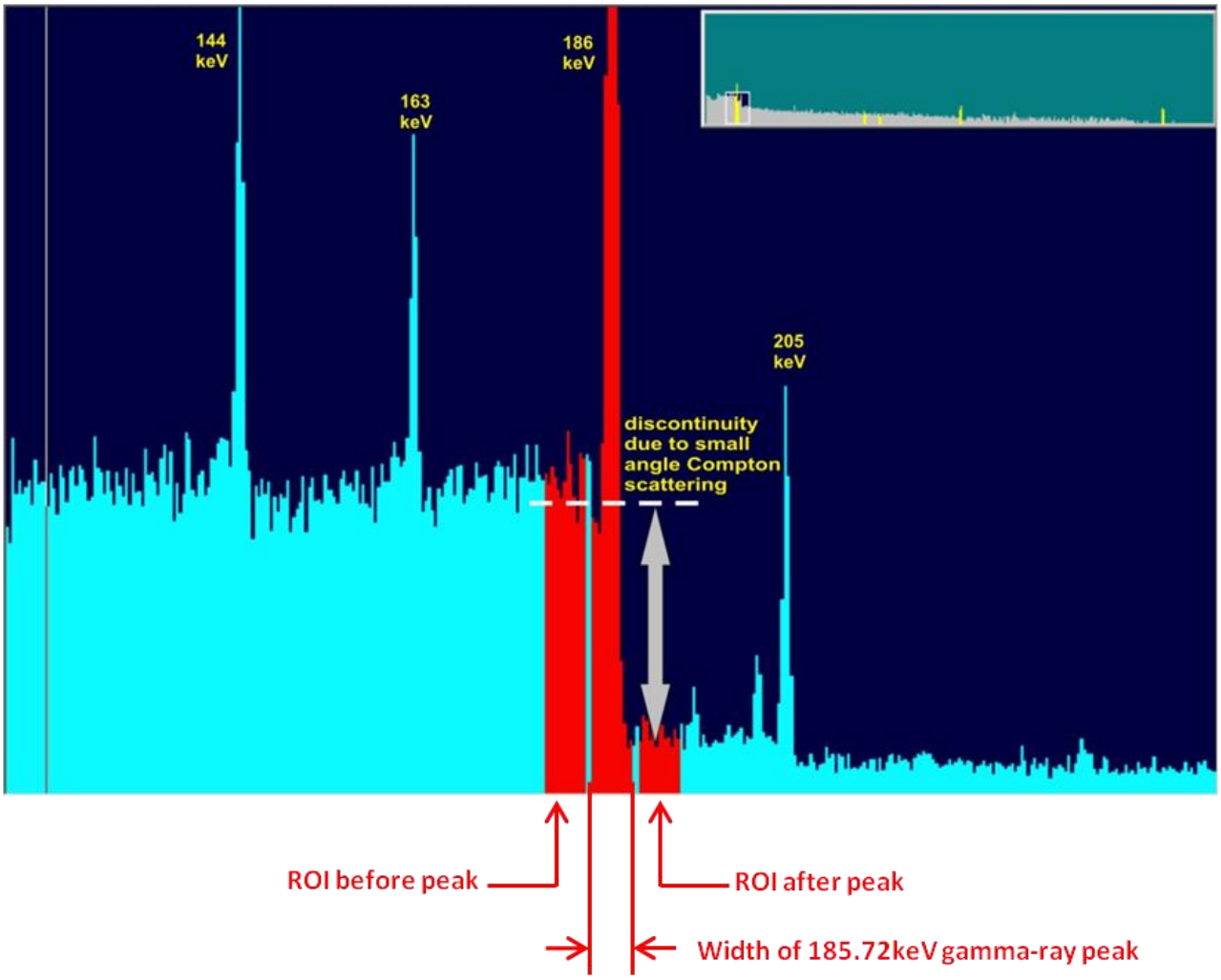

Figure 22: U-235 spectrum at the 185.72keV gamma-ray peak showing the typical discontinuity.

The magnitude of the step increase relative to the net full energy gamma peak area (S/P) is related to the density, thickness, and mass attenuation coefficient of the intervening material by the following equations:

For a radioactive source that is uniformly distributed to some depth,

$$\frac{S}{P} = \frac{(k \cdot dE)[1 - e^{-\mu\rho x}(1 + \mu\rho x)]}{(1 - e^{-\mu\rho x})}$$

where,

S/P is the ratio of the small-angle Compton scattering discontinuity divided by the net gamma-ray peak area,

k $(keV)^{-1}$ is the fraction of interactions which are small-angle Compton scatters,

μ (cm^2/g) is the mass attenuation coefficient of the intervening material,

ρ (g/cm^3) is the density of the intervening material,

x (cm) is the thickness of the material, and

dE (keV) is the energy width of the region of interest used in calculating the S/P ratio.

To prove this theory in practice, a more realistic and practical experiment beyond the calibration was conducted to simulate the spilling of uranium solution on a porous concrete floor using a variety of enriched uranium sources sandwiched between layers of concrete in unique configurations. Where the calibration was done using only one standard, this experiment was done using several different standards within the concrete tiles at the same time. Each configuration of the various standards was measured and the data analyzed to evaluate the effectiveness of the small-angle/differential attenuation strategy in determining the amount of uranium present for each configuration. The same general experimental set-up that was used for the calibration was used for this experimental validation, but now six

different known uranium planar sources were utilized to create the a wide variety of possible uranium configurations within concrete that more aptly mimic what could be seen in the real world. See Figures 23 below for a picture of how the experiment was set up and Table 4 below to understand to different U-235 standards that were used in the experiment.

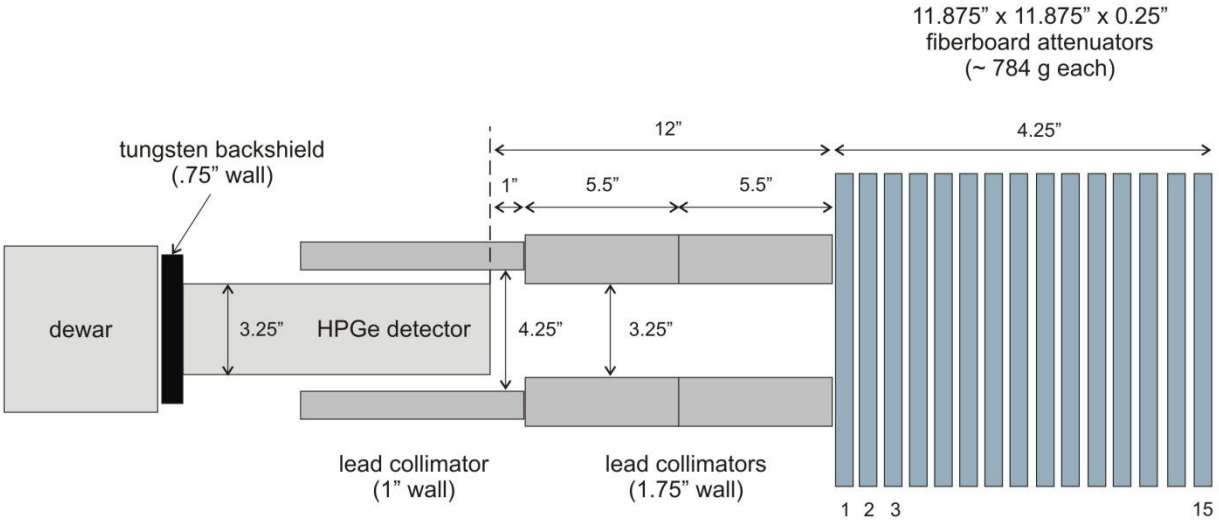

Figure 23: Experimental setup used for measuring enriched uranium deposit concentrations in a concrete matrix.

Table 4: Uranium planar standards used for the U/Concrete measurement study fabricated from uranyl nitrate hexahydrate, UNH, 96% enriched in U-235.

ID	UNH mass (g)	U-235 mass (g)	U-235 areal density (g/cm^2)
P1	44.80	24.45 ± 0.52	0.0333
F1	4.60	2.2 ± 0.19	0.0022
F2	14.30	6.85 ± 0.24	0.0065
F3	14.30	6.85 ± 0.24	0.0065
F4	34.72	16.62 ± 0.42	0.0160
F5	46.30	22.17 ± 0.53	0.0212

A total of forty-nine different deposits were simulated for this study. A high-resolution HPGe spectrum was collected for each simulation. Each arrangement was measured and the data analyzed to evaluate the effectiveness of the small-angle/differential attenuation strategy in determining the amount of uranium present for each configuration. The simulated spills included setups where the sources were placed in decreasing concentration order, increasing concentration order, and in random order. The source depths were varied simulating surface deposits, shallow-depth deposits, deep-deposits, and multiple deposits. The total concentration investigated ranged from a dilute 0.002 gU-235/cm2 up to a maximum concentration of 0.085 gU-235/cm2. The locations of the sources in the 49 measurements conducted in this study were treated as unknown and no foreknowledge of the deposit locations were used in the analysis of this data. Instead, the small angle discontinuity feature in the acquired spectra was used to calculate the effective depth of the deposits.

As discussed in Figure 22 above, the step-to-peak ratio was calculated for each of the 49 acquired spectra by defining three regions of interest (ROIs) – one centered at the full-energy 185.72keV peak, a second region of equal width on the continuum near the peak but at lower energy, and a third region on the continuum near the peak but at higher energy. The step height is calculated as the difference in counts in the regions below and above the 185.72keV peak and the net 185.72keV peak area was calculated using analysis capabilities provided in the off-the-shelf ISOTOPIC software used to collect these spectrum.

The value of the small-angle fraction, *k*, for a uranium/concrete mixture was calculated assuming a 2.5% weight fraction of uranium in the concrete. This assumption was simply selected as a first iteration. The resulting calculations for the small-angle fraction and the mass attenuation coefficient for the mixture are shown in Table 5 below.

Table 5: Calculation of small-angle fraction, k, and mass attenuation coefficient(μ), for a 2.5 % mixture of uranium in concrete.

2.5% U added to concrete

1 barn =	1.00E-24	cm^2
density:	1.39	g/cm^3
Avogadro:	6.02E+23	a/mol

Element	Z	g/mol	Mass fraction (g/g)	Number density n (atom/barn·cm)	Total cross section σ (barn/atom)	Total mass attenuation coefficient $\mu = n\sigma$ (1/cm)	$d\sigma/dE$ $=254.9*Z/E\gamma^2$ (barn/atom/keV)	$d\mu/dE=n.d\sigma/dE$ (1/cm/keV)
H	1	1.01	0.010	0.00813	0.416	3.38E-03	0.007	6.00E-05
C	6	12.01	0.001	0.00007	2.512	1.71E-04	0.044	3.02E-06
O	8	16.00	0.516	0.02709	3.370	9.13E-02	0.059	1.60E-03
Na	11	22.99	0.016	0.00057	4.706	2.68E-03	0.081	4.63E-05
Mg	12	24.31	0.002	0.00007	5.170	3.48E-04	0.089	5.98E-06
Al	13	26.98	0.033	0.00103	5.646	5.81E-03	0.096	9.88E-05
Si	14	28.09	0.329	0.00983	6.137	6.03E-02	0.103	1.02E-03
K	19	39.10	0.013	0.00027	8.930	2.43E-03	0.140	3.82E-05
Ca	20	40.08	0.043	0.00090	9.577	8.61E-03	0.148	1.33E-04
Fe	26	55.85	0.014	0.00021	14.480	2.97E-03	0.192	3.95E-05
U	92	235.00	0.025	0.00009	611.900	5.47E-02	0.680	6.08E-05
Total			1.000			2.33E-01		3.10E-03

μ (cm2/g)		
1.67E-01	k=	0.01334 $(keV)^{-1}$

These values, as well as the energy width of the ROI used in processing the spectra (in keV) were used in the S/P equation discussed above to generate the plot shown in Figure 24 below relating the density-depth of a uranium/concrete mixture to the step-to-peak ratio in a spectrum. The data table that was used to create the plot in Figure 24 below was used in reverse to look up the density-depth associated with the step-to-peak ratio calculated from each measurement spectrum.

μ=	0.167	cm2/g
k=	0.01334	$(keV)^{-1}$
ROI width=	4.90	keV

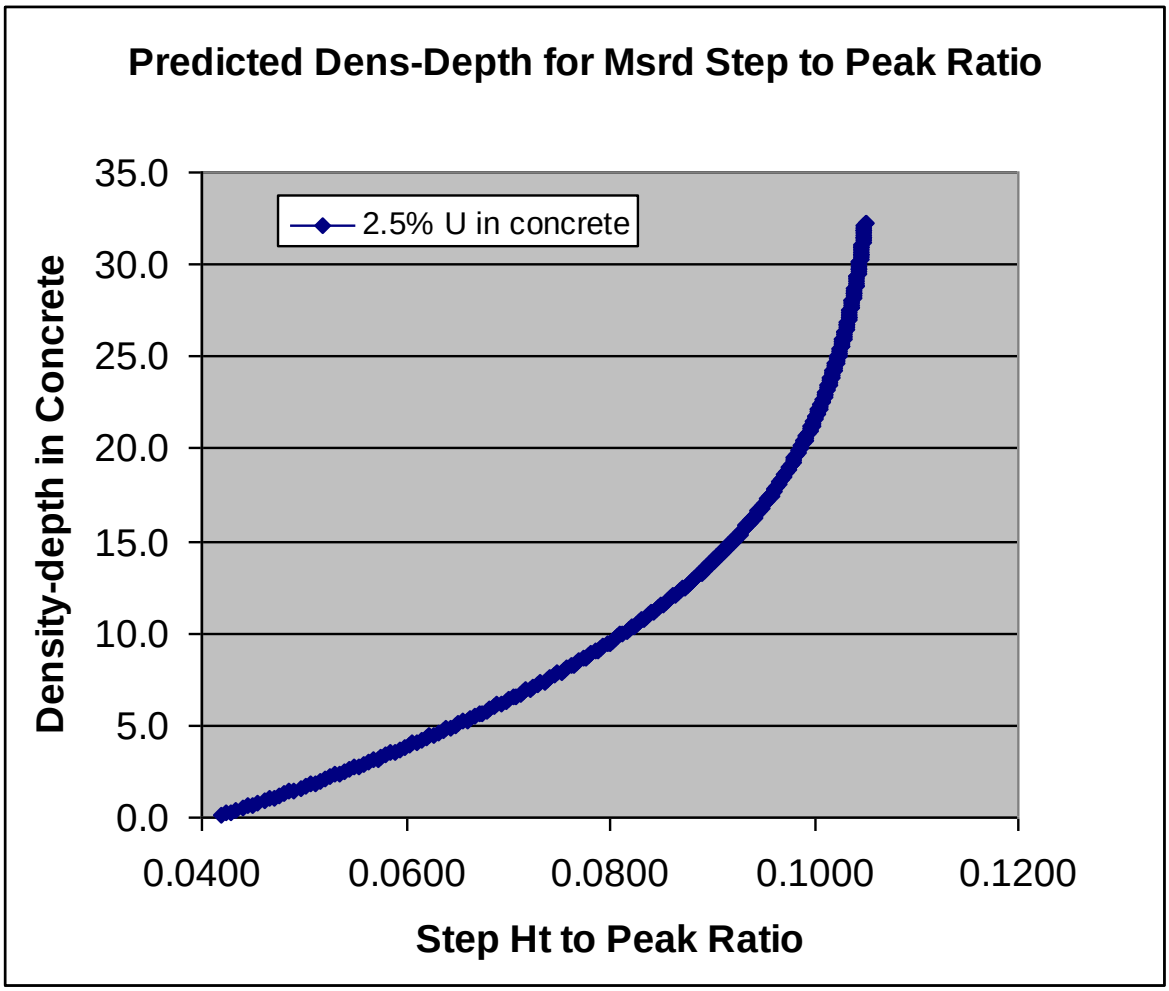

Figure 24: Theoretical small-angle step to peak ratio (S/P) versus density-depth for a distributed mixture of 2.5 weight % uranium in concrete.

In order to complete analysis of the data from the various runs, both ISOTOPIC software and a differential attenuation calculation spreadsheet were used. The uncorrected activities measured for each of the U-235 gamma rays of interest were tabulated from reports available in the ISOTOPIC software. The spreadsheet was then used to calculated background subtraction, geometric correction (using average distance of the deposit to the detector and the effective area of the collimator at the average distance), and matrix attenuation correction. The distance of the deposit to the detector was calculated from the density-depth estimate provided by the small-angle analysis and an assumed concrete density. An initial estimate of the weight fraction of uranium present is obtained from the uncorrected activity of the 185.72keV peak. This fraction of uranium is used to estimate the mass attenuation coefficient of the uranium/concrete mixture which is used in conjunction with the estimated density-depth of the deposit to calculate self-attenuation. The self-attenuation corrected mass is used in the next iteration to estimate the fraction of uranium used to estimate the mass attenuation coefficient of the uranium/concrete mixture. This process is repeated until the estimated mass fraction converges with the calculated mass fraction for the self-attenuation correction.

Differential attenuation is used for the final correction to the fraction of uranium used in the self-attenuation correction. To do this, the corrected activities for each gamma ray are plotted and adjustments are made to the weight fraction to allow the corrected activities to equalize as much as possible. The areal density of the deposit (g U-235 /cm^2) was then calculated by converting the corrected 185.72keV activity to mass using the specific activity of U-235 and dividing by the effective area of the deposit in view. This measured areal density was then compared to the known areal densities determined by summing up the areal densities of the particular planar standards in use for each of the 49 runs.

n. Measurement Results

The results of the small-angle/differential attenuation analyses of the 49 case studies are presented below in Table 6 and plotted in Figure 25. The naming convention for the various runs gives an indication of which sources were placed in which position in the concrete matrix. The source IDs are designated by P1, F1, F2, F3, F4, and F5 as shown above in Table 4. The position of the source is indicated by a number from 1 to 15 in parenthesis following the source ID. For Example, the first case shown in Table 6 is named P1(0)F5(1)F4(2)F3(3)F2(4)F1(5) which indicates that all six sources were used and placed in decreasing mass order starting at position zero and ending at position five. This deposit would be classified as a near-surface deposit extending to 1-1/4" deep into the concrete. Both the known standard areal density and the measured areal density for each of the 49 cases are given for comparison. These results are also plotted in Figure 25 below. The difference between the standard values and measured values ranged from -30% to +37% with an average difference between the standard and measured areal densities being -4%. The plot indicates a good agreement using this approach for the full range of concentrations and variations investigated. The worst results always occurred when the stronger sources were deeper in the concrete with weaker sources closer to the detector. This would represent the most unlikely case in a real world situation because most of the uranium solution would accumulate near the surface with lesser concentrations migrating deeper into the concrete.

The results for the more typical and common real-world situation were quite accurate when using the Small-angle Compton scattering analysis method in conjunction with differential attenuation. The table below only shows raw data and a simple comparison by percent difference between the calculated and measured areal densities, but the sections below this table discuss a more elaborate analysis into statistical correlation and uncertainty regarding the various validation measurements.

Table 6: Comparison of areal density (AD) measurement results (standard vs. measured) for forty-nine (49) validation study runs (g U-235/cm_2).

Validation Study Run	Step/186 Ratio	Theoretical Dens-depth (g/cm2)	Standard AD (g/cm2)	Measured AD (g/cm2)	% diff
P1(0),F5(1),F4(2),F3(3),F2(4),F1(5)	0.055	2.9	0.085	0.076	-12%
P1(0),F5(0),F4(0),F3(0),F2(0),F1(0)	0.044	0.7	0.085	0.072	-16%
P1(0),F5(2),F4(4),F3(6),F2(8),F1(10)	0.060	3.9	0.085	0.072	-16%
F5(0),F4(1),F3(1),F2(2),F1(3)	0.052	2.2	0.052	0.044	-16%
F5(0),F4(1),F3(2),F2(3),F1(4)	0.054	2.7	0.052	0.043	-18%
F5(0),F4(2),F3(4),F2(6),F1(8)	0.059	3.7	0.052	0.043	-18%
F5(0),F4(1),F3(3),F2(6),F1(10)	0.054	2.7	0.052	0.040	-23%
F5(0),F4(2),F3(4),F2(6),F1(8),P1(15)	0.072	6.9	0.085	0.060	-30%
F1(0),F2(2),F3(4),F4(6),F5(8)	0.096	16.1	0.052	0.049	-7%
P1(0) 20120207	0.039	0.10	0.033	0.031	-6%
F1(1)F2(2)F3(3)F4(4)F5(5)	0.092	15.2	0.052	0.062	19%
F1(1)F2(2)F3(3)F4(4)F5(5)P1(6)	0.100	22.1	0.086	0.117	37%
F3(1)F2(2)F1(3)	0.065	5.1	0.015	0.012	-21%
F4(1)F3(2)F1(3)	0.057	3.2	0.025	0.025	0%
F4(1)F3(2)F2(3)	0.058	3.4	0.029	0.027	-8%
F5(1)F3(2)F1(3)	0.055	2.7	0.030	0.026	-12%
F5(1)F3(2)F2(3)	0.057	3.2	0.034	0.029	-15%
F5(1)F4(2)F3(3)F1(4)	0.060	3.9	0.046	0.045	-1%
F5(1)F4(2)F3(3)F2(4)F1(5)	0.061	4.1	0.052	0.049	-6%
F5(1)F4(2)F3(3)F2(4)F1(5)P1(0)	0.053	2.3	0.086	0.077	-10%
P1(1)F5(2)F4(3)F3(4)F2(5)F1(6)	0.064	4.8	0.086	0.079	-7%
P1(2)F5(4)F4(6)F3(8)F2(10)F1(12)	0.081	10	0.086	0.086	1%
P1(0) 20120717	0.035	0.1	0.033	0.037	11%
F2(0) 20120718	0.037	0.1	0.007	0.006	-16%
F5(1)F3(2)F4(3)F2(4)P1(5)	0.068	5.8	0.083	0.086	3%
F5(1)F4(2)F1(3)	0.050	1.7	0.039	0.044	13%
F5(1)F4(2)F3(3)F2(4)P1(15)	0.068	5.8	0.083	0.071	-15%
P1(1)F4(2)F3(3)F1(4)	0.052	2.1	0.058	0.063	8%
P1(1)F4(2)F3(3)F2(4)	0.051	1.9	0.062	0.064	3%
P1(1)F5(2)F3(3)F2(4)	0.053	2.3	0.068	0.070	3%
P1(1)F5(2)F4(3)F1(4)	0.054	2.5	0.072	0.080	10%
P1(1)F5(2)F4(3)F3(4)F1(5)	0.055	2.7	0.079	0.084	7%
P1(1)F5(3)F4(5)F3(7)F1(9)	0.061	4.1	0.079	0.080	1%
P1(1)F5(3)F4(5)F3(7)F2(9)	0.062	4.3	0.083	0.084	0%
P1(2)F5(5)F4(8)F3(11)F2(14)	0.075	7.9	0.083	0.086	2%
F1(0)F2(1)F3(2)	0.054	2.5	0.015	0.014	-9%
F2(0)F1(1)F3(2)	0.046	0.9	0.015	0.013	-14%
F3(0)F2(1)F1(2)	0.043	0.3	0.015	0.014	-6%
F2(0)F3(1)F4(2)F5(3)P1(4)	0.071	6.7	0.083	0.089	7%
F2(1)F3(2)F4(3)P1(4)	0.072	7	0.062	0.065	4%
F2(0)	0.037	0.1	0.007	0.006	-16%
F2(1)	0.045	0.7	0.007	0.006	-15%

Table 6 Continued: Comparison of areal density (AD) measurement results (standard vs. measured) for forty-nine (49) validation study runs (g U-235/cm_2).

Validation Study Run	Step/186 Ratio	Theoretical Dens-depth (g/cm2)	Standard AD (g/cm2)	Measured AD (g/cm2)	% diff
F2(2)	0.053	2.3	0.007	0.006	-11%
F2(3)	0.074	7.6	0.007	0.006	-11%
F2(4)	0.071	6.7	0.007	0.006	-1%
F3(0)F4(1)F5(2)	0.051	1.9	0.044	0.048	9%
F4(0)F3(1)F5(2)	0.047	1.1	0.044	0.047	7%
F5(0)F3(1)F4(2)	0.045	0.7	0.044	0.047	7%
F5(0)F4(1)F3(2)	0.042	0.1	0.044	0.048	10%
				avg:	-4%

o. Statistical Analysis

When first analyzing the results of the validation study, it is critical to ensure that there is statistical relevance between the theoretical values calculated through the small-angle Compton scattering methods described above and the actual real-world results. Testing 49 different validation trials is enough data to make valid statistical conclusions about the data, and the results of the statistical analysis will be important in showing that data is valid and can be applied to similar real-world situations. The statistical analysis also gives a confirmation of the measurement situations that performed the worst and could be considered outliers. Knowing and understanding which measurement conditions give the biggest errors in the validations study can go a long way to understand limitations of the small-angle Compton scattering method/technique and in explaining variations in actual results when this technique is applied to the concrete floor holdup situation. Figure 25 below shows a plot of the data points from the validations studies comparing the theoretical areal density (standard) with the actual measured areal density. This data was plotted using a statistical software tool called JMP Pro.

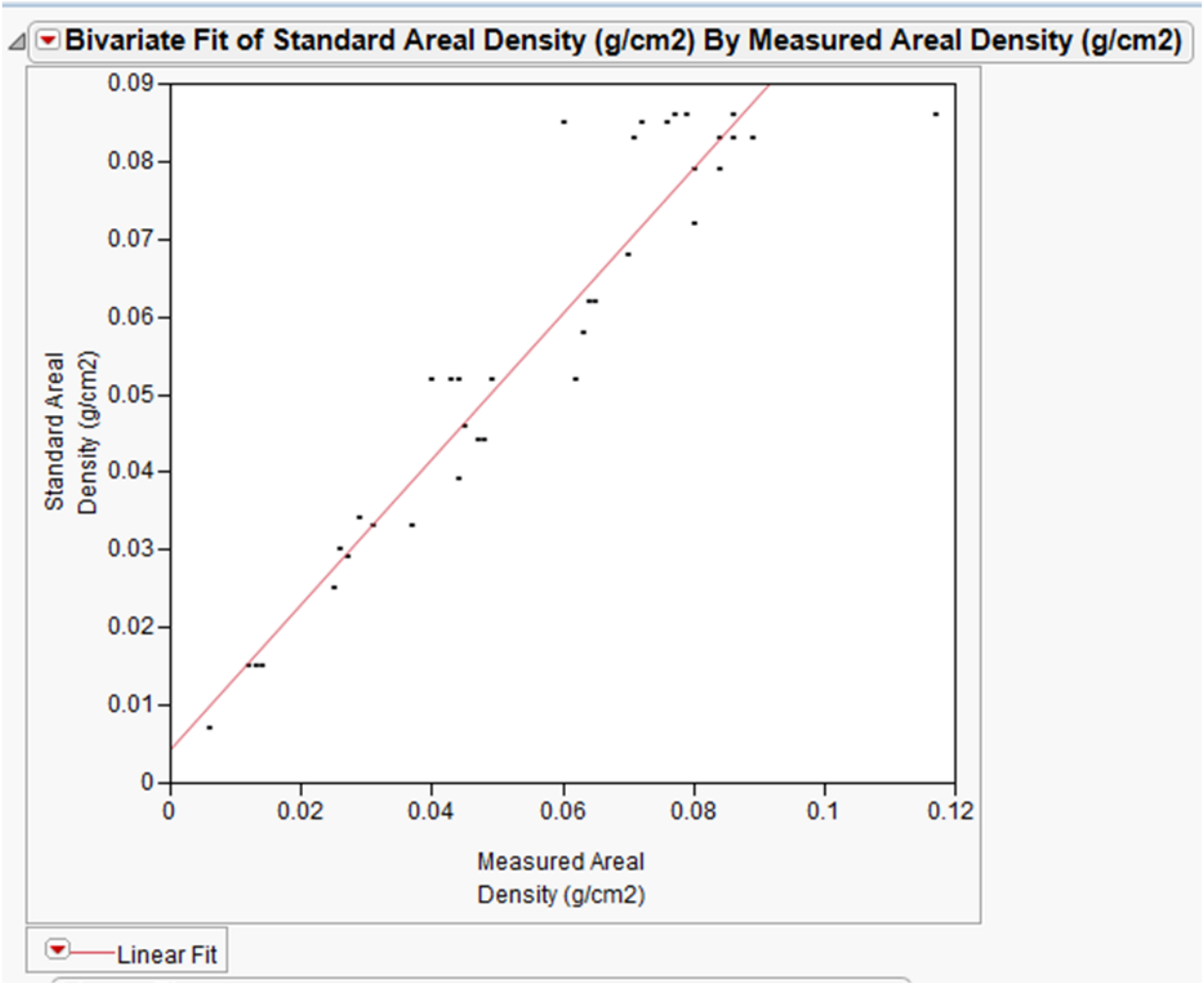

Figure 25: Linear regression analysis of 49 measurements of uranium areal density in concrete (gU-235/cm^2) by HPGe gamma spectroscopy using small-angle/differential attenuation technique.

The red linear line in the plot above shows the best statistical fit between the theoretical and measured areal density values using linear regression. Linear regression is an approach to model the relationship between a scalar dependent variable y (Standard Areal Density) and one or more explanatory variables, x (Measured Areal Density). Besides seeing the close proximity of the majority of data points with the line, a coefficient of determination, or R-squared value, is also calculated by the software to indicate how well the data points fit with the linear line. A perfect linear fit in the data would produce an R-squared value of 1. This is nearly impossible to

achieve in experimental data, but R-squared values close to 1 show a good statistical correlation. Table 7 below shows the JMP output for the "Summary of Fit" conditions.

Table 7: Summary of fit values for linear regression model based on JMP evaluation of validation study data.

Item:	**Value:**
R-Squared	0.921814
R-Squared Adjusted	0.92015
Root Mean Square Error	0.007839
Mean of Response	0.050816
Observations (or Sum Wgts)	49

With an R-squared value of 0.92, this validation study shows great statistical correlation between calculated and measured areal density values. Additionally, if you remove the two data points with the worst percent difference between the calculated and measured areal densities (#8 and #12 from Table 6) the statistical correlation is even better.

Another statistical evaluation that should be done in JMP Pro to ensure that a linear regression model is an appropriate way to statistically evaluate the data from the validation study is to plot the residuals. The residual of an observed value is the difference between the observed value and the estimated function value or predicted value. In other words, it is not a measure of the error between the calculated and measured areal density value, but rather the difference between the measured value and the estimated linear fit line shown above in Figure 25. The key in a residual plot is that the data points should be randomly dispersed in no apparent pattern around the horizontal axis. This shows that a linear regression model is appropriate for the data. In Figure 26 below, the data points are in a random configuration around the horizontal axis confirming that the statistical evaluation is meaningful. Again, the data points for validation test #8 and #12 show up as obvious outliers compared to the other data points.

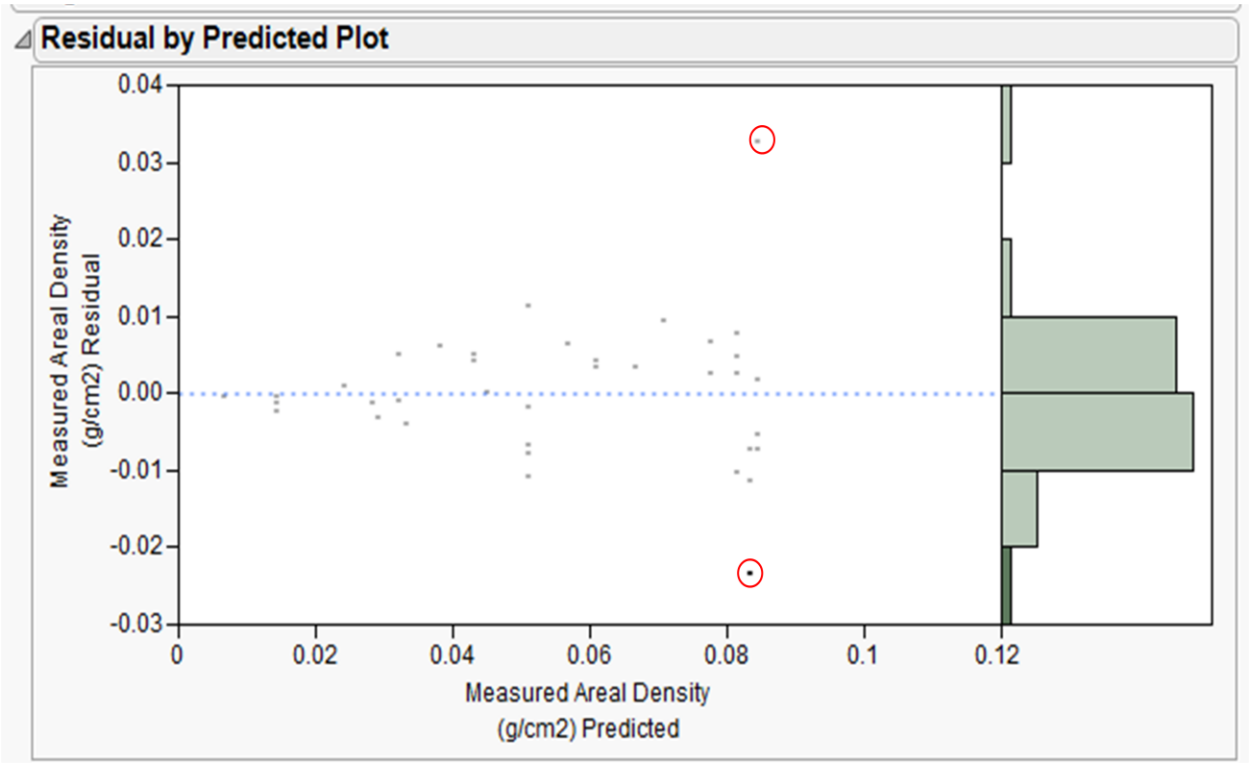

Figure 26: JMP plot of residuals for measured areal density of forty-nine (49) validation measurements of uranium areal density in concrete (gU-235/cm^2) using small-angle/differential attenuation technique.

One final statistical evaluation that will be conducted on the results of this validation study is to look at the confidence region of the data. In this case I will be looking at the 95% confidence region of the validation study results. The confidence region is calculated in such a way that if a set of measurements were repeated many times and a confidence region calculated in the same way on each set of measurements, then on average, 95% of the time the confidence region would include the point representing the "true" values of the set of variables being estimated. In statistics, confidence regions are often set using different intervals of standard deviation, or sigma (σ). 1-sigma uncertainty on each side of the mean typically gives a ~67% confidence that the estimated range of values includes an unknown parameter in a set of sample data, which in this case is the validation study data. 2-sigma uncertainty on each side of the mean gives a ~95% confidence for the data and is typically the most common interval for an uncertainty evaluation. 3-sigma uncertainty on each side of the mean (or six-sigma) is also

frequently used in manufacturing as a goal to ensure there is a 99.99% confidence that products can be built defect free within set specifications. For this validation study related to the small-angle Compton scattering method, the plot shown below in Figure 27 shows the 95% confidence region for the data gathered. Again, only the data points for validation test #8 and #12 show up as obvious outliers that fall outside this region.

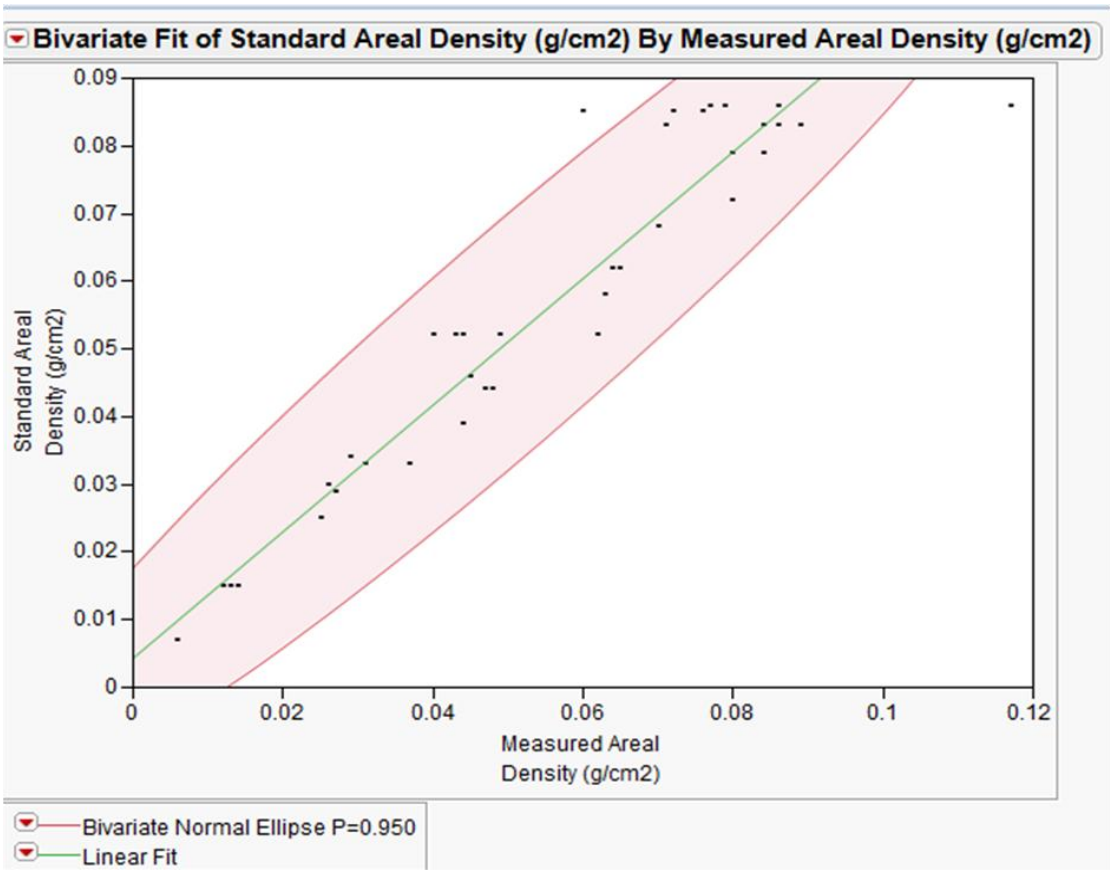

Figure 27: JMP plot showing calculated 95% confidence region from 49 measurements of uranium areal density in concrete (gU-235/cm^2).

Overall, the various statistical evaluations done on this validation data is reassuring to show that the small-angle Compton scattering evaluation method is a valuable and accurate tool for analyzing holdup in shielded situations.

p. Uncertainty Analysis

As previously stated, NDA measurements and analysis involve a large degree of unknowns and assumptions. Although the theoretical analysis methods discussed in this thesis, including differential attenuation corrections and small-angle Compton scattering corrections, improve assumptions and overall accuracy, uncertainty will always exist with non-destructive analysis of radioactive materials. Beyond the statistical variations associated with natural decay of radioactive isotopes (branching ratios, actual activity) and the detectors ability to accurately capture and evaluate those decays (detector efficiency), there are also uncertainties associated with gamma-ray peak areas, actual effects of container and matrix attenuation, and overall geometry estimations. The goal with any non-destructive analysis involving radioactive decay is to incorporate all of these individual uncertainty contributors together and produce an overall Total Measurement Uncertainty (TMU). The ideal way to achieve an accurate estimation of TMU is to use the standard propagation of errors method.

Since HPGe results are based off of the total measurement activity of the nuclide being reported, the standard propagation of errors method is applied to determine the TMU of the gamma ray activity reaching the detector. In this case, we are evaluating the uncertainty in the activity of the various gamma-ray peaks coming from U-235. Therefore, we must again utilize Equation 5 that was explained above on page 26 which is used to determine total activity of nuclide *i* from gamma-ray of energy *E*. This equation is shown below.

$$Q_{i,E} = \left(\frac{R_{i,E}}{Y_{i,E}\epsilon(E)}\right)\left(\frac{\bar{r}}{r_0}\right)^2 (e^{\mu_c\rho_c x_c})\left(\frac{\mu_m\rho_m x_m}{(1-e^{-\mu_m\rho_m x_m})}\right)$$

In more simplistic terms, this same equation can be represented by the following equations:

$$A_{nuc} = \left(\frac{PA_{meas} CF_{geo} CF_{cont} CF_{mat}}{BR_{ray} \epsilon_{det}}\right)$$

Where,

A_{nuc}	Activity of nuclide to be reported
PA_{meas}	Peak area for the reference gamma ray of the reported nuclide
CF_{geo}	Correction factor for geometry
CF_{cont}	Correction factor for container attenuation
CF_{mat}	Correction factor for matrix attenuation
BR_{ray}	Branching ratio for the reference gamma ray of the reported nuclide
ϵ_{det}	Intrinsic detector efficiency

Now, using this simplified equation, the standard propagation of error for nuclide activity can be calculated with the following equation:

$$\left(\frac{\sigma_{A_{nuc}}}{A_{nuc}}\right)^2 = \left(\frac{\sigma_{PA}}{PA_{meas}}\right)^2 + \left(\frac{\sigma_{geo}}{CF_{geo}}\right)^2 + \left(\frac{\sigma_{cont}}{CF_{cont}}\right)^2 + \left(\frac{\sigma_{mat}}{CF_{mat}}\right)^2 + \left(\frac{\sigma_{BR}}{BR_{ray}}\right)^2 + \left(\frac{\sigma_{\epsilon}}{\epsilon_{det}}\right)^2$$

Where, each sigma (σ) term represents the uncertainty associated with the variable in the equation.

The uncertainty in the peak area (σ_{PA}) is determined from counting statistics and is inversely proportional to the amount of radioactive material that is present. The uncertainty in the peak area becomes more significant for low quantities of radioactive material, but this contributor to overall uncertainty can be improved with longer detector counting times. Branching ratios of the various gamma-rays coming from U-235 are well defined and have been tested and

documented by various government and scientific entities. Similarly, the detector efficiency is determined by the detector manufacturer through a series of calibrations and tests. Therefore, the uncertainty contributions from branching ratios (σ_{BR}) and detector efficiency ($\sigma_{\in}$) are typically insignificant compared to other factors and for simplicity, can be ignored for this calculation. The uncertainty correction factor for the container attenuation (σ_{cont}) depends on how well the container material and thickness is understood. For the validation tests conducted, the container material is essentially the plastic used to encase the source standards which is well defined and understood. That makes the container uncertainty small, but it cannot be ignored. Similarly, the container for the practical floor application is the stainless steel installed to cover the floor. This stainless steel cover was constructed to set thickness or gauge by the manufacturer and is also well defined and understood. Therefore, along with the peak area (σ_{PA}), the most significant contributions to uncertainty will come from the geometry correction factor (σ_{geo}) and the matrix correction factor (σ_{mat}). The uncertainty in the geometry correction factor takes into account varying distances between the U-235 sources and the detector. The uncertainty in the matrix attenuation correction factor considers both the varying path lengths through the matrix and inhomogeneity in the matrix composition and density. The uncertainty for the matrix correction becomes significant for high density matrices. Both of these factors are somewhat subjective and depend on assumptions about the actual distribution of matrix and radioactivity within the matrix. The fact that the sources in the validation study must be placed at discrete distances between the concrete tiles also impacts uncertainty because a continuous distribution of uranium would be more ideal and realistic. Overall, for the 49 test cases used in the validation study, the TMU will be calculated using the following formula:

$$TMU = \sqrt{(\sigma_{PA}^2 + \sigma_{geo}^2 + \sigma_{cont}^2 + \sigma_{mat}^2)}$$

Most of these individual uncertainty contributors are automatically calculated within the ORTEC ISOTOPIC software by making comparisons between the defined model and actual information

evaluated from the collected spectrum. Of course, ISOTOPIC cannot account for everything and some subjectivity is involved in applying uncertainty to each of these contributors. An overall estimate of TMU is shown below in Table 8 for each of the 49 validation test cases. The results from this uncertainty analysis will be used as a tool later to apply accurate uncertainty estimates to actual results in the practical application section of this thesis.

Table 8: Calculation of Total Measurement Uncertainty (TMU) for 49 validation study cases using the propagation of error methodology.

Validation Study Run	σ_{PA}	σ_{geo}	σ_{cont}	σ_{mat}	TMU
P1(0),F5(1),F4(2),F3(3),F2(4),F1(5)	6.00%	10.00%	3.50%	6.00%	13.57%
P1(0),F5(0),F4(0),F3(0),F2(0),F1(0)	4.00%	8.00%	3.50%	8.00%	12.50%
P1(0),F5(2),F4(4),F3(6),F2(8),F1(10)	10.00%	10.00%	3.50%	12.00%	18.87%
F5(0),F4(1),F3(1),F2(2),F1(3)	6.00%	6.00%	3.00%	8.00%	12.04%
F5(0),F4(1),F3(2),F2(3),F1(4)	5.00%	6.00%	3.00%	9.00%	12.29%
F5(0),F4(2),F3(4),F2(6),F1(8)	8.00%	7.00%	3.00%	8.00%	13.64%
F5(0),F4(1),F3(3),F2(6),F1(10)	10.00%	10.00%	3.00%	10.00%	17.58%
F5(0),F4(2),F3(4),F2(6),F1(8),P1(15)	14.00%	13.00%	3.50%	12.00%	22.83%
F1(0),F2(2),F3(4),F4(6),F5(8)	9.00%	7.00%	3.00%	7.00%	13.71%
P1(0) 20120207	10.00%	6.00%	1.00%	6.00%	13.15%
F1(1)F2(2)F3(3)F4(4)F5(5)	14.00%	5.00%	3.00%	6.00%	16.31%
F1(1)F2(2)F3(3)F4(4)F5(5)P1(6)	15.00%	13.00%	3.50%	12.00%	23.46%
F3(1)F2(2)F1(3)	8.00%	6.00%	2.00%	5.00%	11.36%
F4(1)F3(2)F1(3)	6.00%	6.50%	2.00%	4.50%	10.12%
F4(1)F3(2)F2(3)	5.50%	6.00%	2.00%	5.50%	10.02%
F5(1)F3(2)F1(3)	4.00%	6.50%	2.00%	5.00%	9.34%
F5(1)F3(2)F2(3)	4.00%	6.00%	2.00%	5.00%	9.00%
F5(1)F4(2)F3(3)F1(4)	8.00%	6.00%	2.50%	6.00%	11.93%
F5(1)F4(2)F3(3)F2(4)F1(5)	7.00%	7.00%	3.00%	6.00%	11.96%
F5(1)F4(2)F3(3)F2(4)F1(5)P1(0)	6.00%	7.00%	3.50%	5.00%	11.06%
P1(1)F5(2)F4(3)F3(4)F2(5)F1(6)	7.00%	8.00%	3.50%	7.00%	13.20%
P1(2)F5(4)F4(6)F3(8)F2(10)F1(12)	4.00%	6.00%	3.50%	5.00%	9.45%
P1(0) 20120717	8.00%	6.00%	1.00%	6.00%	11.70%
F2(0) 20120718	10.00%	6.00%	1.00%	6.00%	13.15%
F5(1)F3(2)F4(3)F2(4)P1(5)	7.00%	5.00%	3.50%	6.00%	11.06%
F5(1)F4(2)F1(3)	8.00%	8.00%	2.00%	6.00%	12.96%
F5(1)F4(2)F3(3)F2(4)P1(15)	10.00%	10.00%	3.50%	10.00%	17.67%
P1(1)F4(2)F3(3)F1(4)	5.00%	6.00%	2.50%	5.50%	9.87%
P1(1)F4(2)F3(3)F2(4)	5.00%	6.00%	2.50%	6.00%	10.16%
P1(1)F5(2)F3(3)F2(4)	4.00%	6.00%	2.50%	6.50%	9.41%
P1(1)F5(2)F4(3)F1(4)	4.00%	6.00%	2.50%	6.50%	10.02%

Table 8 Continued: Calculation of Total Measurement Uncertainty (TMU) for 49 validation study cases using the propagation of error methodology.

Validation Study Run	σ_{PA}	σ_{geo}	σ_{cont}	σ_{mat}	TMU
P1(1)F5(2)F4(3)F3(4)F1(5)	5.00%	7.00%	3.00%	6.00%	10.91%
P1(1)F5(3)F4(5)F3(7)F1(9)	7.00%	8.00%	3.00%	6.00%	12.57%
P1(1)F5(3)F4(5)F3(7)F2(9)	7.00%	8.00%	3.00%	5.00%	12.12%
P1(2)F5(5)F4(8)F3(11)F2(14)	10.00%	14.00%	3.00%	11.00%	20.64%
F1(0)F2(1)F3(2)	8.00%	8.00%	2.00%	6.00%	12.96%
F2(0)F1(1)F3(2)	8.00%	8.00%	2.00%	6.00%	12.96%
F3(0)F2(1)F1(2)	6.00%	7.00%	2.00%	6.00%	11.18%
F2(0)F3(1)F4(2)F5(3)P1(4)	6.00%	4.00%	3.50%	4.00%	8.96%
F2(1)F3(2)F4(3)P1(4)	7.00%	5.00%	3.50%	6.00%	11.06%
F2(0)	14.00%	4.00%	1.00%	6.00%	15.78%
F2(1)	13.00%	5.00%	1.00%	5.00%	14.83%
F2(2)	12.00%	6.00%	1.00%	4.00%	14.04%
F2(3)	11.00%	7.00%	1.00%	4.00%	13.67%
F2(4)	10.00%	8.00%	1.00%	4.00%	13.45%
F3(0)F4(1)F5(2)	8.00%	8.00%	2.00%	6.00%	12.96%
F4(0)F3(1)F5(2)	7.00%	8.00%	2.00%	8.00%	13.45%
F5(0)F3(1)F4(2)	6.00%	7.00%	2.00%	8.00%	12.37%
F5(0)F4(1)F3(2)	6.00%	6.00%	2.00%	8.00%	11.83%
				avg:	13.21%

Overall, the average 1-sigma uncertainty of the 49 different validation studies about 13.21%. The highest uncertainties among the 49 validation studies were in the 20.64-23.46% range. A few consistent patterns can be seen from the uncertainty analysis which will be helpful in analyzing the uncertainty associated with the practical application of this NDA technique discussed later in this thesis. The highest uncertainties typically occurred in two situations. The first is when a stronger source was buried very deep in the concrete while the remaining sources were somewhat shallow in the concrete. This would mean there was a large gap of uncontaminated concrete between a shallow source and a deep source at the same measurement location. This is a very unlikely or virtually impossible situation in the real world, so a higher uncertainty makes sense with this type of mimicked holdup deposit. The other situation that showed a typically larger uncertainty is when stronger sources were placed at position “0” meaning there was no intervening concrete between that source and the detector.

This situation minimized the ability to use small-angle Compton scattering techniques for the source at position "0" because there was no intervening concrete to cause a peak discrepancy. This reduced the ability to use the step-to-peak ratio to pin-point certain variables in the differential attenuation evaluation meaning that some degree of guessing would need to be implemented. Therefore, not being able to utilize small-angle Compton scattering for strong sources at position "0" raised the uncertainty of the final results for those cases. For a final evaluation of the uncertainty associated with this validation study, Figure 28 below is a plot showing the 1-sigma TMU applied to each of the 49 individual data points using error bars.

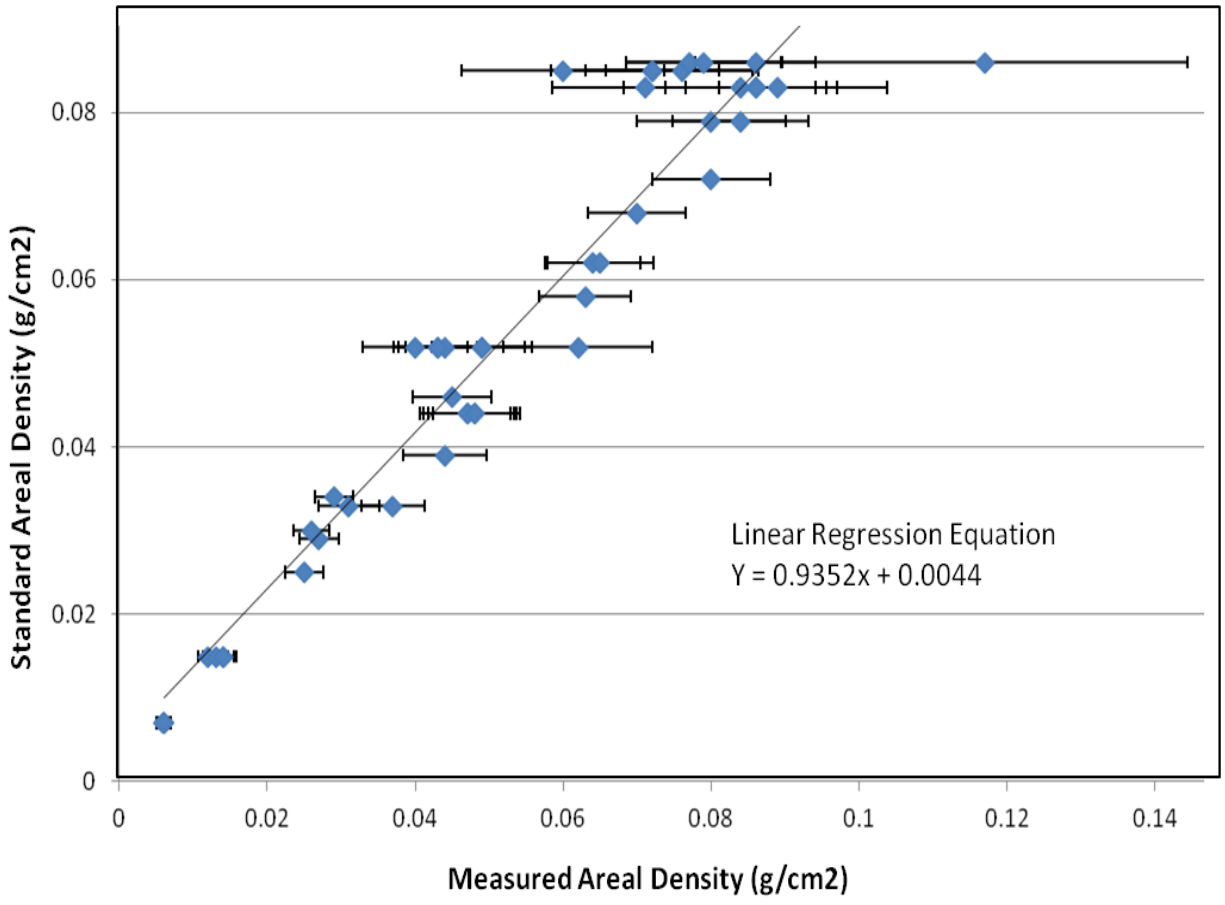

Figure 28: Plot showing the associated 1-sigma Total Measurement Uncertainty (TMU) applied to each data point using error bars for the 49 cases in the validation study.

As stated above on page 58, one standard deviation, or 1-sigma uncertainty, gives a ~67% confidence that the estimated range of values for each point includes the plotted linear regression line determined from the calculated and measured areal densities of the 49 data points. So statistically speaking, the error bars should overlap the linear regression line for 67% of the data points from the validation study (33 of 49). The linear regression equation from Figure 28 was used to determine if the end points of the error bars overlapped the line for each point. After completing this calculation, it was determined that the 1-sigma error bars overlap the linear regression line for 37 of the 49 data points in the validation study. This represents a 75.5% inclusion which is just slightly more than the expected value and still shows good statistical relevance and a good fit of the data.

q. Conclusion

With support from the statistical and uncertainty analysis in the validation study, the overall results of the small-angle/differential attenuation analysis developed for the measurement of uranium solution holdup deposits in concrete flooring have been demonstrated to be effective in measuring a broad range of deposit scenarios. The 49 cases measured for this validation study ranged in concentration from 0.002 g ^{235}U /cm^2 to 0.085 g ^{235}U /cm^2, ranged in concrete depth from 0”- 4” deep, and included various situations that included mockups of increasing concentration as depth increased, decreasing concentration as depth increased, random concentration profiles, and cases of two distinct deposits separate by various thicknesses of uncontaminated concrete. Even with the great variety of cases studied, the small-angle technique was effective in predicting a density-depth that was useful for calculating the self-attenuation of the uranium concrete/mixture and improving the capabilities of the differential attenuation analysis. As mentioned above, certain extreme conditions had results as far as -30% and +37% off from the calculated values, but these were for unanticipated real world situations. The vast majority of results from this validation study which mimicked the situations that would be more commonly seen in the real world were very accurate and promising.

Chapter 5: Practical Application of Small-Angle Compton Scattering

Now that the theory and methods of Small-angle Compton scattering have been discussed along with the details of a validation study showing successful real-world implementation of the theory, this section will discuss a practical application of Small-angle Compton scattering that solved a real-world nuclear problem.

r. Introduction

Nuclear criticality safety considerations and other operating methods used to reprocess highly enriched uranium (HEU) have come a long way in the last several decades. During the 1940's and the peak of the Cold War era, speed and quantity was the name of the game when processing HEU and safety was often a secondary concern. This mode of operation resulted in several documented, and many more undocumented, large quantities of high equity uranyl nitrate solution being spilled onto concrete floors within the processing areas for these materials. Of course, this material was cleaned up and placed back into desired processing equipment or storage containers, but not before some was able to soak into the porous concrete floor or flow into various cracks in the concrete to deeper levels. This condition has led to various accumulations of holdup deposited within and beneath the floor making it extremely difficult to monitor and quantify. At one time, low-resolution sodium-iodide (NaI) detectors were used to monitor the floor and estimate the mass of U-235 that has been deposited over the years, but these measurements are inaccurate and carry a high level of uncertainty. This is because some knowledge of the depth of the U-235 penetration within the concrete is needed to accurately analyze the data. In the case of HEU solution being absorbed into a floor, it is very easy to be deceived when only measuring with a NaI detector. Since the concrete floor acts as a dense attenuator of gamma rays, a low-quantity shallow deposit can appear the same as a high-quantity deep deposit if proper corrections can't be made to account for the different conditions. Figure 28 below again shows some of the different configuration of HEU solution in concrete floors that can make it difficult to accurately analyze and estimate holdup quantities.

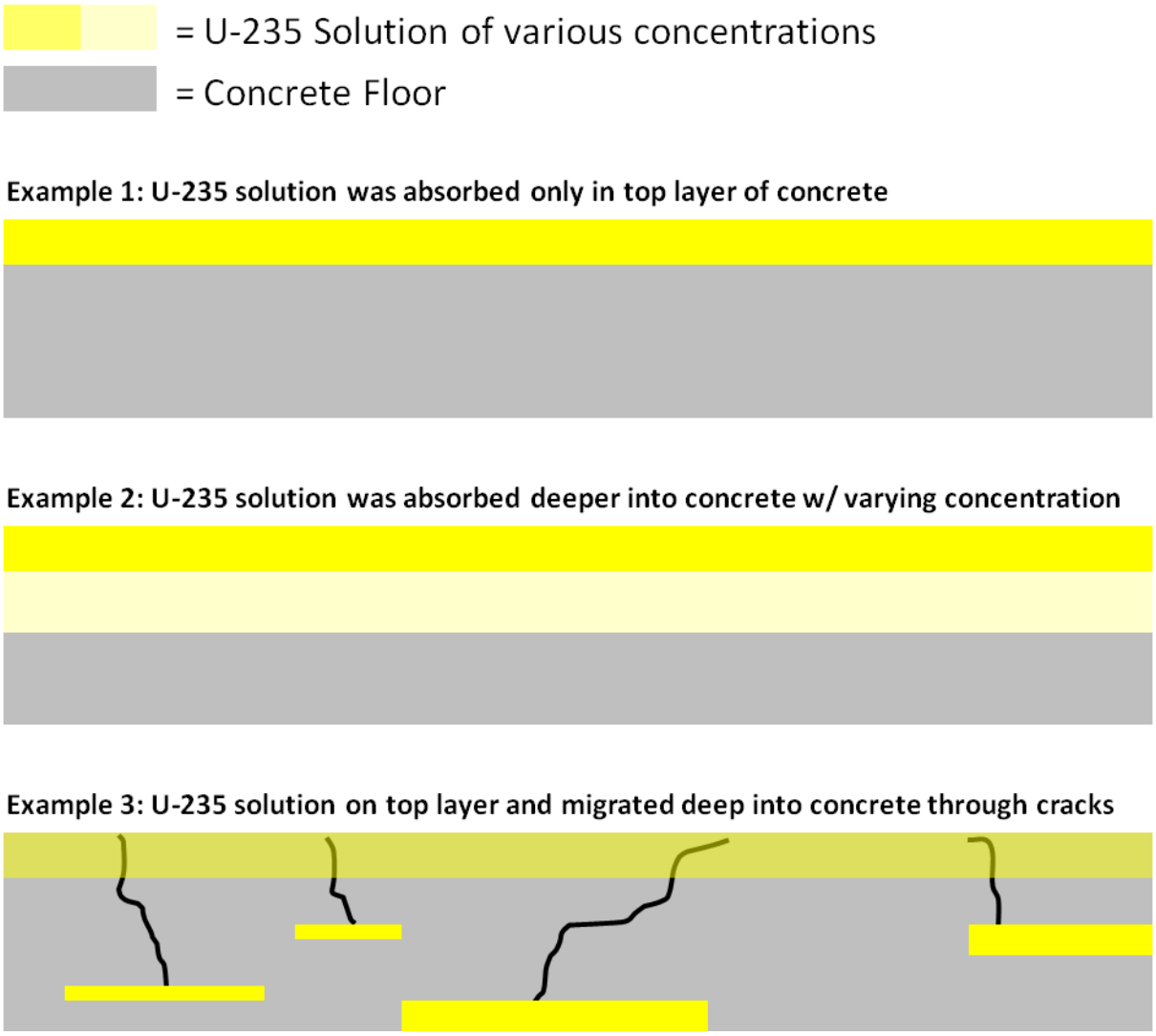

Figure 29: Various possible holdup conditions and penetration depths of U-235 solution spilled onto a concrete floor.

Using a high-resolution HPGe detector and the principles of Small-angle Compton scattering that have been discussed and validated above can provide the needed density-depth estimates of HEU solution deposits within the concrete floor. Having this valuable data in conjunction with uncorrected sodium-iodide measurements of the same areas of a concrete floor can allow for accurate and defensible estimations of HEU holdup accumulations within a floor. This data can then be used for criticality safety planning for continued material processing in those areas as well as for material accountability purposes for material that has been lost into the floor and

cannot be recovered. Additionally, this holdup data will be extremely important in the future if this processing building is ever decommissioned and possibly torn down.

Although low-resolution NaI detectors have their limitations, they still provide valuable data in the process to measure HEU holdup in a concrete floor. The NaI detectors used to measure uranium holdup are specifically set up for measurements of the 185.72keV gamma ray of U-235, but they don't give the user any real information about the attenuation these gamma rays are encountering on their way to the detector. If this was the only equipment available when evaluating a concrete floor with known holdup in it, several assumptions would need to be made unless some other independent means were used to determine the depth of HEU solution in the concrete. One such possibility is core sampling which requires the physical drilling into the concrete floor followed by destructive testing and analysis to see how deep the HEU penetrated the floor. This method of course brings on a whole new level of concerns. Core sampling is very expensive, it creates airborne contamination concerns, it is labor intensive, and when you are done, you really only have information about the exact spot in which the core sampling was done. This does not help much if the area being evaluated is thousands of square feet.

A much better option would be to use an HPGe detector and the principles of small-angle Compton scattering to determine the depth of HEU penetration into the concrete in several locations. This method is non-destructive and much quicker and cheaper than an option like core sampling. And, although it isn't cost effective to check the depth of HEU penetration at every location on a floor, it does allow for multiple data points to be taken without any negative effects to the floor itself. In the end, the combination of data acquired between the NaI detector and the HPGe detector and the application of small-angle Compton scattering analysis can be used to accurately estimate holdup in a concrete floor.

s. Measurement Preparation

Because low-resolution NaI measurements are very quick and the equipment is much more portable compared to HPGe equipment, these types of measurements can be taken quickly and easily covering a large floor area. Once hundreds of these NaI measurements are taken covering the entire floor, the data can be analyzed to determine the uncorrected areal density of HEU detected at each location on the floor. Figure 29 below shows how systematic NaI measurements were taken on a concrete floor to get full coverage and areal density data from HEU holdup within the floor. These measurements were taken by pointing the NaI detector directly down at the floor with an approximate 20 inch standoff. This standoff allowed for a wider field of view from the detector to ensure the entire floor area was covered with somewhat overlapping measurements.

Once this NaI data is acquired, the measurements were analyzed to determine the uncorrected areal density of HEU detected at each location. For these initial calculations, the attenuation of the gamma rays from self attenuation of the deposit was not taken into affect. These uncorrected areal densities were then used to create a topographic map of uranium concentrations in the floor. This map is shown below in Figure 30. The topographic map indicates that holdup in the floor is confined to a limited number of regions where uranyl nitrate solution spills have occurred, with the majority of the floor being unaffected. Although the NaI data can be misleading because it doesn't account for depth of penetration of the HEU solution holdup, it does give you a sense of where spills have occurred and where the gamma rays are the strongest. Knowing this information is extremely helpful when selecting the specific locations to apply the HPGe measurement and the small-angle Compton scattering analysis to determine the depth of penetration of the HEU. The criteria for selecting the locations to use further HPGe and small-angle Compton scattering analysis were areas that indicated spill regions with the greatest concentrations; and areas of the floor where the large HPGe equipment was accessible.

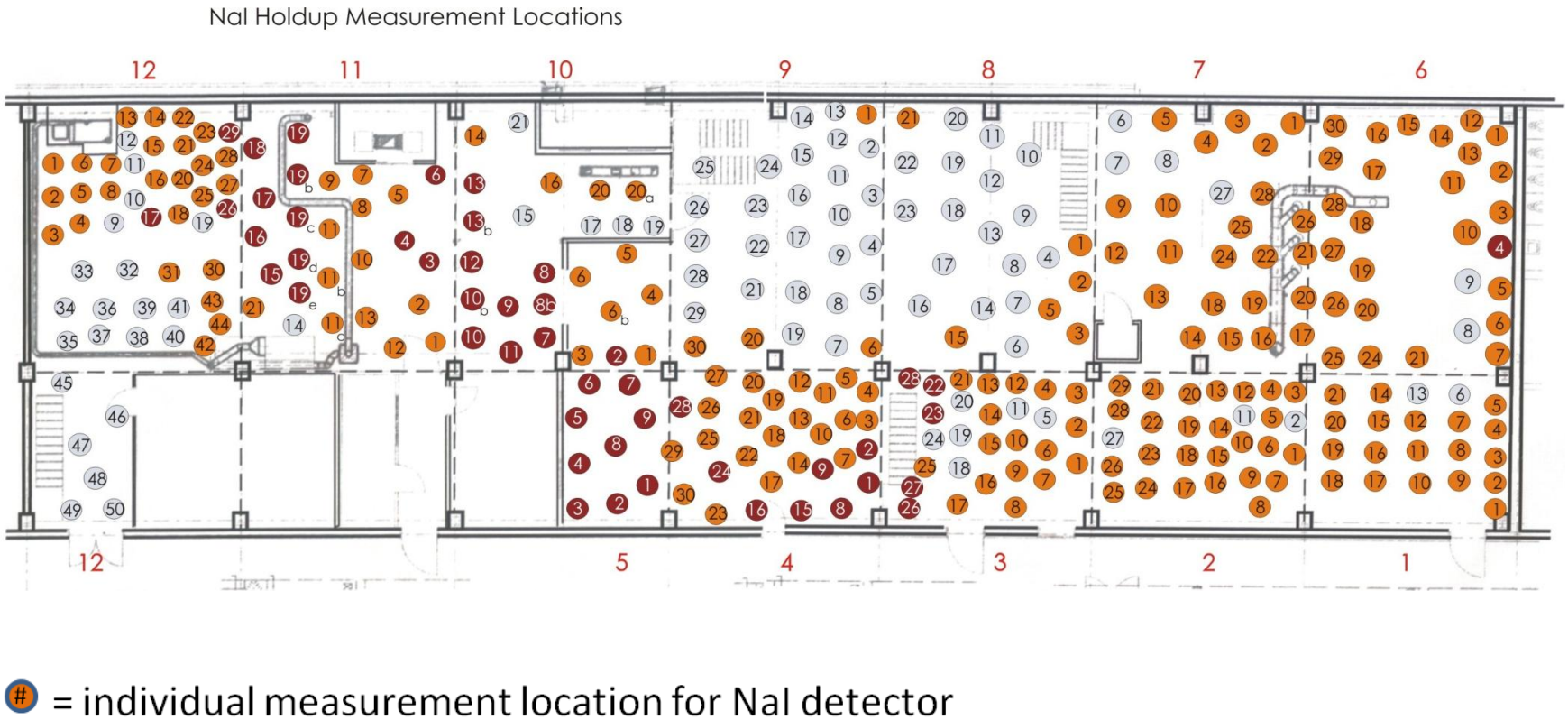

Figure 30: Systematic NaI measurements were taken on a concrete floor to get full coverage and areal density data from HEU holdup within the floor.

Topographical map showing uncorrected areal densities (g U-235/cm^2)

of measured floor using NaI detector only on entire floor.

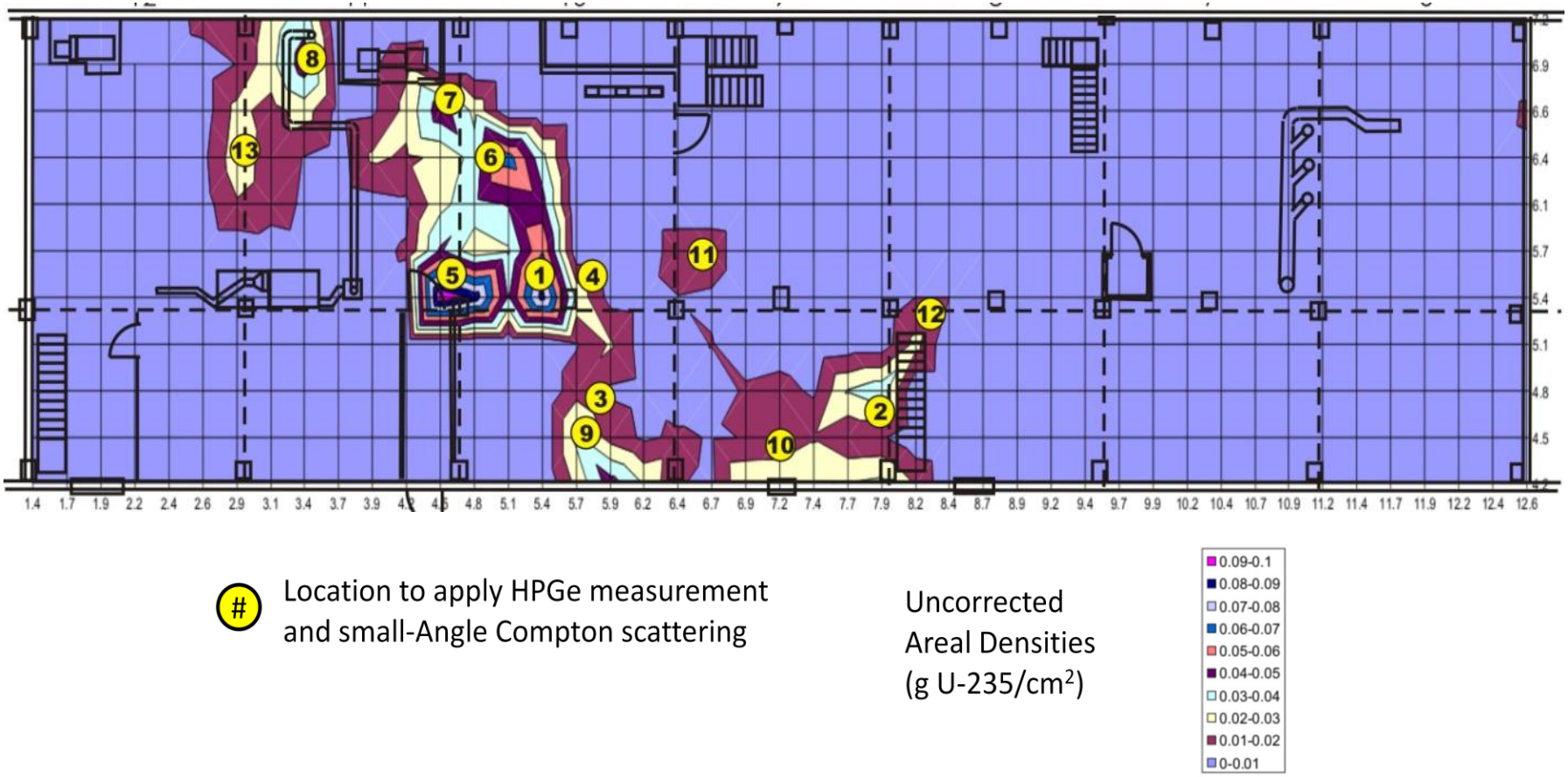

Figure 31: Topographical map showing uncorrected areal densities (g U-235/cm^2) of measured floor from NaI measurements.

t. Performance of measurement

Once the locations were selected to take HPGe measurements and apply the small-angle Compton scattering methodology, the equipment had to be set up in a manner in which it was pointing straight down at the concrete. The setup for the HPGe measurements is shown in Figure 31 below. At each of the selected sites, a background measurement was taken followed by the actual floor measurement. The background was measured by placing a ¾" thick tungsten plug in front of the detector, thereby measuring radiation entering into the detector from directions other than the immediate floor region being sampled. Background radiation typically comes from overhead or nearby processing equipment or storage equipment that contains high quantities of HEU. After the background measurement was completed, the plug was removed and a second spectrum was acquired with the detector/collimator place directly against the floor.

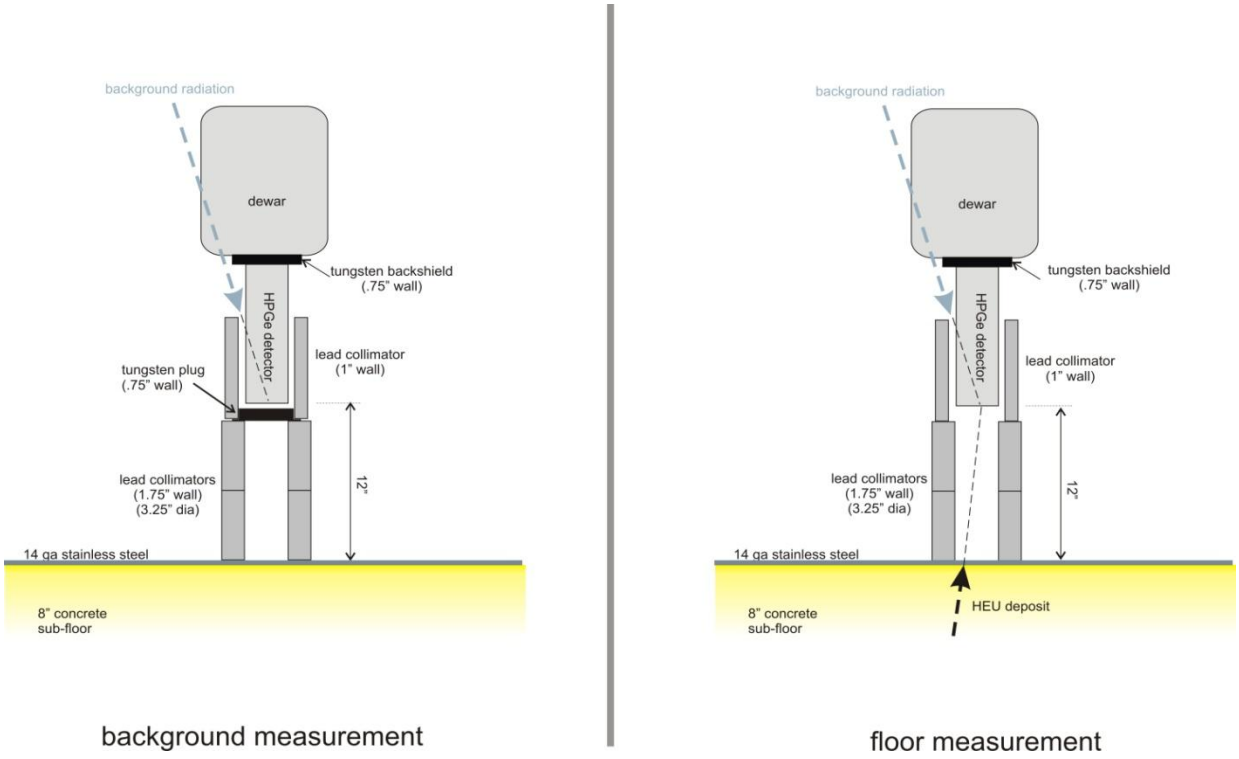

Figure 32: HPGe setup for taking background and actual floor measurements at the selected locations.

The HPGe spectra acquired were analyzed by a combination of both small-angle Compton scattering analysis and differential attenuation analysis to determine the depth of the deposit for each spill region. ISOTOPIC software was used to determine the peak areas and activities for the four dominant gamma rays of U-235, namely the 144, 163, 186, and 205 keV gamma rays. Three regions of interest were defined for the small-angle analysis – one region centered on the 185.72 keV peak and one on each the low and high sides of the Compton scattering continuum on either side of the peak. A spreadsheet was then used to determine the small-angle step-to-peak ratios, the density-depths of the uranium deposit in concrete, the areal density of the deposit (g U-235/cm^2), and to perform the differential attenuation adjustments used to refine the deposit depth calculations.

An example of this differential attenuation analysis is shown below in Figures 32 and 33. In Figure 32, the slope of the activity differences in the U-235 gamma rays indicates that the attenuation correction is not sufficient. To correct the analysis used in generating Figure 32, the fraction of uranium was increased from 0.009 gUNH/g to 0.2 gUNH/g. The resulting differential attenuation plot is shown in Figure 33. When the correct assumptions about matrix composition and density-thickness are used, the activity differences between gamma ray energies are minimized. In this way, the multiple energy peaks provide information on the concrete floor matrix and therefore the appropriate attenuation corrections needed for the U-235 mass calculation.

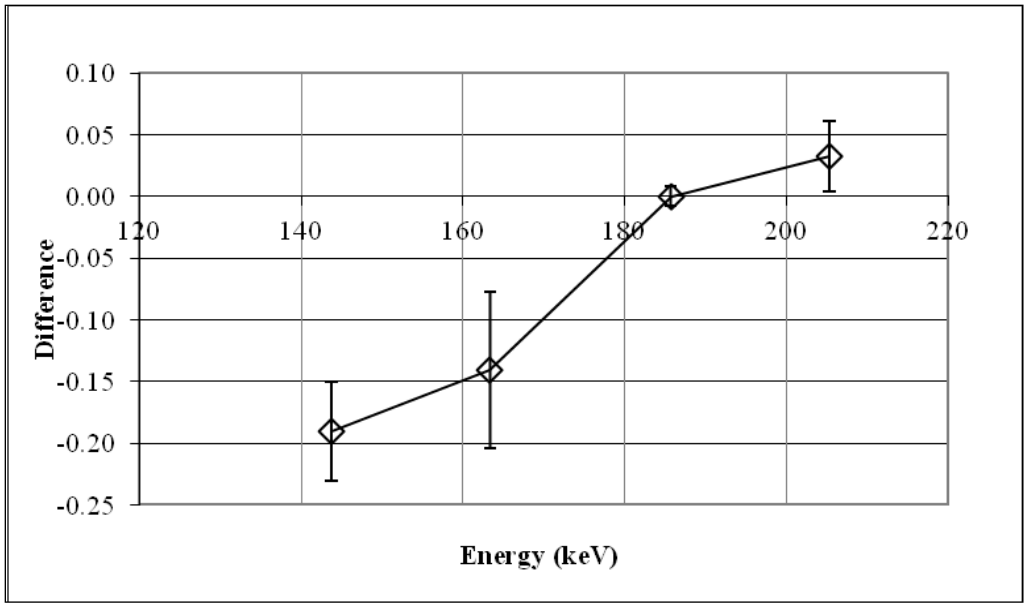

Figure 33: HEU solution in 3.4 cm of concrete with an initially estimated weight fraction of 0.009 gUNH/g.

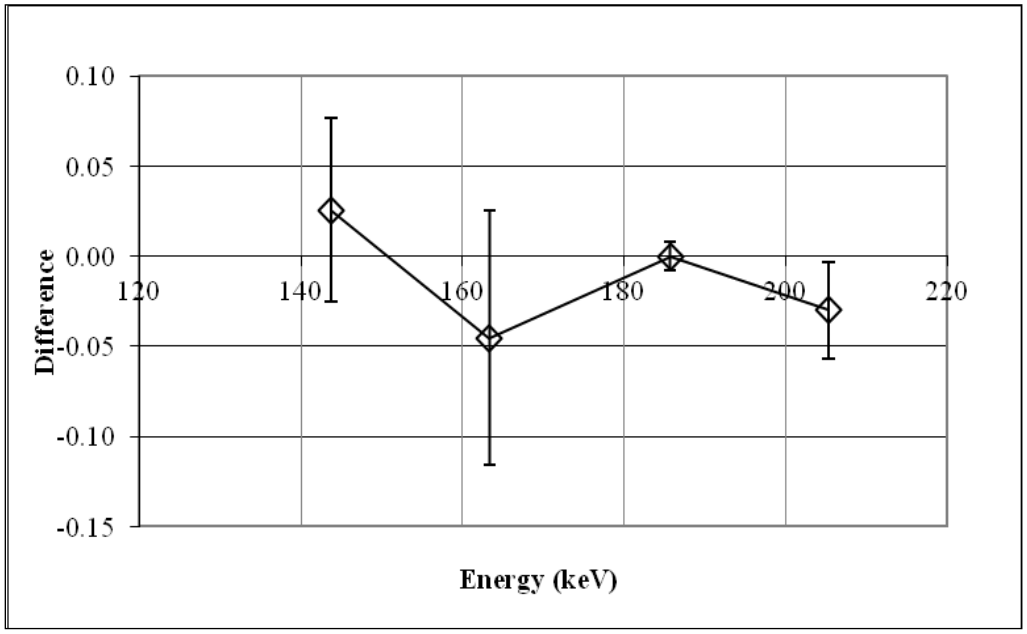

Figure 34: HEU solution in 3.4 cm of concrete with a corrected weight fraction of 0.2 gUNH/g.

The results of the HPGe spectra analysis using the combination of small-angle Compton scattering and differential attenuation techniques are shown below in Table 9.

Table 9: Results of HPGe spectra analyzed by small-angle scatter analysis and differential attenuation methods to determine deposit depths.

Map ID	Small-Angle DensDepth (g/cm2)	Differential Attn DensDepth (g/cm2)	Effective Depth (cm)	1-Sigma Uncertainty (%)
1	1.2	1.2	0.5	11%
2	0.1	0.5	0.2	20%
3	6.2	6.2	3.4	9%
4	0.4	0.4	0.1	13%
5	0.1	0.1	0.02	16%
6	0.1	0.6	0.3	21%
7	0.1	0.5	0.2	20%
8	0.7	0.7	0.3	12%
9	0.2	0.5	0.4	15%
10	Background too high			-
11	Background too high			-
12	3.9	3.9	2.2	10%
13	Background too high			-

The values reported in the second column of the table show the initial estimate of the density-depth of the deposit from small-angle analysis. This is calculated from the formula below which was previously discussed in the theory section of this paper.

$$\frac{N_{sa}}{N_{\gamma}} = \frac{k[1 - e^{-\mu\rho x}(1 + \mu\rho x)]}{(1 - e^{-\mu\rho x})}$$

The third column shows the revised estimate of the density-depth after differential attenuation analysis. In several cases (Map ID #2, #6, #7, and to a lesser degree in #9), the small-angle density depth is shown as 0.1 and is quite different from the differential attenuation density depth shown for the same Map ID location. In the instances where the small-angle density depth value was determined to be 0.1, the analysis of the step-to-peak ratio basically told us

that the uranium deposit was on the surface of the concrete and that there was no intervening concrete between the source and the detector. Therefore, no beneficial data could be gathered from the small-angle Compton scattering analysis at these points and the effective depth was essentially determined from performing the differential attenuation analysis alone. Similar to what was determined during the validation study and the associated uncertainty analysis, surface deposits that are unable to include the effects of small-angle Compton scattering to improve unknowns of the holdup situation must rely solely on assumptions and knowledge from intuition and experience to properly adjust all of the variables in the differential attenuation analysis and get a defensible result. Therefore, this is why the uncertainty associated with these particular point locations is increased above the other locations where the small-angle step-to-peak ratio could be determined and utilized in the overall analysis.

The last column shows the effective depth of the deposit based on the uranium-concrete density determined by differential attenuation analysis. The effective depth is the depth of a uniformly distributed uranium-concrete mixture that would produce the equivalent small-angle scattering ratio as that which was observed in the spectrum for each site.

Of the thirteen HPGe measurements that were taken to utilize Small-angle Compton scattering principles, the majority confirmed that the solution spills became fixed near the top surface of the concrete. The three sites showing the highest concentration of U-235 in concrete, sites 1, 2, and 8, all appear to be within ½ cm of the top. Two of the nine locations indicated a deeper deposit of uranium in the concrete – site 3 at 3.4 cm and site 12 at 2.2 cm. Three of the locations (10, 11, and 13) were not able to produce good data because the background was too high. This means that the strength of the gamma rays coming from the floor in those locations were weaker or identical to the strength of the gamma rays that came from surrounding process equipment of material when the tungsten plug was in front of the detector. If this floor application is ever repeated, it would be ideal to apply this method to different locations on the floor and to devise a better shield that kept gamma rays from entering the detector crystal from the back of the detector.

The results of this N_{SA}/N_{γ} formula that show the density-depth in concrete for a given step-to-peak ratio are also plotted below in Figure 34.

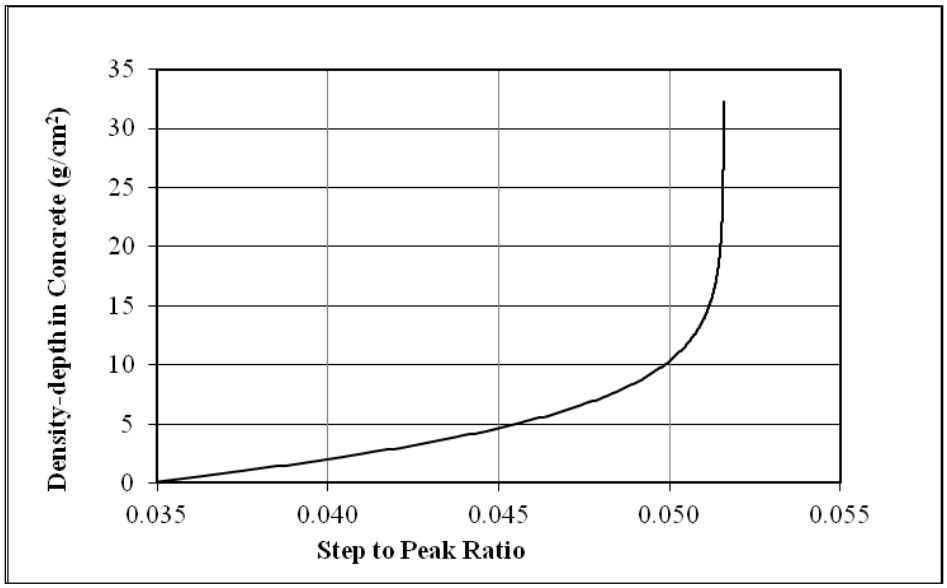

Figure 35: The density-depth in concrete for a step-to-peak ratio based on N_{sa}/N_{γ} formula.

u. Final Results

Low-resolution NaI holdup measurements can be corrected for self-attenuation for a final quantitative holdup result if the amount of concrete interacting with the uranium is known. In the past before Small-angle Compton scattering, a range of final answers had to be reported depending on a range of assumed deposit depth varying between 0" - 1" into the concrete. The high-resolution HPGe measurements and the Small-Angle Compton scattering analysis indicate that the uranium is in fact been deposited near the surface for most of the locations identified, but there were instances of deeper penetrations that had to be considered. In order to complete the analysis of floor holdup, an average deposit depth of 0.23±0.14 cm was applied to the majority of the floor locations that showed activity. A deeper deposit depth was used in the two localized regions, as indicated by sites 3 and 12 in Figure 30 above. Self-attenuation calculations are therefore based on the quantities of both uranium and concrete indicated for each measurement location.

The results of these calculations are presented in Appendix B below. The locations in the table which are highlighted in gray are those locations where a deeper deposit depth was used. Points # 22, 23, and 28 in Section 3 correspond to the spill region represented by HPGe site 12, and Points # 4 and 8 in Section 5 correspond to the region represented by HPGe site 3. In order to calculate a total holdup quantity, the results are averaged for each of the twelve sections defined for the floor, then that average is applied to the area of the floor section. These results are shown in Appendix B and are also summarized in Table 10 below.

Table 10: Summary of final U-235 holdup quantities in entire concrete floor**.**

Concrete Floor Section	Holdup Quantity (g U-235)	Average Areal Density (g U-235/cm^2)
1	978	0.0022
2	821	0.0018
3	2144	0.0048
4	5136	0.0115
5	5104	0.0229
6	1656	0.0027
7	784	0.0013
8	445	0.0007
9	829	0.0013
10	10487	0.0168
11	6871	0.0110
12	1863	0.0022
Total:	**37119**	**0.0056**

The total estimated U-235 holdup in the concrete floor based on both low-resolution and high-resolution measurements is 37.1 kg U-235. The specific NaI measurement locations corresponding to the entries in Appendix B, column labeled 0.23 cm depth, are shown in Figure 29 above. The most probable result of 37.1kg U-235, using the average depth of 0.23cm, is bracketed with calculations using a depth that is two standard deviations below (0.0cm) and two standard deviations above (0.51cm) the average depth of 0.23cm. The lower two-sigma bound is shown in Appendix B, column labeled "0 cm depth." In addition, the area of the two deep deposits was expanded to include larger regions in the upper bound. The upper bound results are shown in Appendix B, column labeled 0.51 cm depth. Again, the deep deposits are shaded in gray in Appendix B. Using these depths results gives a lower two-sigma bound of 35.2kg U-235 and an upper two-sigma bound of 40.0kg of U-235 within the concrete floor.

Chapter 6: Additional Applications and Future Work

Using Small-Angle Compton scattering as a way to determine the depth of U-235 penetration into a concrete floor is a very specific and unique application of this non-destructive analysis technique, but there are many other practical applications that can be used across the nuclear industry and in nuclear non-proliferation work. This section will discuss these other potential uses for the Small-angle Compton scattering NDA methods that were described in this paper.

v. Other uses of Small-angle Compton Scattering

Shielding and attenuation, whether intentional or not, are very prominent when dealing with gamma rays and must be accounted for when trying to analyze the quantity or condition of nuclear materials. Unfortunately, shielding thicknesses are often unknown and require the use of gross assumptions and guesses when trying to model a situation. Small-angle Compton scattering is a proven method to provide detailed information about the shielding condition of nuclear materials and can allow nuclear engineers and nuclear investigators to have another method of analyzing nuclear materials correctly.

One obvious place this analysis method can be used is in DOE nuclear production facilities. These facilities often create copious amounts of contaminated trash or process equipment that must be properly disposed of. In order to dispose of these radioactive items, a full characterization and quantitative analysis must be done to identify the contents of the item, ensure it meets criticality safety limitations for the chosen container, and ensure quantities and activities of the radioactive contents of the container are known for proper handling and final disposition. Radioactive materials discarded from DOE facilities are often comingled with other matrix materials (combustibles, metal, plastic, etc.) or even inside dense process equipment (glove boxes, ductwork, pipes, etc.). All of these conditions cause attenuation and shielding of the gamma rays that make analysis very difficult, especially when using non-destructive methods. Non-destructive analysis is too cost effective and versatile compared to other analysis methods to be replaced, so it is not going away. But, any improvements that can be implemented to strengthen the capabilities of non-destructive analysis are highly desirable.

Using Small-Angle Compton Scattering to identify the amount of shielding that is present is extremely important in getting accurate results when analyzing nuclear waste materials. This method takes unknown situations that cause high levels of uncertainty away and gives you valuable information that otherwise is almost impossible to obtain.

Another situation that Small-angle Compton scattering can be used is in nuclear non-proliferation work or nuclear inspection work. Several countries around the world already have nuclear weapons capabilities and several more are desperately trying to achieve these capabilities. The efforts of the United States, the Nuclear Regulatory Commission (NRC), the United Nations (UN), and several international watchdog groups that monitor nuclear activity are some of the major reasons why most of these dangerous countries have not been able to create nuclear weapons. These groups often monitor and perform routine inspections of all countries' nuclear sites to ensure enrichment of U-235 or possession of large quantities of U-235 is not taking place. Obviously, countries that do not want these watchdog groups to know that they possess U-235 materials are going to try their best to hide them. Ultimately, the only way to hide U-235 material is to shield it and claim that it is not there or it is in extremely low quantities for peaceful power production purposes.

Figure 35 below shows another rough example of what an adversary could do to shield nuclear material away from a UN inspector.

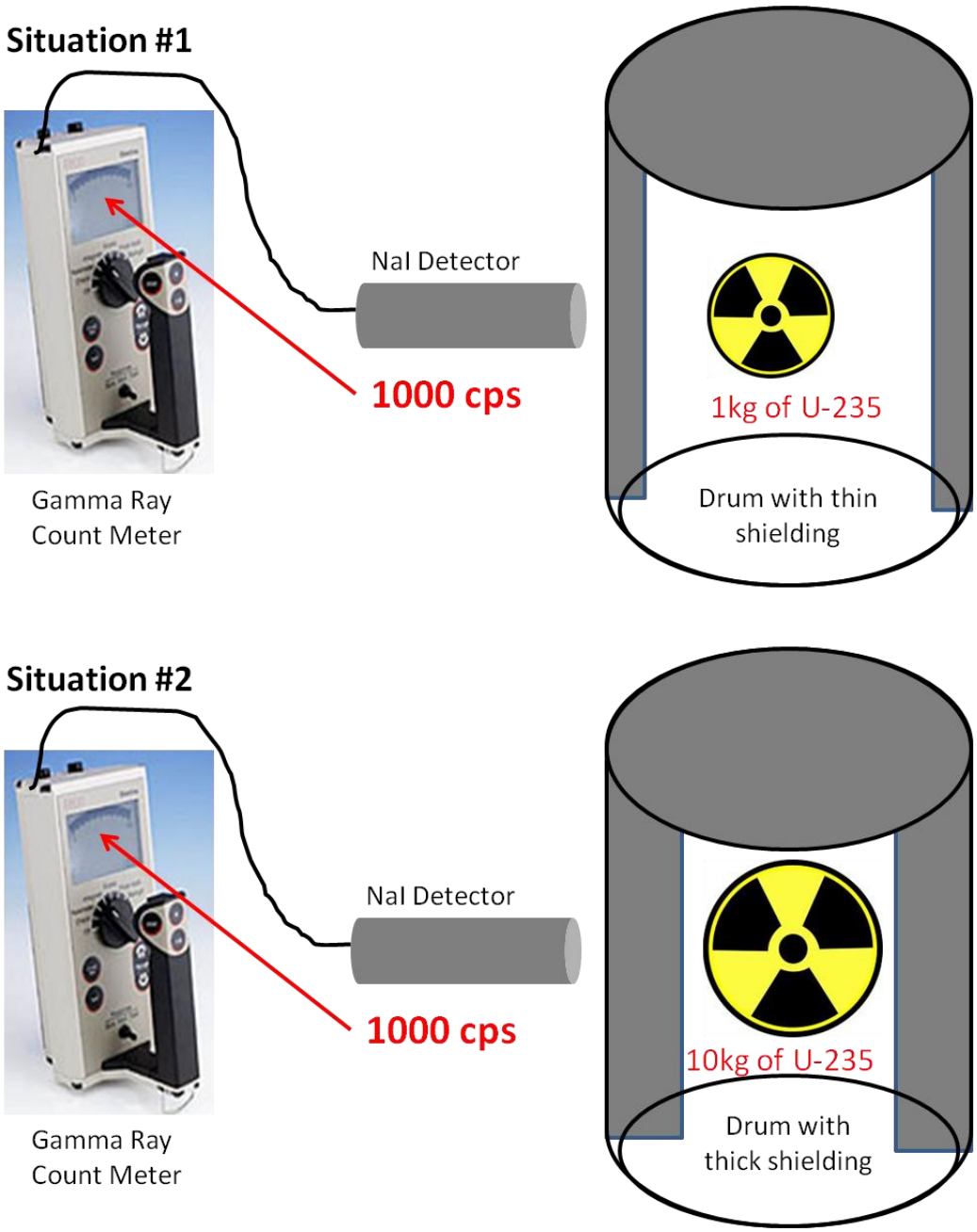

Figure 36: Example of shielding U-235 material in a storage drum.

The gamma rays coming off the U-235 materials appear to be equal even though the quantities of U-235 are very different. This is solely due to the thickness of shielding material that the gamma rays must traverse to get to the NaI detector. If an adversary said both of the drum

conditions were the same, there would be no way to tell that they were hiding large quantities of U-235 unless you were able to inspect the drums thoroughly inside and out or weigh them. Additionally, these quantities could be hidden behind a dense wall and even if nuclear investigators suspected that U-235 materials were present, they could grossly underestimate the quantities that are there because they have no way to determine or account for the effects of the shielding.

Using a high-resolution HPGe detector in the same situations along with the principles of Small-Angle Compton scattering would very quickly and easily give you a much better understanding of the shielding that is present directly between your detector and the radioactive material in almost any situation. Even if detailed analysis couldn't be done on the spot, simply understanding what it means when you see a large discontinuity in the 185.72keV peak could make all the difference in identifying a potentially dishonest situation with an adversary trying to shield or hide U-235 material. Also, if it were desired to try and quantify the amount of U-235 that was present in a drum or another container, knowing the thickness of the attenuating material would be a principle piece of information in trying to get an accurate estimation of the quantity. Figure 36 below shows how a quick evaluation of this discontinuity discloses that more shielding is present and deeper investigation should be conducted.

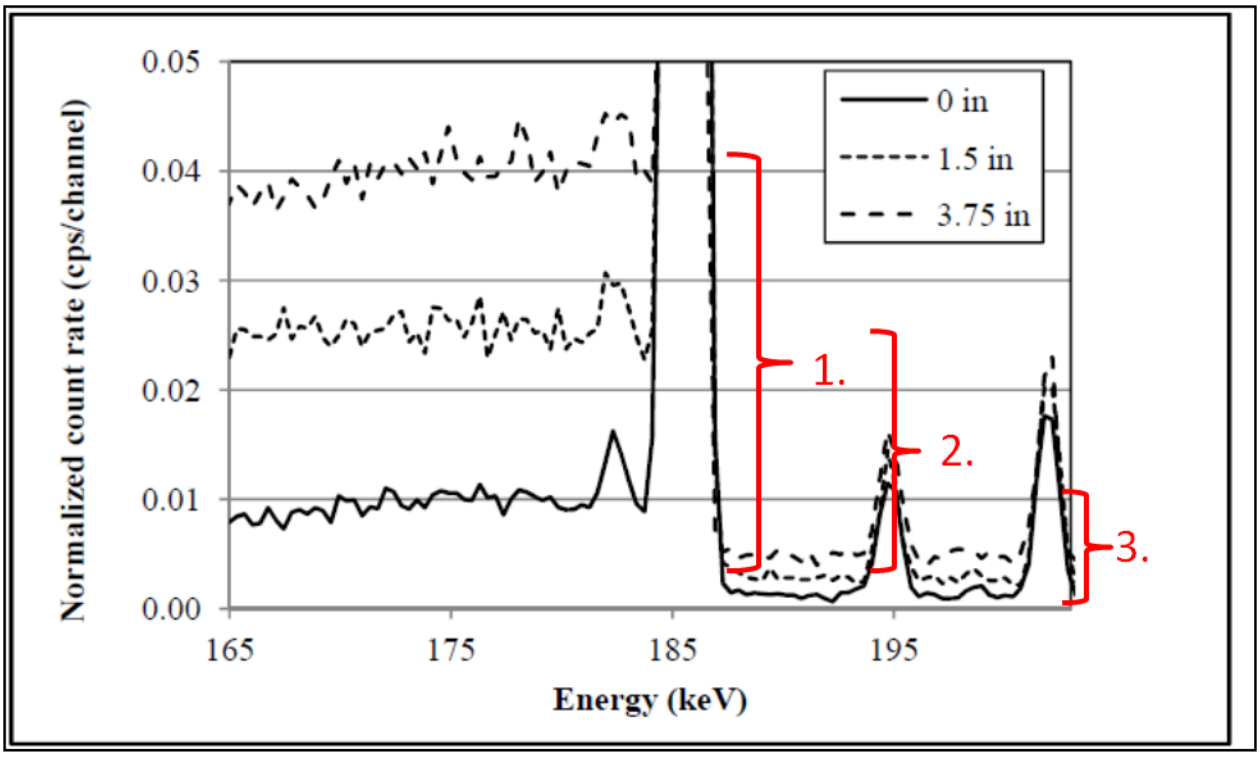

1. Discontinuity from Small-angle Compton scattering is large around the 185.72keV peak meaning U-235 gamma rays are being heavily shielded.

2. Discontinuity from Small-angle Compton scattering is medium around the 185.72keV peak meaning U-235 gamma rays are being moderately shielded.

3. Discontinuity from Small-angle Compton scattering is negligible around the 185.72keV peak meaning U-235 gamma rays are not being shielded.

Figure 37: Example of 3 possible shielding conditions which would give very easily identifiable discontinuities in the 185.72keV gamma ray coming from U-235 material.

If a nuclear engineer at a DOE facility or a nuclear inspector at an adversary's nuclear facility took a high resolution spectrum of a contaminated waste container or a sophisticated storage container for U-235 material, understanding the principles and meanings of the Small-Angle Compton scattering phenomenon could be a critical tool in making accurate assumptions and judgments.

w. Future Work

Since Small-angle Compton scattering is a new and exceptionally unknown analysis technique, very little has been done to expand its application beyond the initial validation studies and contaminated floor experiment that are explained above. Small-angle Compton scattering could have an unlimited amount of uses and applications that could improve or revolutionize the way non-destructive analysis is done on nuclear materials, but very few of these conditions have been investigated or verified. Therefore, experiments and validations of Small-angle Compton scattering using different shielding materials, quantities of U-235, and other radioactive materials could be done to continue to strengthen the understanding of this analysis technique and the best ways to apply it. If desired or needed, additional experiments could be set up to continue to refine this analysis technique and increase its applicability to a wide range of real-world and important situations. Furthermore, the process of analyzing data using the Small-angle Compton scattering techniques discussed in this thesis paper is very cumbersome and error prone. Much work could be done to automate some of the data capture and analysis methods to reduce errors and ensure consistent and accurate results.

Chapter 7: Overall Conclusions

In the most simplistic definition, Small-angle Compton scattering can be used to determine the amount of intervening material between a radioactive source and a detector. While this doesn't sound like a game changing piece of information, understanding the amount of shielding and attenuation that intervening material has on gamma rays is critical to the understanding and analysis of most nuclear material investigations. Not knowing the amount of intervening material that is attenuating critical gamma rays causes the need for gross assumptions and leads to inaccurate results with high levels of uncertainty. Non-destructive analysis can be a challenging method for evaluating nuclear materials, but it has enough advantages to make it a method of choice in many situations. Many other unknowns and assumptions exist when performing non-destructive analysis, but few have as big of an effect on the final results as shielding and attenuation. Being able to understand and accurately estimate the shielding conditions surrounding various nuclear materials through the use of Small-angle Compton scattering methods is a game changing technique that can have far reaching applications and benefits as it becomes better known and implemented into different situations. The invention of this analysis technique as well as the promising results of the initial validations studies and real-world applications are extremely impressive, but only scratch the surface of how Small-angle Compton scattering may change the landscape of non-destructive testing and analysis throughout the nuclear industry. If the method can be refined and some of the analysis requirements can be automated, the applications of Small-angle Compton scattering can be far reaching and instrumental in advancing the capabilities of non-destructive techniques in many beneficial situations. Only time will tell if the concept of using Small-angle Compton scattering will catch on amongst the nuclear industry as a non-destructive analysis tool and if others are willing to spend research dollars to further develop and utilize it, but the groundwork and initial proof of this concept has definitely been shown to be a legitimate and beneficial NDA tool by Dr. Oberer, Dr. Chiang, and Ms. Gunn.

BIBLIOGRAPHY

1. R. B. Oberer, C. A. Gunn, L. G. Chiang, *Small-angle Compton scattering used to determine the depth of a radioactive source in material and to estimate gamma ray attenuation*, submitted to Nuclear Instruments and Methods in Physics Research Section A: Accelerators, Spectrometers, Detectors and Associated Equipment.

2. C.A. Gunn, R.B. Oberer, L.G. Chiang, *Validation Study of the Measurement of Holdup Deposits in Concrete by Gamma Spectrometry Using Differential Attenuation Coupled with Small-Angle Analysis Technique*, NSRD status report, October 18, 2012

3. Berger, M.J., Hubbell, J.H., Seltzer, S.M., Chang, J., Coursey, J.S., Sukumar, R., Zucker, D.S., and Olsen, K. (2010), XCOM: Photon Cross Section Database (version 1.5). National Institute of Standards and Technology, Gaithersburg, MD. [Online] http://physics.nist.gov/xcom

4. M.J. Berger, J.S. Coursey, M.A. Zucker and J. Chang, "Stopping-Power and Range Tables for Electrons, Protons, and Helium Ions." Material composition http://physics.nist.gov/cgi-bin/Star/compos.pl, Concrete http://physics.nist.gov/cgi-bin/Star/compos.pl?matno=144

5. C. A. Gunn, R. B. Oberer, L. G. Chiang, "Comparison Study of B-1 Wing Floor Holdup (2006 to 2012)," June 7, 2012

6. J. G. Hackworth,"Nuclear Criticality Safety Evaluation of Holdup in the 9212 B-1 and C-1 Wing Floors", Y/DD-1377, April 2010

7. R. B. Oberer, L. G. Chiang, C. A. Gunn, "The Use of High Resolution Gamma Spectroscopy to Improve Floor-Holdup Measurements," Y/EN-8269, May 26, 2009

8. R.B. Oberer, C.A. Gunn, L.G. Chiang, "Evaluation of Uranium Holdup in a Concrete Floor Using High and Low Resolution Gamma Spectrometry" Technical Report Y12-NDA-12-055, Y-12 National Security Complex, November 2012

9. Russo, P.A. June 2005. "Gamma Ray Measurements of Holdup Plant-Wide: Application Guide for Portable, General Approach," LA-14206.

10. T.P. Donohoue, R. Martin, J. McCague, "Performance Testing and Validation Plan for HMS4 Quantitative Gamma Measurements, K-25/K-27 D&D Project, East Tennessee Technology Park, Oak Ridge, Tennessee." Technical Report BJC/OR-2931/R2, Prepared for U.S. Department of Energy by Bechtel Jacobs Company, May 2008.

11. ORTEC, "A Complete In-Situ NDA Gamma ray Analysis for a Wide Variety of Samples." Iso-Cart Mobile Assay System, Prepared by Advanced Measurement Technology (AMETEK), January 2012.

12. Rick B. Oberer, Cynthia A. Gunn, Lisa G. Chiang, Michael C. Mattmann, "Small-angle Compton Scattering to Determine the Attenuation of Gamma Rays from HEU," Proceedings of the American Nuclear Society: 2011 Winter Meeting, October 30 – November 3, 2011, Washington, D.C.

13. R.B. Oberer, C.A. Gunn, L.G. Chiang, R.E. Valiga, J.A. Cantrell, "Small-angle Compton Scattering to Determine the Depth of a Radioactive Source in Matter," Technical Report RP 900000-0006, Y-12 National Security Complex, April 2011.

14. R. B. Oberer, L. G. Chiang, M. J. Norris, C. A. Gunn, B. C. Adaline, "The use of Tl-208 gamma rays for safeguards, nondestructive-assay (NDA) measurements," INMM Central Regional Chapter, 2009 Fall Meeting, Oak Ridge, Tennessee, November 3-4, 2009, Y/EN-8270 May 26, 2009.

15. ORTEC Online White Paper, “Why High-Purity Germanium (HPGe) Radiation Detection Technology is Superior to Other Detector Technologies for Isotope Identification.” http://www.ortec-online.com/papers/la_ur_03_4020.pdf.

16. J.K. Sprinkle, Jr., R. Cole, M.L. Collins, T-S Hsue, P.A. Russo, R. Siebelist, H.A. Smith, Jr., R.N. Ceo, S. E. Smith, "Low-resolution Gamma ray Measurements of Process Holdup," LA-UR-96-3482, September 1996.

APPENDIX

APPENDIX A

The details of converting the Klein-Nishina differential cross section from solid angle are provided in this appendix. This equation relates the differential cross-section by angle of scatter for Compton scattering. It is typically written as

$$\frac{d\sigma}{d\Omega} = \frac{Z}{2}\alpha^2 r_c^2 \left(\frac{E}{E_\gamma}\right)^2 \left[\left(\frac{E}{E_\gamma}\right) + \left(\frac{E_\gamma}{E}\right) - 1 + \cos^2(\theta)\right]$$

Where Ω is the solid angle, E_γ is the original gamma-ray energy, 185.72keV in the case of a U-235 measurement, E is the energy of the scattered gamma ray, θ is the angle of scatter from the original direction, Z is the atomic-number of the element, and $\alpha^2 r_c^2 = 0.0794\text{barns}$ is the square of the classical electron radius.

The ratio of the scattered energy to the original energy comes from conservation of energy and momentum

$$\left(\frac{E}{E_\gamma}\right) = \frac{1}{1 + \frac{E_\gamma}{m_e c^2}(1 - \cos(\theta))}$$

where $m_e c^2 = 511keV$ is the rest-mass energy of an electron. Because the small-angle scatter results in a continuum from the peak energy E_γ downward, it must be normalized by energy.

The count rate in the continuum depends on the width in energy of the region counted. Therefore the differential cross-section with respect to energy is needed. This differential cross section is determined by

$$\frac{d\sigma}{dE} = \frac{d\sigma}{d\Omega}\frac{d\Omega}{d\theta}\frac{d\theta}{dE}$$

Where

$$\frac{d\Omega}{d\theta} = 2\pi \sin(\theta)$$

And

$$\frac{d\theta}{dE} = -\frac{[\cos^2(\theta) - 2\cos(\theta) + 1]\mathrm{E}_\gamma^2 + 2m_e c^2[1 - \cos(\theta)]\mathrm{E}_\gamma + (m_e c^2)^2}{m_e c^2 \mathrm{E}_\gamma^2 \sin(\theta)}$$

Multiplying the three factors results in

$$\frac{d\sigma}{d\mathrm{E}} = \pi \mathrm{Z}\alpha^2 \mathrm{r}_\mathrm{c}^2 \left(\frac{\mathrm{E}}{\mathrm{E}_\gamma}\right)^2 \left[\left(\frac{\mathrm{E}}{\mathrm{E}_\gamma}\right) + \left(\frac{\mathrm{E}_\gamma}{\mathrm{E}}\right) - 1 + \cos^2(\theta)\right]$$

$$\cdot \left[\frac{[\cos^2(\theta) - 2\cos(\theta) + 1]\mathrm{E}_\gamma^2 + 2m_e c^2[1 - \cos(\theta)]\mathrm{E}_\gamma + (m_e c^2)^2}{m_e c^2 \mathrm{E}_\gamma^2}\right]$$

The small-angle scattering continuum intersects the peak at a zero scattering angle θ. Therefore the differential cross-section is evaluated at zero.

$$\left.\frac{d\sigma}{d\mathrm{E}}\right|_{\theta=0} = 2\pi \mathrm{Z}\alpha^2 \mathrm{r}_\mathrm{c}^2 \left[\frac{m_e c^2}{\mathrm{E}_\gamma{}^2}\right] = 254.9(\mathrm{keV} \cdot \mathrm{barn}) \left(\frac{\mathrm{Z}}{\mathrm{E}_\gamma{}^2}\right)$$

The differential cross-section for $\theta = 0$ depends only on the atomic-number Z of the material and the energy E_γ of the gamma ray. The fraction of interactions which are small-angle Compton scatters k, is given by

$$k = 254.9(\mathrm{keV} \cdot \mathrm{barn}) \left(\frac{\mathrm{Z}}{\sigma \times \mathrm{E}_\gamma{}^2}\right) =$$

where the total cross-section σ is taken from XCOM data.

APPENDIX B

This is the corrected areal density measurements of the concrete floor taken in May 2012 (g ^{235}U/cm2). Holdup in concrete was measured with a NaI detector. Calculations for self-attenuation included depth of the deposit determined by HPGe measurements and small angle/differential attenuation analysis. An average deposit depth of 0.23 cm in the concrete was used in calculating holdup for the majority of the floor, with deeper deposits used for specific sites, if indicated.

Table B1: Uncorrected areal density of floor measurements (g ^{235}U/cm2).

Section	Point ID #	Date	0 cm depth Corrected Areal Dens ($g^{235}U/cm2$)	0.23 cm depth Corrected Areal Dens ($g^{235}U/cm2$)	0.51 cm depth Corrected Areal Dens ($g^{235}U/cm2$)
1	1	5/8/2012	0.0035	0.0036	0.0038
1	2	5/8/2012	0.0017	0.0018	0.0019
1	3	5/8/2012	0.0045	0.0047	0.0048
1	4	5/8/2012	0.0011	0.0012	0.0012
1	5	5/8/2012	0.0019	0.0019	0.0020
1	6	5/8/2012	0.0020	0.0020	0.0021
1	7	5/8/2012	0.0011	0.0011	0.0012
1	8	5/8/2012	0.0011	0.0011	0.0012
1	9	5/8/2012	0.0016	0.0016	0.0017
1	10	5/8/2012	0.0027	0.0028	0.0029
1	11	5/8/2012	0.0029	0.0030	0.0032
1	12	5/8/2012	0.0012	0.0012	0.0013
1	13	5/8/2012	0.0008	0.0008	0.0009
1	14	5/8/2012	0.0014	0.0015	0.0016
1	15	5/8/2012	0.0011	0.0012	0.0012
1	16	5/8/2012	0.0045	0.0047	0.0048
1	17	5/8/2012	0.0030	0.0031	0.0032
1	18	5/3/2006	0.0015	0.0015	0.0016
1	19	5/8/2012	0.0040	0.0041	0.0043
1	20	5/8/2012	0.0008	0.0008	0.0009
1	21	5/8/2012	0.0020	0.0021	0.0022
		Section 1 Average Areal Density:	0.0021	0.0022	0.0023
		Section 1 Area (cm2):	445935		
		Section 1 Holdup Sub-total (g U-235):	945	978	1018

Table B1 Continued: Uncorrected areal density of floor measurements (g ^{235}U/cm2).

Section	Point ID #	Date	0 cm depth Corrected Areal Dens ($g^{235}U/cm2$)	0.23 cm depth Corrected Areal Dens ($g^{235}U/cm2$)	0.51 cm depth Corrected Areal Dens ($g^{235}U/cm2$)
2	2	5/8/2012	0.0008	0.0008	0.0008
2	3	5/8/2012	0.0011	0.0011	0.0011
2	4	5/8/2012	0.0013	0.0014	0.0014
2	5	5/8/2012	0.0011	0.0011	0.0011
2	6	5/8/2012	0.0064	0.0066	0.0069
2	7	5/8/2012	0.0038	0.0039	0.0040
2	8	5/8/2012	0.0010	0.0010	0.0010
2	9	5/8/2012	0.0021	0.0022	0.0023
2	10	5/8/2012	0.0039	0.0040	0.0042
2	11	5/8/2012	0.0014	0.0014	0.0015
2	12	5/8/2012	0.0012	0.0012	0.0013
2	13	5/8/2012	0.0010	0.0010	0.0010
2	14	5/8/2012	0.0008	0.0009	0.0009
2	15	5/8/2012	0.0032	0.0033	0.0034
2	16	5/8/2012	0.0011	0.0012	0.0012
2	17	5/8/2012	0.0006	0.0007	0.0007
2	18	5/8/2012	0.0026	0.0027	0.0028
2	19	5/8/2012	0.0011	0.0011	0.0011
2	20	5/8/2012	0.0014	0.0014	0.0015
2	21	5/8/2012	0.0019	0.0020	0.0021
2	22	5/8/2012	0.0020	0.0021	0.0021
2	23	5/8/2012	0.0002	0.0002	0.0002
2	24	5/8/2012	0.0002	0.0002	0.0002
2	25	5/8/2012	0.0003	0.0003	0.0003
2	26	5/8/2012	0.0003	0.0003	0.0003
2	27	5/8/2012	0.0049	0.0050	0.0052
2	28	5/8/2012	0.0025	0.0026	0.0027
2	29	5/8/2012	0.0010	0.0011	0.0011
		Section 2 Average Areal Density:	0.0018	0.0018	0.0019
		Section 2 Area (cm2):	445935		
		Section 2 Holdup Sub-total (g U-235):	795	821	856

Table B1 Continued: Uncorrected areal density of floor measurements (g ^{235}U/cm2).

Section	Point ID #	Date	0 cm depth Corrected Areal Dens ($g^{235}U/cm2$)	0.23 cm depth Corrected Areal Dens ($g^{235}U/cm2$)	0.51 cm depth Corrected Areal Dens ($g^{235}U/cm2$)
3	1	5/8/2012	0.0022	0.0023	0.0024
3	2	5/8/2012	0.0016	0.0017	0.0017
3	3	5/8/2012	0.0012	0.0012	0.0013
3	4	5/8/2012	0.0008	0.0008	0.0008
3	5	5/8/2012	0.0007	0.0008	0.0008
3	6	5/8/2012	0.0014	0.0015	0.0016
3	7	5/8/2012	0.0013	0.0014	0.0014
3	8	5/8/2012	0.0048	0.0050	0.0052
3	9	5/8/2012	0.0026	0.0027	0.0028
3	10	5/8/2012	0.0017	0.0017	0.0018
3	11	5/8/2012	0.0009	0.0009	0.0009
3	12	5/8/2012	0.0008	0.0008	0.0008
3	13	5/8/2012	0.0007	0.0007	0.0010
3	14	5/8/2012	0.0019	0.0020	0.0026
3	15	5/8/2012	0.0013	0.0014	0.0014
3	16	5/8/2012	0.0045	0.0047	0.0049
3	17	5/8/2012	0.0010	0.0010	0.0014
3	18	5/8/2012	0.0003	0.0003	0.0004
3	19	5/8/2012	0.0004	0.0004	0.0005
3	20	5/8/2012	0.0008	0.0008	0.0011
3	21	5/8/2012	0.0012	0.0012	0.0016
3	22	5/8/2012	0.0087	0.0118	0.0118
3	23	5/3/2006	0.0201	0.0273	0.0273
3	24	5/3/2006	0.0003	0.0003	0.0004
3	25	5/3/2006	0.0019	0.0020	0.0026
3	26	5/8/2012	0.0165	0.0170	0.0224
3	27	5/8/2012	0.0114	0.0117	0.0154
3	28	5/8/2012	0.0231	0.0313	0.0313
		Section 3 Average Areal Density:	0.0041	0.0048	0.0053
		Section 3 Area (cm2):	445935		
		Section 3 Holdup Sub-total (g U-235):	1818	2144	2349

Table B1 Continued: Uncorrected areal density of floor measurements (g ^{235}U/cm2).

Section	Point ID #	Date	0 cm depth Corrected Areal Dens ($g^{235}U/cm2$)	0.23 cm depth Corrected Areal Dens ($g^{235}U/cm2$)	0.51 cm depth Corrected Areal Dens ($g^{235}U/cm2$)
4	1	5/8/2012	0.0286	0.0295	0.0308
4	2	5/8/2012	0.0097	0.0100	0.0104
4	3	5/8/2012	0.0323	0.0332	0.0346
4	4	5/8/2012	0.0031	0.0032	0.0042
4	5	5/8/2012	0.0031	0.0032	0.0033
4	6	5/8/2012	0.0272	0.0280	0.0292
4	7	5/8/2012	0.0095	0.0098	0.0101
4	8	5/8/2012	0.0268	0.0276	0.0288
4	8	5/3/2006	0.0255	0.0263	0.0274
4	9	5/3/2006	0.0165	0.0170	0.0177
4	10	5/3/2006	0.0071	0.0073	0.0076
4	11	5/3/2006	0.0010	0.0010	0.0011
4	12	5/8/2012	0.0038	0.0039	0.0040
4	13	5/8/2012	0.0121	0.0124	0.0130
4	14	5/8/2012	0.0094	0.0097	0.0101
4	15	5/8/2012	0.0260	0.0268	0.0280
4	16	5/8/2012	0.0075	0.0078	0.0081
4	17	5/8/2012	0.0089	0.0092	0.0096
4	18	5/8/2012	0.0104	0.0108	0.0112
4	19	5/8/2012	0.0017	0.0018	0.0019
4	20	5/8/2012	0.0091	0.0094	0.0098
4	21	5/8/2012	0.0022	0.0023	0.0024
4	22	5/8/2012	0.0080	0.0082	0.0086
4	23	5/8/2012	0.0091	0.0093	0.0097
4	24	5/8/2012	0.0105	0.0108	0.0112
4	25	5/8/2012	0.0028	0.0028	0.0030
4	26	5/8/2012	0.0041	0.0042	0.0044
4	27	5/8/2012	0.0071	0.0073	0.0076
4	28	5/8/2012	0.0054	0.0056	0.0058
4	29	5/8/2012	0.0070	0.0073	0.0076
4	30	5/3/2006	0.0109	0.0112	0.0117
		Section 4 Average Areal Density:	0.0112	0.0115	0.0120
		Section 4 Area (cm2):	445935		
		Section 4 Holdup Sub-total (g U-235):	4982	5136	5361

Table B1 Continued: Uncorrected areal density of floor measurements (g ^{235}U/cm2).

Section	Point ID #	Date	0 cm depth Corrected Areal Dens ($g^{235}U/cm2$)	0.23 cm depth Corrected Areal Dens ($g^{235}U/cm2$)	0.51 cm depth Corrected Areal Dens ($g^{235}U/cm2$)
5	1	5/8/2012	0.0257	0.0265	0.0406
5	2	5/8/2012	0.0401	0.0413	0.0637
5	3	5/8/2012	0.0200	0.0206	0.0316
5	4	5/8/2012	0.0287	0.0454	0.0454
5	5	5/8/2012	0.0146	0.0151	0.0230
5	6	5/8/2012	0.0077	0.0080	0.0083
5	7	5/8/2012	0.0187	0.0192	0.0200
5	8	5/8/2012	0.0142	0.0223	0.0223
5	9	5/8/2012	0.0074	0.0076	0.0079
		Section 5 Average Areal Density:	0.0197	0.0229	0.0292
		Section 5 Area (cm2):	222967		
		Section 5 Holdup Sub-total (g U-235):	4385	5104	6515

Table B1 Continued: Uncorrected areal density of floor measurements (g ^{235}U/cm2).

Section	Point ID #	Date	0 cm depth Corrected Areal Dens ($g^{235}U/cm2$)	0.23 cm depth Corrected Areal Dens ($g^{235}U/cm2$)	0.51 cm depth Corrected Areal Dens ($g^{235}U/cm2$)
6	1	5/8/2012	0.0026	0.0027	0.0028
6	2	5/8/2012	0.0020	0.0021	0.0021
6	3	5/8/2012	0.0106	0.0110	0.0114
6	4	5/8/2012	0.0057	0.0059	0.0061
6	5	5/8/2012	0.0047	0.0049	0.0051
6	6	5/8/2012	0.0046	0.0047	0.0049
6	7	5/8/2012	0.0022	0.0023	0.0024
6	8	5/8/2012	0.0001	0.0001	0.0001
6	9	5/8/2012	0.0048	0.0050	0.0052
6	10	5/8/2012	0.0040	0.0042	0.0044
6	11	5/8/2012	0.0018	0.0019	0.0020
6	12	5/8/2012	0.0020	0.0021	0.0022
6	13	5/8/2012	0.0016	0.0017	0.0018
6	14	5/8/2012	0.0011	0.0011	0.0012
6	15	5/8/2012	0.0017	0.0017	0.0018
6	16	5/8/2012	0.0029	0.0030	0.0032
6	17	5/4/2006	0.0014	0.0015	0.0015
6	18	5/8/2012	0.0028	0.0029	0.0030
6	19	5/8/2012	0.0026	0.0027	0.0028
6	20	5/8/2012	0.0013	0.0014	0.0014
6	21	5/8/2012	0.0015	0.0016	0.0016
6	24	5/8/2012	0.0011	0.0011	0.0012
6	25	5/8/2012	0.0015	0.0015	0.0016
6	26	5/8/2012	0.0006	0.0006	0.0006
6	27	5/8/2012	0.0009	0.0009	0.0009
6	28	5/8/2012	0.0029	0.0030	0.0032
6	29	5/8/2012	0.0006	0.0006	0.0006
6	30	5/8/2012	0.0020	0.0021	0.0022
		Section 6 Average Areal Density:	0.0026	0.0027	0.0028
		Section 6 Area (cm2):	624308		
		Section 6 Holdup Sub-total (g U-235):	1600	1656	1723

Table B1 Continued: Uncorrected areal density of floor measurements (g ^{235}U/cm2).

Section	Point ID #	Date	0 cm depth Corrected Areal Dens ($g^{235}U/cm2$)	0.23 cm depth Corrected Areal Dens ($g^{235}U/cm2$)	0.51 cm depth Corrected Areal Dens ($g^{235}U/cm2$)
7	1	5/8/2012	0.0024	0.0025	0.0026
7	2	5/8/2012	0.0023	0.0024	0.0025
7	3	5/8/2012	0.0014	0.0014	0.0015
7	4	5/8/2012	0.0006	0.0007	0.0007
7	5	5/8/2012	0.0009	0.0009	0.0010
7	6	5/8/2012	0.0014	0.0014	0.0015
7	7	5/8/2012	0.0006	0.0006	0.0007
7	8	5/8/2012	0.0004	0.0004	0.0005
7	9	5/8/2012	0.0014	0.0014	0.0015
7	10	5/8/2012	0.0015	0.0015	0.0016
7	11	5/8/2012	0.0023	0.0024	0.0025
7	12	5/8/2012	0.0008	0.0008	0.0008
7	13	5/8/2012	0.0011	0.0012	0.0012
7	14	5/8/2012	0.0005	0.0005	0.0006
7	15	5/8/2012	0.0010	0.0011	0.0011
7	16	5/8/2012	0.0013	0.0014	0.0014
7	17	5/8/2012	0.0012	0.0013	0.0013
7	18	5/8/2012	0.0022	0.0022	0.0023
7	19	5/8/2012	0.0012	0.0012	0.0013
7	20	5/8/2012	0.0008	0.0009	0.0009
7	21	5/8/2012	0.0011	0.0011	0.0012
7	22	5/8/2012	0.0013	0.0014	0.0014
7	24	5/8/2012	0.0008	0.0008	0.0008
7	25	5/8/2012	0.0010	0.0010	0.0011
7	26	5/8/2012	0.0011	0.0011	0.0011
7	27	5/8/2012	0.0009	0.0009	0.0010
7	28	5/8/2012	0.0012	0.0012	0.0013
		Section 7 Average Areal Density:	0.0012	0.0013	0.0013
		Section 7 Area (cm2):	624308		
		Section 7 Holdup Sub-total (g U-235):	760	784	820

Table B1 Continued: Uncorrected areal density of floor measurements (g ^{235}U/cm2).

Section	Point ID #	Date	0 cm depth Corrected Areal Dens ($g^{235}U/cm2$)	0.23 cm depth Corrected Areal Dens ($g^{235}U/cm2$)	0.51 cm depth Corrected Areal Dens ($g^{235}U/cm2$)
8	1	5/8/2012	0.0010	0.0010	0.0011
8	2	5/8/2012	0.0007	0.0007	0.0008
8	3	5/8/2012	0.0023	0.0024	0.0025
8	4	5/8/2012	0.0001	0.0001	0.0001
8	5	5/8/2012	0.0003	0.0003	0.0004
8	6	5/8/2012	0.0011	0.0012	0.0012
8	7	5/8/2012	0.0007	0.0007	0.0008
8	8	5/8/2012	0.0003	0.0003	0.0003
8	9	5/8/2012	0.0004	0.0004	0.0004
8	10	5/8/2012	0.0004	0.0004	0.0004
8	11	5/8/2012	0.0017	0.0017	0.0018
8	12	5/8/2012	0.0002	0.0002	0.0002
8	13	5/8/2012	0.0003	0.0003	0.0003
8	14	5/8/2012	0.0018	0.0019	0.0020
8	15	5/8/2012	0.0020	0.0021	0.0028
8	16	5/8/2012	0.0010	0.0010	0.0011
8	17	5/8/2012	-0.0001	-0.0001	-0.0001
8	18	5/8/2012	-0.0001	-0.0001	-0.0001
8	19	5/8/2012	0.0000	0.0000	0.0000
8	20	5/8/2012	0.0000	0.0000	0.0000
8	21	5/8/2012	0.0015	0.0016	0.0016
8	22	5/8/2012	0.0001	0.0001	0.0001
8	23	5/8/2012	0.0001	0.0001	0.0001
		Section 8 Average Areal Density:	0.0007	0.0007	0.0008
		Section 8 Area (cm2):	624308		
		Section 8 Holdup Sub-total (g U-235):	430	445	480

Table B1 Continued: Uncorrected areal density of floor measurements (g ^{235}U/cm2).

Section	Point ID #	Date	0 cm depth Corrected Areal Dens ($g^{235}U/cm2$)	0.23 cm depth Corrected Areal Dens ($g^{235}U/cm2$)	0.51 cm depth Corrected Areal Dens ($g^{235}U/cm2$)
9	1	5/8/2012	0.0003	0.0003	0.0004
9	2	5/4/2006	0.0003	0.0003	0.0003
9	3	5/8/2012	0.0000	0.0000	0.0000
9	4	5/8/2012	0.0001	0.0001	0.0001
9	5	5/8/2012	0.0004	0.0004	0.0004
9	6	5/8/2012	0.0019	0.0020	0.0026
9	7	5/8/2012	0.0015	0.0016	0.0017
9	8	5/4/2006	0.0004	0.0004	0.0004
9	9	5/8/2012	0.0002	0.0002	0.0003
9	10	5/8/2012	0.0002	0.0002	0.0002
9	11	5/8/2012	0.0000	0.0000	0.0001
9	12	5/8/2012	0.0002	0.0002	0.0002
9	13	5/8/2012	0.0005	0.0005	0.0005
9	14	5/4/2006	0.0001	0.0001	0.0001
9	15	5/4/2006	0.0001	0.0001	0.0002
9	16	5/4/2006	0.0000	0.0000	0.0000
9	17	5/4/2006	0.0001	0.0001	0.0001
9	18	5/4/2006	0.0002	0.0002	0.0002
9	19	5/4/2006	0.0002	0.0002	0.0002
9	20	5/8/2012	0.0006	0.0006	0.0006
9	21	5/8/2012	0.0002	0.0002	0.0002
9	22	5/8/2012	0.0004	0.0004	0.0004
9	23	5/8/2012	0.0002	0.0002	0.0003
9	24	5/8/2012	0.0002	0.0002	0.0002
9	25	5/8/2012	0.0002	0.0002	0.0002
9	26	5/8/2012	0.0001	0.0001	0.0001
9	27	5/8/2012	0.0046	0.0047	0.0049
9	28	5/8/2012	0.0019	0.0020	0.0020
9	29	5/8/2012	0.0149	0.0154	0.0160
9	30	5/8/2012	0.0084	0.0087	0.0090
		Section 9 Average Areal Density:	0.0013	0.0013	0.0014
		Section 9 Area (cm2):	624308		
		Section 9 Holdup Sub-total (g U-235):	804	829	875

Table B1 Continued: Uncorrected areal density of floor measurements (g ^{235}U/cm2).

Section	Point ID #	Date	0 cm depth Corrected Areal Dens ($g^{235}U/cm2$)	0.23 cm depth Corrected Areal Dens ($g^{235}U/cm2$)	0.51 cm depth Corrected Areal Dens ($g^{235}U/cm2$)
10	1	5/8/2012	0.0038	0.0039	0.0041
10	2	5/8/2012	0.0054	0.0056	0.0058
10	3	5/8/2012	0.0243	0.0250	0.0261
10	4	5/8/2012	0.0011	0.0011	0.0012
10	5	5/8/2012	0.0009	0.0010	0.0010
10	6	5/8/2012	0.0015	0.0016	0.0016
10	6b	5/8/2012	0.0026	0.0026	0.0028
10	7	5/8/2012	0.0649	0.0668	0.0697
10	8	5/8/2012	0.0444	0.0458	0.0477
10	8b	5/8/2012	0.0291	0.0300	0.0313
10	9	5/8/2012	0.0234	0.0242	0.0252
10	10a	5/7/2012	0.0918	0.0944	0.0985
10	10	5/8/2012	0.0686	0.0706	0.0737
10	10b	5/8/2012	0.0324	0.0334	0.0348
10	11	5/8/2012	0.0347	0.0357	0.0372
10	12	5/8/2012	0.0285	0.0294	0.0306
10	13	5/8/2012	0.0243	0.0250	0.0261
10	13b	5/8/2012	0.0008	0.0008	0.0008
10	14	5/8/2012	0.0018	0.0019	0.0020
10	15	5/8/2012	0.0007	0.0007	0.0007
10	16	5/8/2012	0.0003	0.0003	0.0004
10	17	5/8/2012	0.0007	0.0007	0.0008
10	18	5/8/2012	0.0006	0.0006	0.0006
10	19	5/8/2012	0.0002	0.0002	0.0002
10	20	5/8/2012	0.0002	0.0002	0.0003
10	20a	5/8/2012	0.0005	0.0005	0.0006
10	21	5/8/2012	0.0004	0.0004	0.0004
10	21	5/8/2012	0.0004	0.0004	0.0004
10	21	5/8/2012	0.0004	0.0004	0.0004
10	21	5/8/2012	0.0004	0.0004	0.0004
Section 10 Average Areal Density:			0.0163	0.0168	0.0175
Section 10 Area (cm2):			624308		
Section 10 Holdup Sub-total (g U-235):			10181	10487	10933

Table B1 Continued: Uncorrected areal density of floor measurements (g ^{235}U/cm2).

Section	Point ID #	Date	0 cm depth Corrected Areal Dens ($g^{235}U/cm2$)	0.23 cm depth Corrected Areal Dens ($g^{235}U/cm2$)	0.51 cm depth Corrected Areal Dens ($g^{235}U/cm2$)
11	1	5/29/2012	0.0055	0.0057	0.0059
11	2	5/7/2012	0.0079	0.0082	0.0085
11	3	5/7/2012	0.0066	0.0068	0.0070
11	4	5/7/2012	0.0278	0.0287	0.0299
11	5	5/7/2012	0.0065	0.0067	0.0070
11	6	5/7/2012	0.0095	0.0098	0.0102
11	7	5/8/2012	0.0031	0.0032	0.0033
11	8	5/8/2012	0.0024	0.0025	0.0026
11	9	5/8/2012	0.0249	0.0256	0.0267
11	10	5/8/2012	0.0042	0.0044	0.0045
11	11	5/8/2012	0.0076	0.0078	0.0081
11	11b	5/8/2012	0.0059	0.0061	0.0063
11	11c	5/8/2012	0.0046	0.0047	0.0049
11	12	5/7/2012	0.0064	0.0066	0.0069
11	13	5/8/2012	0.0035	0.0036	0.0038
11	14	5/7/2012	0.0041	0.0043	0.0044
11	15	5/7/2012	0.0166	0.0171	0.0178
11	16	5/7/2012	0.0229	0.0236	0.0246
11	17	5/7/2012	0.0204	0.0211	0.0219
11	18	5/7/2012	0.0090	0.0092	0.0096
11	19	5/7/2012	0.0208	0.0215	0.0224
11	19b	5/8/2012	0.0193	0.0199	0.0207
11	19c	5/8/2012	0.0140	0.0144	0.0150
11	19d	5/8/2012	0.0128	0.0132	0.0137
11	19e	5/8/2012	0.0094	0.0096	0.0100
11	21	5/7/2012	0.0020	0.0021	0.0021
		Section 11 Average Areal Density:	0.0107	0.0110	0.0115
		Section 11 Area (cm2):	624308		
		Section 11 Holdup Sub-total (g U-235):	6664	6871	7156

Table B1 Continued: Uncorrected areal density of floor measurements (g ^{235}U/cm2).

Section	Point ID #	Date	0 cm depth Corrected Areal Dens ($g^{235}U/cm2$)	0.23 cm depth Corrected Areal Dens ($g^{235}U/cm2$)	0.51 cm depth Corrected Areal Dens ($g^{235}U/cm2$)
12	1	5/7/2012	0.0030	0.0031	0.0033
12	2	5/7/2012	0.0077	0.0079	0.0082
12	3	5/7/2012	0.0009	0.0009	0.0010
12	4	5/7/2012	0.0033	0.0034	0.0036
12	5	5/7/2012	0.0035	0.0036	0.0037
12	6	5/7/2012	0.0015	0.0016	0.0017
12	7	5/7/2012	0.0020	0.0020	0.0021
12	8	5/7/2012	0.0016	0.0016	0.0017
12	9	5/7/2012	0.0013	0.0014	0.0014
12	10	5/7/2012	0.0010	0.0010	0.0011
12	11	5/7/2012	0.0011	0.0012	0.0012
12	12	5/7/2012	0.0011	0.0012	0.0012
12	13	5/7/2012	0.0013	0.0013	0.0014
12	14	5/7/2012	0.0015	0.0016	0.0017
12	15	5/7/2012	0.0008	0.0008	0.0008
12	16	5/7/2012	0.0010	0.0010	0.0011
12	17	5/7/2012	0.0012	0.0013	0.0013
12	18	5/7/2012	0.0018	0.0019	0.0020
12	19	5/7/2012	0.0040	0.0041	0.0043
12	20	5/7/2012	0.0011	0.0011	0.0011
12	21	5/7/2012	0.0020	0.0020	0.0021
12	22	5/7/2012	0.0026	0.0026	0.0028
12	23	5/7/2012	0.0034	0.0035	0.0037
12	24	5/7/2012	0.0021	0.0022	0.0022
12	25	5/7/2012	0.0027	0.0028	0.0029
12	26	5/7/2012	0.0063	0.0065	0.0068
12	29	5/7/2012	0.0124	0.0128	0.0134
12	30	5/7/2012	0.0047	0.0049	0.0051
12	31	5/7/2012	0.0012	0.0013	0.0013
12	32	5/7/2012	0.0016	0.0017	0.0017
12	33	5/7/2012	0.0012	0.0012	0.0013
12	34	5/7/2012	0.0012	0.0012	0.0013
12	35	5/7/2012	0.0007	0.0007	0.0008
12	36	5/7/2012	0.0007	0.0008	0.0008
12	37	5/7/2012	0.0007	0.0007	0.0008
12	38	5/7/2012	0.0007	0.0007	0.0008
12	39	5/7/2012	0.0009	0.0009	0.0009
12	40	5/7/2012	0.0009	0.0009	0.0010
12	41	5/7/2012	0.0011	0.0011	0.0011
12	42	5/7/2012	0.0011	0.0012	0.0012

Table B1 Continued: Uncorrected areal density of floor measurements (g ^{235}U/cm2).

Section	Point ID #	Date	0 cm depth Corrected Areal Dens ($g^{235}U/cm2$)	0.23 cm depth Corrected Areal Dens ($g^{235}U/cm2$)	0.51 cm depth Corrected Areal Dens ($g^{235}U/cm2$)
12	43	5/7/2012	0.0022	0.0022	0.0023
12	44	5/7/2012	0.0038	0.0039	0.0040
12	45	5/7/2012	0.0012	0.0013	0.0013
12	46	5/7/2012	0.0010	0.0010	0.0010
12	47	5/7/2012	0.0005	0.0005	0.0005
12	48	5/7/2012	0.0005	0.0005	0.0006
12	49	5/7/2012	0.0004	0.0004	0.0004
12	50	5/7/2012	0.0002	0.0002	0.0003
		Section 12 Average Areal Density:	0.0021	0.0022	0.0023
		Section 12 Area (cm2):	847276		
		Section 12 Holdup Sub-total (g U-235):	1803	1863	1942
		Concrete Floor Total:	35167	37119	40027

Note: Shaded entries indicate a depth deeper than the average was used for calculating self-attenuation for a specific spill region.

VITA

Cory Jake Hudson was born in Lorain, OH and grew up in the suburbs of Cleveland, OH. He also spent two years living in Dayton, OH before graduating high school and pursuing a college degree. Cory earned a Bachelor of Science degree in Electrical Engineering from Clemson University in Clemson, SC in 2005. After that, Cory spent 5 years working as a Design and Quality Engineer for Denso Manufacturing Tennessee (DMTN) in Maryville, TN. In 2010, Cory completed is Master's in Business Administration (MBA) from The University of Tennessee. In 2010 he also accepted a job as a Process Engineer within the Non-Destructive Analysis (NDA) Engineering Group at the Y-12 National Security Complex where he presently works. Cory is pursuing a Master's in Nuclear Engineering from The University of Tennessee with the expected graduation date of May 2014.